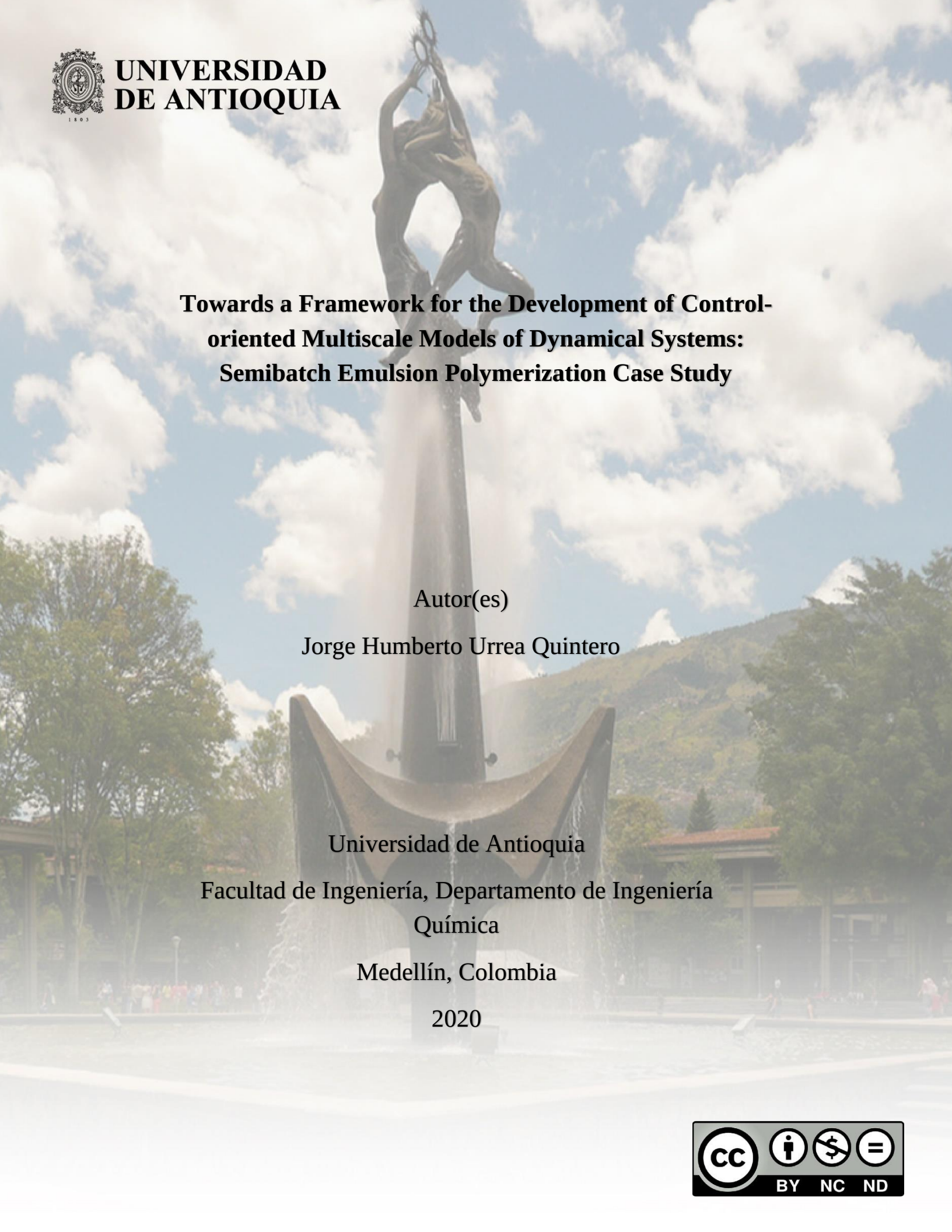

UNIVERSIDAD DE ANTIOQUIA

Towards a Framework for the Development of Control-oriented Multiscale Models of Dynamical Systems: Semibatch Emulsion Polymerization Case Study

Autor(es)

Jorge Humberto Urrea Quintero

Universidad de Antioquia

Facultad de Ingeniería, Departamento de Ingeniería Química

Medellín, Colombia

2020

DOCTORAL THESIS

Towards a Framework for the Development of Control-oriented Multiscale Models of Dynamical Systems: Semibatch Emulsion Polymerization Case Study

Author:
Jorge-Humberto
URREA-QUINTERO

Supervisors:
Prof.Dr.Ing. Silvia OCHOA,
Dr.rer.nat. Hugo HERNÁNDEZ

A thesis submitted in fulfillment of the requirements
for the degree of Doctor of Chemical Engineering

in the

Research Group on Simulation, Design, Control and Optimization of Chemical Processes (SIDCOP)
Departamento de Ingeniería Química

August 9, 2020

Declaration of Authorship

I, Jorge-Humberto URREA-QUINTERO, declare that this thesis titled, "Towards a Framework for the Development of Control-oriented Multiscale Models of Dynamical Systems: Semibatch Emulsion Polymerization Case Study" and the work presented in it are my own. I confirm that:

- This work was done wholly or mainly while in candidature for a research degree at this University.
- Where any part of this thesis has previously been submitted for a degree or any other qualification at this University or any other institution, this has been clearly stated.
- Where I have consulted the published work of others, this is always clearly attributed.
- Where I have quoted from the work of others, the source is always given. With the exception of such quotations, this thesis is entirely my own work.
- I have acknowledged all main sources of help.

Signed:

Date:

"Be plural like the universe."

Fernando Pessoa

UNIVERSIDAD DE ANTIOQUIA

Abstract

Facultad de Ingeniería

Departamento de Ingeniería Química

Doctor of Chemical Engineering

Towards a Framework for the Development of Control-oriented Multiscale Models of Dynamical Systems: Semibatch Emulsion Polymerization Case Study

by Jorge-Humberto URREA-QUINTERO

This work develops a framework for the construction of a control-oriented model from a multiscale perspective, using a semibatch emulsion polymerization process as a case study. First, a so-called full multiscale model (considering the macro-, meso-, and micro-scopic scales) was developed which is composed of a set of Partial/Ordinary Differential Equations and a kinetic Monte Carlo simulation (PDE/ODE - kMC). Then, to obtain a reduced-order representation of the multiscale model, Variance Algebra concepts are used as a tool for representing, at the mesoscopic scale, a disperse-phase system from which only statistical information is available. After that, a dataset considering several process operational conditions is built to capture the main dynamics at the microscopic scale. This dataset is used to derive a closed-form model of the microscopic state variables by adopting a statistical modeling approach. The final obtained control-oriented model is composed of a set of ODEs comprising the macroscopic and the mesoscopic scales that can be solved by using standard ODEs integration schemes, whereas the microscopic scale variables are conveniently defined as some of the system outputs, represented by a set of algebraic equations. In order to consistently solve the full multiscale model, a numerical scheme based on the Finite Element Method is developed capturing the nonlinear evolution of the Particle Size Distribution (PSD). The validity of the obtained reduced-order model is verified through several simulations with respect to the system inputs. Finally, the multiscale control-oriented representation is employed to perform a batch output-controllability analysis based on a set-theoretic approach. The proposed framework might be adopted as a tool for the derivation of dynamical multiscale models keeping a good balance between their tractability and predictive capability, which can constitute an advantage when implementing real-time optimization and process control.

Acknowledgements

First and foremost, I would like to express my sincere gratitude to my advisor, Professor Silvia Ochoa from Universidad de Antioquia, for her much-valued guidance, suggestions, pertinent corrections, and encouragement throughout this work. I would also like to thank my co-advisor, Dr.rer.nat Hugo Hernández. His patience, enthusiasm, and immense knowledge about the polymerization processes made this thesis possible.

Part of this thesis was completed thanks to the advise and support of Dr.-Ing Michele Marino at the Institute of Continuum Mechanics (IKM) in Leibniz Universität Hannover, Germany. After arriving in there, he made room for an excellent research environment. I learned a lot about the Finite Element Method, Continuum Mechanics and many other things. I would like to thank him for his willingness, diligence and generosity in sharing his thoughts and broad knowledge. I really appreciate all the interest and time he placed in my research topic and all the support provided since the first contact established and even after the completion of this process.

I was also fortunate to meet and get to know several the IKM members which made the experience of being there much more comfortable. I would like to thank Aidin for our numerous discussions about both the polymerization mechanism taking part in the Ca-alginate hydrogel and the implementation of the numerical solution in a new programming language I was just getting used to. Thank you, Alex and Darcy, for sharing so many coffees while discussing about the Colombian, German, and Australian culture. It was always a pleasure to me to prepare the Colombian coffee for us. Thank you Meike, Philipp, Blaž, Lukas, Jan, and all the IKM staff who always kept the door opened when I needed some help.

I would like to express my gratitude to both Professor Nicolás Muñoz and Professor Lina Gómez as well, who always kept track of my Ph.D. process and were willing to support me at anytime. My appreciations extend, likewise, to Duban, my college and friend, who helped a lot during this stage and always asked for a beer in every meet.

A lot of things have changed during these last years but one, the love of my unconditional wife. She is the only one who has been at my side in the hard times. It certainly allowed me to successfully complete this endeavor, stay positive and look forward.

Last but not least, I would like to thank COLCIENCIAS and its doctoral grant 727 − 2015. This funding made it possible to focus in my research and to bring my Ph.D. to a successful conclusion.

Contents

List of Figures

List of Tables

List of Abbreviations

CFD	**C**omputational **F**luid **D**ynamics
CTS	**C**ontrollable **T**rajectories **S**et
EM	**E**mulsion **P**olymerization
FEM	**F**inite **E**lement **M**ethod
FPE	**F**okker **P**lanck **E**quation
kMC	**k**inetic **M**onte **C**arlo
LTI	**L**inear **T**ime **I**nvariant
MD	**M**olecular **D**ynamics
MPC	**M**odel **P**redictive **C**ontrol
ODE	**O**rdinary **D**ifferential **E**quation
PBE	**P**opulation **B**alance **E**quation
PDE	**P**artial **D**ifferential **E**quation
p.d.f.	**p**robability **d**ensity **f**unction
PSE	**P**ower **S**eries **E**xpansion
PSD	**P**article **S**ize **D**istribution

List of Symbols

Nomenclature

Symbol	Description	Units
a_0	sum of the all propensity functions	
a_ν	propensity function of the νth reaction channel	
b_0	independent coefficient of the predictor functions	
b_i	dependent coefficients of the predictor functions	
B_D	Bhattacharyya distance	
$C_{[I]_{aq}}$	initiator concentration in the microscopic scale	$\mathrm{mol\,cm^{-3}}$
$C_{[M]_w}$	monomer concentration in the microscopic scale	$\mathrm{mol\,cm^{-3}}$
C_n	free-radicals concentration in the microscopic scale	$\mathrm{mol\,cm^{-3}}$
$C_{[P]}$	Polymer concentration in the microscopic scale	$\mathrm{mol\,cm^{-3}}$
C_p	mixture heat capacity (water, monomer, polymer P_2)	$\mathrm{J\,g^{-1}\,K^{-1}}$
C_{p_M}	monomer heat capacity	$\mathrm{J\,g^{-1}\,K^{-1}}$
C_{p_w}	water heat capacity	$\mathrm{J\,g^{-1}\,K^{-1}}$
d_p	polymer particles diameter	cm
$D(r)$	diffusion of the particles size distribution	$\mathrm{m^2\,s^{-1}}$
D_{rd}	reactor diameter	cm
D_r	diffusion coefficient of the primary radicals	$\mathrm{m^2\,s^{-1}}$
$\mathcal{D}$	reduced-order model polymer particles diffusion	$\mathrm{nm^2\,s^{-1}}$
dW_t	differential update of a Wiener process	
F_I	initiator flow	$\mathrm{cm^3\,s^{-1}}$
F_M	monomer flow	$\mathrm{cm^3\,s^{-1}}$
$G(r,t)$	polymer growth rate kernel	
$\mathcal{G}$	reduced-order model polymer growth rate kernel	
I	a initiator unit	
$[I]_{aq}$	initiator concentration at the aqueous phase	$\mathrm{mol\,cm^{-3}}$
$[I]_{aq_0}$	initiator concentration in the feed stream	$\mathrm{mol\,cm^{-3}}$
j_{max}	monomer chains length to being considered a polymer particle	
K	a function determining the fluctuation of the polymer particles around their mean value	
k_c	apparent radical absorption coefficient	$\mathrm{s^{-1}}$
k_d	initiator decomposition rate	$\mathrm{s^{-1}}$
k_p	propagation reaction coefficient	$\mathrm{cm^3\,mol^{-1}\,s^{-1}}$
m_i	predictor functions	
M	a monomer unit	
$[M]_{aq}$	monomer units at the aqueous phase	
$[M]_{aq}^{sat}$	saturation concentration of the monomer at the aqueous phase	$\mathrm{mol\,cm^{-3}}$
$[M]_p$	monomer concentration at the polymer phase	$\mathrm{mol\,cm^{-3}}$
$[M]_{p_0}$	monomer concentration in the feed stream	$\mathrm{mol\,cm^{-3}}$

$[M]_{p_k}$	monomer units at the polymer phase	
M_{wM}	monomer molecular weight	g mol^{-1}
$\bar{n}$	average number of the free-radicals	
N_A	Avogadro number	molecules mol^{-1}
N_p	particle number concentration	
$\mathcal{N}_p$	number of particles within V_{cell}	
N_s	secondary nucleation rate	Num particles s^{-1}
P_1	seeded polymer particles	
P_2	structured polymer particles	
Pe	Péclet number	
P_{i+j}	the sum of two monomeric radical chains	
P_ν	probability of the νth reaction channel	
q	any linear or nonlinear transformation of the response variables	
$R_0^\bullet$	primary free-radicals formed by the initiator decomposition	
$R_{i+1}^\bullet$	radicals chains plus one monomer unit	
$R_{i,j}^\bullet$	radical chains	
$R_{j_{max}-1}^\bullet$	a radical chain formed by $j_{max} - 1$ monomer units	
$[R_i^\bullet]_{aq}$	radical chains at the aqueous phase	
$[R_i^\bullet]_p$	radical chains at the polymer phase	
$[R_{j_{max}}^\bullet]_p$	a radical chain formed by j_{max} monomer units	
$[R_{i,j}^\bullet]_{p_k}$	free-radical radical chains at the polymer phase	
$[R_{i+1}^\bullet]_{p_k}$	free-radical radical chains at the polymer phase plus one monomer unit	
R_{new}	number of growing polymer chains that have reached j_{max}	
r	polymer particles size	cm
$r_{1,2,3}$	random numbers generated for the kMC simulation	
$\bar{r}$	average polymer particles size	cm
r_p	polymerization rate	
t_f	final batch reaction time	s
T	reactor temperature	K
T_I	initiator temperature	K
T_M	monomer temperature	K
T_j	jacket temperature	K
U	overall heat transfer coefficient	W cm^{-2} K
V	reactor volume	cm^3
V_{cel}	reference volume at the microscopic scale	cm^3
V_w	aqueous phase volume at the microscopic scale	cm^3
$\mathbf{Y}$	random response variables	
$\mathbf{Y}^*$	standardized transformed random response variables	
$Y_{\bar{n}}$	closed-form of the average of free-radicals	
Y_{N_s}	closed-form of the secondary nucleation rate	

Greek letters

Symbol	Description	Units
ΔH_r	reaction enthalpy	J mol^{-1}
Δr	particles space-step size	
Δt	time-step size	

$\partial\Omega_r$	boundary of the polymer particles domain	
$\eta_r(r,t)$	particles population density function	
η_{r_0}	initial condition of the particles population density function	
γ	scales interface	
Ω_0	set of state variables initial conditions	
Ω_r	polymer particles size domain	
Π	time-stepper function describing the system at the microscopic scale	
Φ_{aq}	water volume fraction	
ρ	mixture density (water, monomer, and polymer P_2)	$\mathrm{g\,cm^{-3}}$
ρ_M	monomer density	$\mathrm{g\,cm^{-3}}$
ρ_{Pol}	P_2 polymer density	$\mathrm{g\,cm^{-3}}$
ρ_w	water density	$\mathrm{g\,cm^{-3}}$
σ_n	free-radicals per particle standard deviation	
σ_r	particles size standard deviation	cm
τ	time-steps between reaction events in the kMC simulation	
τ_i	time in which a reaction occurs in the kMC simulation	
τ_t	controllable trajectories set	
θ	system parameters	
μ	index of the selected reaction channel	
ε	residuals of the original model	

Spaces, vectors and matrices notation

Symbol	Description	Units
$\mathbf{C}(t)$	advection matrix	
$\mathcal{C}_t$	controllable set	
$\mathcal{C}^1$	space of those functions whose their first derivative along with themselves are continuous	
$\mathcal{H}^1((0,T)$	Hilbert space consisting of functions, along with their weak partial derivatives, are integrable on Ω_r and vanish on the boundary $\partial\Omega_r$	
$\mathbf{K}$	diffusion matrix	
$\mathcal{L}^2(\Omega_r)$	space of the quadratically integrable functions	
$\mathbf{M}$	mass matrix	
$\boldsymbol{\eta}_r$	vector of the unknowns	
$\dot{\boldsymbol{\eta}}_r$	vector of the derivatives of the unknowns	
$\mathbf{P}$	dead polymer chains arrays	
$\mathbf{R}$	living polymer chains arrays	
$\mathcal{R}_t$	reachable set	
$\mathcal{S}_t$	space of the real-valued functions η_r defined on Ω_r	
$\mathbf{u}$	inputs of the system	
$\mathcal{U}$	space of the admissible inputs	
$\mathcal{V}$	space of the weighting functions w	
$\mathbf{x}$	state variables	
$\dot{\mathbf{x}}$	state derivatives	
$\mathbf{X}$	set of random predictor variables	
$\mathcal{X}$	space of state variables	
$\mathbf{y}$	output variables	
$\mathcal{Y}$	space of the outputs	
$\mathcal{Y}_f$	end-batch specification set	

To my unconditional wife.

Chapter 1

Introduction

Multiscale modeling is a term employed in several fields which commonly refers to a specific set of methods used for simultaneously describing the dynamics of a system at a different time and length scales (Keil, 2012). For lumped processes, Ordinary Differential Equations (ODEs) are adopted to describe the time evolution of the system. For distributed processes, hyperbolic/parabolic Partial Differential Equations (PDEs) are preferred to describe not only the temporal but also the spatial evolution of the system. For instance, Navier-Stokes and Population Balance Equations (PBEs) are the basis for the design and optimization of a wide variety of dynamic processes (Christofides, 2001). In contrast, for processes where important phenomena at microscopic scales take place, multiscale approaches coupling continuum-type lumped/distributed parameter models with Molecular Dynamics (MD) or kinetic Monte Carlo (kMC) simulations are implemented because of their ability to describe phenomena that are inaccessible using macroscopic continuum laws and equations (Vlachos, 2005).

All physical and chemical phenomena are inherently multiscale in nature, the macroscopic behavior observed at human scale is just the result of the interaction of elementary particles, either at the microscopic, molecular, atomic or sub-atomic scales. Modeling these types of processes requires understanding the behavior of the system at each scale having a relevant effect on the overall phenomenon. Accurate and efficient multiscale models could be required for a better prediction of the behavior of a studied system, as well as for the design of better optimization/control strategies. Given all the details and specificity found for each multiscale system of interest, they must be considered as particular case studies (Christofides and Armaou, 2006; Majumder and Broadbelt, 2006; Varshney and Armaou, 2008; Rasoulian and Ricardez-Sandoval, 2014; Crose et al., 2015; Rasoulian and Ricardez-Sandoval, 2015; Crose et al., 2017).

PDE/ODEs - kMC-based multiscale modeling approaches have been receiving a lot of attention in the international research community in the last few years in order

to be used in optimization and control tasks (Christofides and Armaou, 2006; Majumder and Broadbelt, 2006; Varshney and Armaou, 2008; Rasoulian and Ricardez-Sandoval, 2014; Crose et al., 2015; Rasoulian and Ricardez-Sandoval, 2015; Crose et al., 2017; Kimaev and Ricardez-Sandoval, 2017). There is a significant number of publications on multiscale processes modeling, optimization, and control, including some recent reviews (Braatz et al., 2006; Ricardez-Sandoval, 2011; Vlachos, 2012; Karolius and Preisig, 2018). Within those reviews, the main tools available to address this kind of problems as well as some open research questions are well explained. It is important to remark that because of the curse of dimensionality associated to the multiscale models (Ricardez-Sandoval, 2011; Kimaev and Ricardez-Sandoval, 2017), model-order reduction techniques are commonly applied for optimization/control applications based on PDE/ODEs - kMC models (Rusli et al., 2006; Kwon et al., 2013b; Chaffart, Rasoulian, and Ricardez-Sandoval, 2016; Chaffart and Ricardez-Sandoval, 2017; Chaffart and Ricardez-Sandoval, 2018a). Model-order reduction has been mainly focused on the development of a closed-form model for the microscopic-scale in order to both reduce the model computational load and to quantify the associated uncertainty due to the stochastic nature of the kMC simulations. However, less attention has been paid to the dimensional reduction of the mesoscopic scale in order to reduce the number of the degrees of freedom would result from adopting, e.g., a discretization technique to numerical approximate its solution, while indirectly also decreasing the amount of the kMC executions. That could be another alternative to deal with the curse of dimensionality.

A wide range of complex chemical processes could require a multiscale perspective for the description of their dynamical evolution if high-quality product specifications are required, such as: the manufacture of on-chip copper inter-connections by electrochemical deposition of copper into a trench (Rusli et al., 2006; Braatz et al., 2006; Li et al., 2007), the growth mode transitions that occur during physical vapor deposition of thin films from a fluid in a vertical, stagnation-flow geometry (Lam and Vlachos, 2001; Christofides and Armaou, 2006); concentration variations in the fluid in two dimensions for catalytic flow reactor (Majumder and Broadbelt, 2006; Ulissi, Prasad, and Vlachos, 2011); batch crystallization process to produce tetragonal hen-egg-white lysozyme crystals (Kwon et al., 2013a; Kwon et al., 2013b; Kwon et al., 2014a; Kwon et al., 2014b; Kwon et al., 2014c); electrochemistry applications as CO electro-oxidation, fuel cells, and batteries (Röder, Braatz, and Krewer, 2019; Röder, Laue, and Krewer, 2019), among others.

In the chemical vapor deposition process, particularly, during the epitaxial thin film growth process in the stagnation point flow chamber, the evolution of the surface microstructure is captured through kMC simulations which represent the surface roughness trajectories as a combination of absorption, desorption and migration stochastic events (Christofides and Armaou, 2006). The multiscale nature of the process has been captured using nonlinear PDEs embedded with lattice-based kMC

simulations. Moreover, the control problem of obtaining thin films with uniform surface roughness had been solved based on this PDE-kMC dynamical model (Rasoulian and Ricardez-Sandoval, 2015; Rasoulian and Ricardez-Sandoval, 2016).

On the other hand, stochastic fluctuations in the microscopic-scale has been handled in a crystallization process, particularly, in the crystal growth of the tetragonal form of hen-egg-white lysozyme. Kwon et al. (2013a); Kwon et al. (2013b) modeled and controlled this protein crystallization process taking into account both nucleation and growth rates. In that work, the growth of each crystal was simulated via kMC comprising adsorption, desorption and migration events on the (110) and (101) crystal faces. PBE were used to describe the evolution of the particle size and shape distribution inside the reactor. Kwon et al. (2014a), Kwon et al. (2014b), and Kwon et al. (2014c) coupled the PBE and the kMC simulation with the mass and energy balances obtaining a multiscale representation for the crystallizer. Then, the multiscale model was used for the design of a Model Predictive Control (MPC) scheme to regulate the average shape of the crystal population in a continuous operation mode.

In summary, well-defined approaches for modeling at least the nanoscopic, microscopic, mesoscopic, and macroscopic scales in a variety of chemical processes have been already developed (Gooneie, Schuschnigg, and Holzer, 2017; D'hooge et al., 2016). Additionally, several algorithms to simulate multiscale systems have been reported (Keil, 2012; Kwon, Nayhouse, and Christofides, 2015; Xie and Luo, 2017; Xie, Liu, and Luo, 2018; Röder, Braatz, and Krewer, 2019), where the latest developments are focused on assuring the numerical stability and reduction of the computational cost (both, of integrating the different scales and of solving the complete multiscale model). However, despite the similarities between the crystallization and Emulsion Polymerization (EP) process for synthesizing structured polymer particles, the latter has not yet been tackled by means of a multiscale approach that simultaneously takes into account scales below the mesoscopic-scale, e.g., the microscopic-scale through a kMC simulation.

1.1 Motivation and objectives

Multiscale representation of batch processes has opened the possibility of a better control of relevant microscopic state variables allowing the manufacture of specialized products with microscopic specifications (Braatz et al., 2006). Consequently, it would be desirable to have a formal approach to evaluate the process capabilities to meet the desired end-product quality specifications. One alternative of doing that could be the process controllability verification from a multiscale perspective (Ricardez-Sandoval, 2011). Notwithstanding some controllability analyses have been successfully applied to one-scale (semi)batch processes to design some trajectories through the process can be controlled to achieve the desired system performance

(Srinivasan and Bonvin, 2007; Aumi and Mhaskar, 2009; Gómez-Pérez, Gómez, and Alvarez, 2015), they have never been applied to the controllability analysis of batch processes adopting a multiscale perspective. Two main limitations of the controllability verification from a multiscale perspective are: ***i.*** the natural complexities arise from the multiscale representation because of the inherently uncertainty at the finer scales (Ricardez-Sandoval, 2011), and ***ii.*** the general absence a closed-form model at the finer scales (Christofides and Armaou, 2006; Varshney and Armaou, 2008). However, by applying a suitable model-order reduction procedure, it would be possible to derive a control-oriented representation of the multiscale model such that, e.g., a set-theoretic approach to verify the system controllability could be applied (Gómez et al., 2015; Gómez-Pérez, Gómez, and Alvarez, 2015).

1.1.1 Main objective

To develop a framework for evaluating the controllability of multiscale systems that explicitly considers the effect of microscopic variables over the final product quality by the manipulation of macroscopic variables.

1.1.2 Specific objectives

1. Propose a control-oriented multiscale dynamical model for the selected case study (i.e. core-shell morphology control in a free-radical polymerization process).
2. Select an algorithm to solve the proposed multiscale model.
3. Analyze the effect of model parameter uncertainties on the process (uncertainty analysis).
4. Extend the range of applicability of the set-theoretic controllability analysis to the controllability analysis of a multiscale process.
5. Evaluate the process capabilities of achieving the desired product quality specifications via simulation.

1.2 Thesis contributions

In this work, a framework for the development of a control-oriented model from a multiscale perspective is developed, using a semibatch emulsion polymerization process as case study. This work adopts multiscale models represented by Partial/Ordinary Differential Equations - kinetic Monte Carlo (PDE/ODE - kMC) set of equations. The proposed framework is composed of the following stages: ***i.*** to build a multiscale dynamical model combining the most representative scales of the process; ***ii.*** to solve the full multiscale model adopting suitable numerical algorithms for each of the considered scales; ***iii.*** to build a reduced-order model by

means of the Variance Algebra concepts for the disperse-phase scale represented by a PDE; ***iv.*** to generate a database by solving the full multiscale model considering as much as possible admissible process operational conditions to capture the most relevant dynamics of the microscopic scale; ***v.*** to apply a statistical modeling approach for developing a closed-form model of the microscopic scale, while keeping a good predictive capability of the model; and ***vi.*** to validate the obtained reduced-order model by the verification of the process output controllability from the set-theoretic approach.

The multiscale model representing the emulsion polymerization process is proposed attempting to keep a good balance between model predictions accuracy and tractability. It integrates microscopic-scale calculations based on kMC simulations (stochastic). On the other hand, the mesoscopic scale representing the PSD (the dispersed media) is carried out by adopting the FPE. The macroscopic scale is described based on mass and energy balances (deterministic). The Variance Algebra concepts are used to describe the stochastic nature of the particles growth kernel at the mesoscopic scale. This approach is precisely the main step towards the construction of a reduced-order multiscale model. To deal with the curse of dimensionality, the procedure based on the statistical modeling approach introduced by Hernandez (2018) is adopted to derive a closed-form model for the microscopic scale. The proposed method relies on testing hypotheses based on a wide range of versatile distribution models instead of assuming a single specific distribution. A statistical model is obtained by minimizing the variance of the error model, instead of the variance of the data sample, thus reducing the effect of over-fitting. Based on such a procedure, the problem of fitting a model based on a dataset generated by several realizations performed from the kMC model solution is addressed. The developed control-oriented model from the multiscale representation predicts the traditional macro- and mesoscopic variables of the emulsion polymerization process, along with the average number of free radicals and the secondary nucleation rate at the microscopic scale, all with a low computational load.

Accordingly, this work develops a reasonable computational control-oriented model while preserving a good level of detail in the formulation capturing information from three different length scales. Although the macroscopic-scale description is kept simple, it must be noticed that the modeling effort is on the microscopic-scale representation (where an integration of chemical, colloidal and hydrodynamic events is performed using the kMC technique (Hernández and Tauer, 2008a)), as well as in the mesoscopic-scale (where even a reduced-order model is proposed for describing the mean and standard deviation of the particle size distribution by means of only two ODEs), and in an efficient scales integration. Considering these key points, the model can be used as a base for developing a control strategy towards improving the process productivity while avoiding secondary particle nucleation. For instance, it is showed here that the batch output-controllability analysis based on a set-theoretic

approach allows to verify whether it is possible or not to achieve a set of end-batch quality specifications and how the definition of those specifications affects the size of the so-called Controllable Trajectories Sets. Additionally, it is shown how the information of the computed sets can be used to define different reachable end-batch specifications.

1.3 Thesis outline

Chapter 2: Theoretical foundations and literature review

This chapter reviews the literature pertaining to multiscale modeling approaches and highlights the relevance of developing these models to bridge microscopic and macroscopic domains. The challenges regarding multiscale modeling are summarized in Section 2.1. Numerical methods that have been developed to approximate the solution of multiscale models are analyzed in Section 2.2. Section 2.3 deals with the approximations reported in the literature to obtain computational inexpensive closed-form models at lower scales. Finally, controllability analyses to address this problem are described at the end of this chapter in Section 2.4.

Chapter 3: Multiscale model of a free-radical semibatch emulsion polymerization process

This chapter presents all the procedure for the multiscale model derivation and its numerical solution. Chapter 3 is organized as follows. The process description and multiscale mathematical model deduction are presented in Section 3.1. The computational strategy derived by using the FEM for numerically solving the multiscale mathematical model is presented in Section 3.2. Finally, some concluding remarks of the chapter are presented in Section 3.4.

Chapter 4: Multiscale model order reduction

This chapter contains the mathematical formulation regarding the derivation of a reduced-order model for the mesoscopic scale and the statistical modeling procedure adopted to build the closed-form model for the microscopic scale. Chapter 4 is organized as follows. The mesoscopic reduced-order model derivation based on the Variance Algebra concepts is presented in Section 4.1. The closed-form model derivation of the microscopic scale is presented in Section 4.2. Finally, chapter conclusions are presented in Section 4.5.

Chapter 5: Set-theoretic output-controllability analysis

In this chapter all the concepts about the bath output-controllability analysis from a multiscale perspective are introduced and applied to a particular case study. Then the output-controllabilty for the semibatch emulsion polymerization process is performed. Chapter 5 is organized as follows. In Section 5.1, the foundations of the

set-theoretic based batch output-controllability analysis are presented and the general mathematical representation of the multiscale system addressed in this paper is stated. In Section 5.2, the output-controllability analysis is performed for the free-radical emulsion polymerization process. Afterwards, the simulation results are reported. Finally, some concluding remarks of the chapter are presented in Section 5.3.

Chapter 6: Conclusions and future work

Finally, in this chapter some general conclusions are presented and a number of suggestions for future work are presented.

1.4 List of publications

Following three papers encompassing the whole thesis were published as the result of this research work:

1. Urrea-Quintero, J. H., Ochoa, S., & Hernández, H. (2019). A reduced-order multiscale model of a free-radical semibatch emulsion polymerization process. *Computers & Chemical Engineering*, 127, 11-24.

2. Urrea-Quintero, J. H., Michele, M., Ochoa, S., & Hernández, H. (2020). Multiscale modeling of a free-radical emulsion polymerization process: Numerical approximation by the Finite Element Method. *Computers & Chemical Engineering*, 106974.

3. Urrea-Quintero, J. H., Hernández, H., & Ochoa, S. (2020). Towards a controllability analysis of multiscale systems: application of the set-theoretic approach to a semi-batch emulsion polymerization process. *Computers & Chemical Engineering*, 106833.

Chapter 2

Theoretical foundations and literature review

2.1 Modeling of Emulsion Polymerization (EP) processes

The most common approaches for modeling and simulating processes containing a dispersed media (as is the case for EP processes) represent the system of interest as a set of coupled ODEs-PDEs. However, such approximations assume that the system behaves as a continuum entity, which does not represent closely the actual phenomenon. A suggested approximation for overcoming this is to combine continuum models with coarse models by assuming that the system is not a continuum but a collection of a very large number of particles. Thus, allowing to observe the behavior of each of those particles separately, i.e., multiscale approaches (Matous et al., 2017). For the specific case of EP processes, the most recurrent approach employed for modeling a particular EP process couples mass and energy balances with PBEs (Crowley et al., 2000; Kiparissides, 2006; Sweetman et al., 2008; Hosseini, Bouaswaig, and Engell, 2012). This type of approaches have shown to be very effective only in the simplest case of pure growth processes (Sheibat-Othman et al., 2017).

However, the real picture is more complicated than that because the particle size is not the only factor distinguishing the particles from each other. Besides the size of the particle, the characteristic length, volume, mass, age, composition, and other characteristics of an entity in a distribution should be taken into account (Gunawan, Fusman, and Braatz, 2004). This can be achieved by considering any of the above particle characteristics as internal coordinates to describe the evolution of the Particle Size Distribution (PSD). The main issue in doing so is that by considering additional internal coordinates leads to a multidimensional PBE system. Main drawbacks of this are: ***i.*** reaching a solution of a multidimensional PBE is very challenging, still an open research problem up to four internal variables or dimensions (Gunawan, Fusman, and Braatz, 2004; Reinhold and Briesen, 2015); ***ii.*** the stochastic nature of the evolution of the internal variables is still neglected (Hosseini, Bouaswaig,

and Engell, 2012); and ***iii.*** it is still not clear how to validate multidimensional PBE-based models while models from different scales can be separately validated and afterwards integrated in a coupled simulation scheme (D'hooge et al., 2016). For instance, an alternative approach for solving the problem could be extending the model by incorporating additional scales and representing the evolution of the system in those scales through stochastic simulation approaches as Brownian Dynamics or kMC simulations (Hernández and Tauer, 2008a).

Modeling EP processes is a challenging task because the rate of events that take place in this process range from about 10^0 to 10^9 s^{-1} involving entities of very different length scales, such as ions and molecules ($< 1nm$), macromolecules ($1 - 10nm$), polymer particles ($10nm - 1\mu m$) and monomer droplets ($> 1\mu m$) (Hernández and Tauer, 2008b). Those difficulties in the modeling of EP reactors coupled with the lack of robust online measurements for critical process parameters have forced practitioners to use several empirical or semi-empirical equations. Furthermore, industrial EP reactors suffer from process variability, that usually makes the process irreproducible from batch to batch (Dimitratos, Elicabe, and Georgakis, 1994). This variability includes random disturbances in the process operating conditions, which in the EP case corresponds to stochastic fluctuations occurring at the finest scales (D'hooge et al., 2016). For example, fluctuations of the particle state around the mean size cause a stochastic broadness in the PSD (Hosseini, Bouaswaig, and Engell, 2012). For all these reasons, a very precise representation of the process is only possible if different simulation techniques are integrated into a multiscale simulation approach (D'hooge et al., 2016).

The integration of different scales in EP was initially done by incorporating the mesoscopic scale of PSD in the macroscopic polymerization model (Dimitratos, Elicabe, and Georgakis, 1994). Almost in parallel, the microscopic scale of radical dynamics and chain growth was considered using Gillespie's stochastic simulation algorithm (Gillespie, 1976), also known as kMC simulation. kMC was originally used for modeling the molecular weight distribution of polymers (Tobita, Takada, and Nomura, 1994), although without a multiscale integration. Integration of polymerization models at different scales, including the micro-scale was explored for both emulsion (Hernández, 2008) and mini-emulsion polymerization (Rawlston, 2010). However, integrating the micro-, meso- and macro-scopic scales in a single model is still challenging, particularly from the computational load point of view.

Up-to-date modeling approaches for describing the dynamic evolution of polymerization processes include sophisticated descriptions at the meso- and micro-scopic scales (Xie, Liu, and Luo, 2018; Xie and Luo, 2017; Yao, Su, and Luo, 2015; Yan, Luo, and Guo, 2011). For example, full Computational Fluid Dynamic (CFD) simulations have been developed, which include the turbulence characteristic of the fluid pattern inside the reactor (Xie, Liu, and Luo, 2018; Xie and Luo, 2017). Most of the proposed approaches have resulted in an accurate representation of the studied

phenomenon. However, they might be impractical for carrying out model-based optimization and control tasks in real-time implementations. Furthermore, it must be noticed that selecting an adequate solution strategy for integrating continuum with coarse models (in order to exchange information among the scales) is a very important task (Gooneie, Schuschnigg, and Holzer, 2017). Such exchange of information could lead to numerical instability during the numerical solution of the problem (Ricardez-Sandoval, 2011). Additionally, numerical solution of the multiscale models imposes several restrictions as high computational load or the need for parallelizable numerical schemes, not to mention that those models can hardly be used for subsequent tasks such as process optimization and/or control because of the computational load and the lack of a closed-form of the scales below the mesoscopic-scale (Xie and Luo, 2017).

There are two predominant modeling approaches of EP processes, classified by Vale and McKenna (2005) as level-one and level-two models. Level-one models assume that all polymer particles have the same average volume. In contrast, level-two models incorporate the latex PSD by means of PBEs, allowing to investigate on the link between the reaction kinetics, particle nucleation, and growth (Vale and McKenna, 2005). However, PBE-based models require refined constitutive models of the phenomena occurring in the process to extend their predictive capabilities, which are not always easy to derive. Another limiting factor of the PBE-based models adoption is that the more complete the models, more complex they are and more computationally extensive they numerical solution become (Vale and McKenna, 2005; Sheibat-Othman et al., 2017).

There are several ways in which the constitutive models regarding the EP process can be improved. For instance, by including additional mechanisms of the reaction, by accounting for the hydrodynamics effects on coagulation (Sheibat-Othman et al., 2017), by extracting semi-deterministic kernels for the physical phenomena (e.g., the particle growth kernel) directly from the experimental data (Hosseini, Bouaswaig, and Engell, 2013), by incorporating the stochastic nature of the PSD evolution (e.g., an stochastic term to account for the growing particle fluctuations (Hosseini, Bouaswaig, and Engell, 2012; Urrea-Quintero, Ochoa, and Hernández, 2019)) or by taking into account additional length scales into the simulation and representing the system evolution in those scales through stochastic approaches as Brownian Dynamics (Hernández and Tauer, 2008a) or kMC simulations (Urrea-Quintero, Ochoa, and Hernández, 2019).

2.2 Numerical methods for solving multiscale models described by PDE/ODEs – kMC system of equations

In recent years, many papers have been published dealing with the numerical solution of multiscale models described by a PDE/ODEs – kMC set of equations (see

Ricardez-Sandoval (2011) and Röder, Braatz, and Krewer (2019), and the references therein, for a review of the already proposed numerical schemes). In general terms, the numerical solution of such multiscale models possess two main bottlenecks: ***i.*** the need of the solution of the PBE by means of an efficient numerical scheme and ***ii.*** the stochastic nature of the microscopic scale evolution, properly capture by the kMC simulation but still too expensive. Regarding the numerical solution of the PBEs, many papers have been published dealing with their numerical approximation in recent years. Some relevant works and reviews are the following: Rigopoulos and Jones (2003); Immanuel and III (2003); Gunawan, Fusman, and Braatz (2004); Vale and McKenna (2005); Vale and McKenna (2007); Schütte and Wulkow (2010); Bouaswaig and Engell (2010); Hosseini, Bouaswaig, and Engell (2012); Bertin et al. (2016); Sheibat-Othman et al. (2017); Omar and Rohani (2017). Roughly speaking, the numerical methods used to solve the PBEs can be classified into moment methods, stochastic methods (such as Monte Carlo simulations), and discretization methods (such as finite element methods, finite difference/volume methods, and sectional methods). The lowest computation time can be obtained by using moment methods, but they only capture a few statistical moments of the PSD. Stochastic methods are suitable when random dynamics of the population want to be simulated (e.g., nucleation and aggregation), but the evolution of only a small number of particles can be included. Discretization methods allow the computation of the full PSD, but although the first statistical moment of the PSD is accurately capture, sometimes they fail capturing the higher moments due to the high numerical diffusion and dispersion (Bouaswaig and Engell, 2010). Among discretization methods, finite differences and finite volume methods are more practical due to their easy implementation, but the finite element method (FEM) can be adapted to represent more complex PSDs (Rigopoulos and Jones, 2003; Vale and McKenna, 2005; Sheibat-Othman et al., 2017).

Discretization techniques are one of the most popular numerical methods to solve PBEs-based models. Those discretization techniques basically differ in the choice of the mesh selection as well as the global population properties that want to be conserved (Bertin et al., 2016). High-resolution methods are an interesting option for solving PBEs which are advection-dominated. These techniques are able to capture a high accurate solution on coarse meshes by conditioning the solution through a function called flux limiter. That function tends to high order accuracy in the PSD smooth region and a first order scheme is used in the vicinity of large gradients. These methods reduce numerical diffusion present in first order discretization and also eliminating the oscillations caused by higher order discretization schemes (Gunawan, Fusman, and Braatz, 2004). The main drawback of these methods is that still require large computational time and often cannot be used to perform neither sensitivity analyses nor optimization tasks (Majumder et al., 2010).

Another class of discretization methods often used to solve PBEs is the method of

weighted residuals (Finlayson, 2013), which is a general technique to solve problems formulated as differential equations in science and engineering. The methods associated with this technique retrieve the full distribution by approximating the solution with a series of basis functions. Local basis functions that lead to the so-called FEM can be adopted to preserve the generality and flexibility of the numerical scheme by capturing highly irregular distributions (Zienkiewicz, Taylor, and Zhu, 2013). The main feature of the FEM over the finite difference methods and other discretization techniques is the recovery of the entire PSD as well as their flexibility in coping with any possible formulation of the PBE (Rigopoulos and Jones, 2003). Several applications of the FEM to solve PBEs-based problems are summarized in (Vale and McKenna, 2005; Sheibat-Othman et al., 2017). It has been argued that the adoption of the FEM to solve PBEs typically results in severe oscillations that cannot be alleviated neither by introducing an artificial diffusion term nor by increasing the number of elements (Mesbah et al., 2009). However, it is also well documented that if the Péclet (Pe) number is kept small enough, i.e. $Pe < 1$, it is possible to obtain a satisfactory solution of the problem if a smooth function is transported far from Dirichlet boundaries (Donea and Huerta, 2003b), which is the case, for example, of the Fokker-Planck equation (FPE) formulation to represent the evolution of the PSD presented in (Hosseini, Bouaswaig, and Engell, 2012; Urrea-Quintero, Ochoa, and Hernández, 2019) or the example presented in (Donea and Huerta, 2003b) to cope with the advection-diffusion of a Gaussian hill.

In the FEM, the solution is approximated through linear combinations of predefined interpolation functions and the PDE is translated into an algebraic system by means, for instance, of the minimization of the weighted residual (Wriggers, 2008; Zienkiewicz, Taylor, and Zhu, 2013). The main advantages of the FEM over other discretization techniques are the recovery of the entire PSD and its flexibility in coping with any possible formulation of the PBE (Rigopoulos and Jones, 2003). As a disadvantage of the FEM, the numerical solution might be characterized by severe oscillations that require special attention in setting up the simulation, such as mesh discretization associated with a low Péclet number (Pe) or the use of a stabilizing term (Donea and Huerta, 2003b).

2.3 Closed-form for microscopic scales

Small scale chemical reactions are well studied and recognized to be stochastic by nature (Schnoerr, Sanguinetti, and Grima, 2017). At fine scales, chemical reactions are better modeled by the Chemical Master Equation (CME) which describes reactions as discrete probabilistic events (Gillespie, 1976; Gillespie, 2007). While the solution of the CME can be obtained using traditional numerical methods for solving ODEs, the challenge of finding a solution lies in the number of states that need to be evaluated. For systems with even a relatively small size, the CME cannot be solved

since the number of possible states is prohibitively large Gillespie (2007). This imposes a limitation towards the direct application of the CME to obtain an estimate of system states. In fact, no analytic solutions to the CME are known for most systems. Moreover, stochastic simulations are computationally expensive, making systematic analysis and statistical inference a challenging task (Schnoerr, Sanguinetti, and Grima, 2017; Evans and Ricardez-Sandoval, 2014). The scope of this work is not to present a detailed literature review on the topic, but numerous solution methods have been designed to approximate the solution of the CME. Some relevant references on the topic are Jahnke (2011); Kazeev et al. (2014); Schnoerr, Sanguinetti, and Grima (2017). Particularly, Evans and Ricardez-Sandoval (2014) presented an interesting work where the so-called Multiple Scenario Chemical Master Equation (MSCME) algorithm is introduced. MSCME models and analyze uncertainty propagation in the CME. Analysis indicated that the proposed algorithm showed a good prediction of uncertain parameters and could be an alternative to the most widely used method, the kinetic Monte Carlo algorithm.

The microscopic scale of PDE/ODEs – kMC multiscale models, which is represented by the kMC simulation, is the most critical part from the computational viewpoint since it requires a computationally intensive stochastic solution. The main concern is that it lacks a closed mathematical form. Few authors have already proposed some approaches to obtain closed-forms estimates from the kMC simulations (Rasoulian and Ricardez-Sandoval, 2015; Rasoulian and Ricardez-Sandoval, 2016; Crose et al., 2015; Crose et al., 2017; Chaffart and Ricardez-Sandoval, 2018a; Kimaev and Ricardez-Sandoval, 2019). The drawbacks of such approximations are that they are limited only to the linear regime of the problem (Crose et al., 2015; Crose et al., 2017), require a sensitivity analysis via a Monte Carlo simulation over the parameters domain, which entails a large number of samples from the uncertain parameter distribution (Rasoulian and Ricardez-Sandoval, 2015; Rasoulian and Ricardez-Sandoval, 2016), requires a large dataset to train the model (Kimaev and Ricardez-Sandoval, 2019), or leads to the construction of a stochastic PDE, which is later solving in conjunction with the other scales, increasing the dimension of the problem (Chaffart and Ricardez-Sandoval, 2018a). Furthermore, those procedures were developed for each case and it is not clear how to generalize them as a tool to build closed-form models based on kMC simulations for the EP case here considered.

Crose et al. (2015, 2017) developed a multiscale model and operation framework for plasma-enhanced chemical vapor deposition (PECVD) on thin film silicon solar cells. The model captures the gas-phase reaction and transport phenomena that lead to the deposition of the thin film across the wafer. They were able to study the evolution of the thin film surface microstructure at different spatial locations across the wafer. The relationships among substrate temperature, gas-phase mole fraction of SiH_3, and the thing film growth rate were plotted were a clear nonlinear behavior

appears above 500 K. Thus, the data from the kMC simulation was used to construct linear growth rate equations which depend on the temperature by ignoring the non-linear effects restricting the study to the region below 500 K. The linear growth rate equations were fitted using standard least square methods.

Rasoulian and Ricardez-Sandoval (2015a,b, 2016) presented an algorithm to design a robust estimator that can mimic the multiscale model of an epitaxial thin film growth process for online control and optimization purposes. The model parameter uncertainties were considered by using first-order power series expansion (PSE). It was shown that the robust estimator bounded multiple realizations of the multiscale model under parameter uncertainty. The algorithm presented by the authors is quite straightforward and its capabilities to obtain closed-form models of the microscopic states was proved. It is fair to say that the algorithm presented by the authors is the best up to date candidate to be applied to multiscale systems represented by PDE/ODEs - kMC models. However, the requirement of the sensitivity analysis as a prerequisite of the algorithm imposed a challenge in its adoption as the authors already pointed out. The reason is that the sensitivity analysis requires a Monte Carlo simulation over the parameters domain and this requires a large number of samples from the uncertain parameter distribution (Rasoulian and Ricardez-Sandoval, 2014). It is not always possible to perform such a Monte Carlo simulation over the parameters domain by taking enough samples to reconstruct the full probability distribution of the microscopic states due to the curse of dimensionality associated with the multiscale models. Additionally, although the authors mentioned that their proposed algorithm is applicable regardless of the type of probability distribution assigned to the uncertain parameters, such an uncertainty was assumed to be normally distributed in the study. This means the closed-form models of the microscopic states represent normally distributed uncertainty as well. Therefore, if a different distribution on the parameters is assumed and if additional statistical moments rather than the mean value and the standard deviation are required to characterize the microscopic states, it not clear how this procedure can be generalized.

Aside from the methods developed with aim of a closed-form model derivation at the microscopic effect, there are some additional works that have focused on the quantification and uncertainty propagation at this scale (see, e.g., Rasoulian and Ricardez-Sandoval (2014); Chaffart and Ricardez-Sandoval (2017); Kimaev and Ricardez-Sandoval (2017); Kimaev, Chaffart, and Ricardez-Sandoval (2020)). Those works are worth to be mentioned because the PCE method, that leads to a deterministic description of a stochastic process and can be used to approximate the kMC simulation, has been adopted as an efficient technique to uncertainty propagation in the multiscale system where discrete scales are modeled without the need of considering a closed-form expression, just as in the case of the microscopic scale in the polymerization application presented in this work.

The capabilities and functionality of the PCE are acknowledged as a way to approximate the kMC simulation in multiscale approaches, specially because of the critical role uncertainty might play at fine scales for the accurate prediction of variables at coarser scales. However, in the case study presented in this work, the goal was not to propagate the uncertainty, but to handle high computational complexity at the microscopic scale as a statistical modeling problem where exploiting the advantages of the method proposed by Hernandez (2018), bearing in mind other statistical modeling approaches could be adopted as well. Consequently, the importance of quantify and propagates microscopic scale uncertainty is admitted studying its effect but will be left to future.

In summary, approaches to handle probability distribution functions other than Gaussian distributions have been developed in the literature and used in the context of multiscale modeling, see e.g. Kimaev and Ricardez-Sandoval (2017); Chaffart and Ricardez-Sandoval (2017); Chaffart and Ricardez-Sandoval (2018b). However, no closed-form model of the microscopic scale accounting for distributions beyond the Gaussian have been reported.

2.4 Set-theoretic based controllability analysis of batch processes

One key property that must be evaluated when designing a control structure for a dynamic system is the controllability. According to Kalman (1959), controllability is the property of dynamical systems by which an initial state of a system can be steered to another state by a control input sequence in a finite time interval. However, in most cases, controllability is taken for granted, perhaps, since some influence of the system inputs over its outputs is observed when open-loop simulations are performed. Currently, determining to what extent a multiscale system is controllable (i.e. whether a set of microscopic state variables can be driven to meet some desired product quality specification), is still an open research topic. In a very complete review of the topic design and control of multiscale systems, by Ricardez-Sandoval (2011), the author pointed out that one of the limitations when designing control strategies from a multiscale perspective is the lack of availability to measure on-line the system properties at the lower scales. In that review, it was argued that maybe the most promising strategy to overcome this limitation is to improve the system controllability, by proposing a robust design at the smaller length scales. This could avoid the need for on-line sensors measuring molecular or microscopic state variables, which is fundamental for classical control, at the expense that any external perturbation or uncertainties that were not considered while designing the underlying microscopic or molecular system may result in loss of performance and poor product quality. The mentioned review closed by calling for more research on this

subject to validate this promising alternative, which seems to be the most practical method that may exist to control multiscale systems.

A controllability analysis could be performed following different approaches based on system characteristics. For example, if the system can be approximated by a liner representation around a stable operating point, then Kalman rank condition can be applied for investigating its controllability (Kalman, 1959). However, if a suitable linear approximation of the system is not available, and/or it lacks a stable operating point (which is the case in batch processes), another kind of approximation must be adopted in order to evaluate the system controllability. This implies that batch processes are not controllable in Kalman's sense. That is why, from the classical control theory viewpoint, batch processes are simply not controllable (Gómez et al., 2015).

Only few works have addressed the controllability problem of batch processes in the open literature, which are: (Srinivasan and Bonvin, 2007; Gómez, Gómez, and Alvarez, 2010; Gómez et al., 2015; Gómez-Pérez, Gómez, and Alvarez, 2015). Controllability analysis of batch processes possess additional challenges in comparison to continuous, because: ***i.*** they lack a steady-state operating point and ***ii.*** at least one of state variables is irreversible. Hence, it is expected that batch processes evolve far away from their initial conditions to reach some end-point product quality specifications (Srinivasan and Bonvin, 2007; Gómez et al., 2015).Some of these mentioned drawbacks have been addressed in the work by Gómez et al. (2015). In that work, authors claimed that, from the set-theoretic viewpoint, it is possible to find a state-space region in which an admissible control action sequence exists such that the system is driven from an initial condition to a final desired point. This state-space region is defined by the Controllable Trajectories Set (CTS). The computation of the CTS can be viewed as an approach to perform a state controllability analysis for batch processes. In this direction, controllability analysis based on a set-theoretic approach has been successfully applied to batch processes from a single-scale point of view (e.g. macroscopic scale) (Gómez-Pérez, Gómez, and Alvarez, 2015; Gómez et al., 2015). However, to the author's knowledge, such approximation has not been applied to the output-controllability analysis of batch processes from a multiscale perspective (i.e., in processes represented by PDE/ODEs – kMC multiscale models). Two main limitations for applying the mentioned set-theoretic approach to the controllability analysis from a multiscale perspective are: ***i.*** the intrinsic curse of dimensionality of sets computation, which increases exponentially as the number of state variables increases, and ***ii.*** the methodology requires a closed-form model of the process, which is usually not available when scales below the mesoscopic scale are included in a multiscale modeling approach (Christofides and Armaou, 2006; Varshney and Armaou, 2008). These two limitations are addressed in the present work, in order to extend the range of applicability of the controllability analysis

based on a set-theoretic approach to the batch output-controllability analysis of processes represented by PDE/ODE-kMC multiscale models. First, in order to obtain a multiscale model suitable for the controllability analysis, a statistical modeling approach is proposed as a tool to formulate a closed-form model of the microscopic states. On the other hand, to face the curse of dimensionality in sets computation, a variance algebra approach is used for deriving a reduced-order model of the mesoscopic scale model. As a case study, a semi-batch emulsion polymerization process represented by a multiscale approach recently introduced by Urrea-Quintero, Ochoa, and Hernández (2019) is considered. This problem is relevant because a lack of controllability could represent a limitation in some polymerization processes when high product quality is required. In many polymer production processes, high product quality requires minimizing/maximizing multiple product quality specifications. Such a problem may result in a limited set of viable process trajectories, giving more relevance to process controllability analysis to get the most out of its dynamical properties (Murray, 2003). By adopting the procedure proposed in this work, it would be possible to carry out a controllability analysis for any system represented by a PDE/ODEs - kMC multiscale model. As it will be shown in Chapter 5, the batch output-controllability analysis proposed here (based on a set-theoretic approach) allows verifying whether it is possible or not to achieve a set of end-batch quality specifications from a multiscale perspective, given the available admissible inputs. This means, that it allows verifying if the available manipulated inputs have the desired effect on the microscopic state variables. Other advantages of performing a batch output-controllability analysis are: ***i.*** the verification of the feasibility of the end-product quality specifications prior to the definition of a control policy. This could be particularly helpful for designing reference trajectories such that the end-product quality specifications are achieved even if external disturbances appear (Gómez-Pérez, Gómez, and Alvarez, 2015). ***ii.*** The possibility of implementing optimal control structures (e.g. a model predictive controller), such that the process can be safely steered from an initial condition to the desired final state while remaining inside the CTS. This means that neither the inputs nor the states constraints are violated (Aumi and Mhaskar, 2009).

State-space controllability was defined by Kalman (1959) for Linear Time Invariant (LTI) systems and later extended to the nonlinear case by Sussmann and Jurdjevic (1972). To verify if a LTI system is controllable, it is enough to compute Kalman's controllability matrix and verify if its rank is equal to the state-space dimension. In that case, it is said that the system is fully controllable. For the nonlinear case, one option is to iteratively compute Lie's brackets to verify the system accessibility (Sussmann and Jurdjevic, 1972). However, the accessibility property is weaker than the state controllability property. Then, in order to claim a nonlinear system as controllable, not only the accessibility rank condition must be fulfilled, but it must be reversible (Sontag, 1998). State-space controllability in the nonlinear case is only a local property, that is, a nonlinear system is locally controllable around a system

equilibrium or operating point but seldom anything else can be said in the global sense (Sontag, 1998).

Skogestad and Postlethwaite (2007) defined the output-controllability as the ability to achieve an acceptable control performance; that is, to keep the system outputs within specified bounds from a reference value using available inputs and available measurements of the outputs, even if unknown but bounded disturbances appear. A common characteristic in both, the state-space controllability and the output-controllability is that the result of the analysis is a yes/no answer (i.e. the system is/is not controllable). However, it is not possible to conclude to what extent a nonlinear system is controllable (in any, the state-space or the output- controllability sense), or how much effort (energy) is required to reach the desired final state. In the authors' opinion, such missing information would be very valuable for being used in the simultaneous design-control of multi-scale systems.

In a batch process, the objective is to obtain a product with a defined specification that is set by conducting a sequence of steps (i.e. to obtain a set of states within defined final conditions from an initial condition within a given process time) (Gómez-Pérez, Gómez, and Alvarez, 2015). Then, the control problem can be seen as a steering problem in which the system must be safely driven from an initial condition to a final desired one (Aumi and Mhaskar, 2009). Commonly, the final specification is reached by tracking a predetermined reference trajectory (Chen and Sheui, 2003). Such a reference trajectory should be designed by taking into account the system state-space domain to guarantee the end-product specification feasibility (Aumi and Mhaskar, 2009). However, there is not only one safe path that could be followed, but a bounded hypervolume can be computed which contains on all the possible controllable trajectories given the set of admissible inputs and a suitable model of the system.

The following considerations must be taken into account to address the batch output-controllability problem: ***i.*** full state controllability is not required to achieve the final product specifications. Indeed, a system that is not fully state controllable still could be output controllable (Yuan, Chen, and Zhao, 2011). In batch processes, the output is typically composed only by a subset of the system states. ***ii.*** The number of outputs that can be independently controlled cannot exceed the number of available inputs to be manipulated (Srinivasan and Bonvin, 2007). ***iii.*** Two types of control objectives are desired to be met in batch processes, namely, run-time profiles tracking and run-end values fulfillment (Srinivasan and Bonvin, 2007). ***iv.*** Since controllability addresses the problem of the existence of inputs that result in the desired system performance, some deviations from the nominal run-time profiles are accepted as long as the run-end values are reached (Gómez-Pérez, Gómez, and Alvarez, 2015).

Srinivasan and Bonvin (2007) introduced a definition of batch output-controllability and a quantitative notion of stability that takes into account the finite-time nature

of batch processes. Additionally, they pointed out that since two types of objectives need to be met in batch processes, namely, run-time profiles and run-end values, these two aspects must be combined in an appropriate definition of controllability. The authors stated that controllability is a property that should inform whether or not there exist (open-loop) inputs that bring about the desired performance of the system. Consequently, they defined that a batch system is output-controllable if it is possible to find a sequence of control actions that can simultaneously guarantee the run-time tracking profiles while run-end values are met. This batch output-controllability definition certainly incorporates all the elements to verify whether a batch process is or is not controllable. However, some drawbacks of this approach are: ***i.*** in order to verify the controllability of a nonlinear system, it is necessary to linearize its model; ***ii.*** the analysis still gives a yes/no answer about the controllability of the batch system, but no further information about, e.g., the process limitations are given; ***iii.*** it is assumed that the run-time profiles have been already predefined (usually by means of offline optimization) which does not leave room to improve the process performance while it is running on through, e.g., a run-time redesigning trajectory approach that could deal with unexpected disturbances/uncertainties. Therefore, it would be desirable that the results of a controllability analysis allow finding a group of trajectories that could be used for fulfilling the end-batch requirements, instead of having a one-single trajectory to follow.

In order to address some of the above mentioned drawbacks, Gómez et al. (2015) proposed a set-theoretic based approach for the controllability analysis of batch systems. As stated by the authors, some remarkable points of this approach are: ***i.*** the results obtained by this approach go beyond a yes/no answer, i.e. quantitative information about the system capabilities and limitations can be obtained from sets computation. Using this information, further analyses could be performed, as for example, process optimization, trajectories design and control structure selection (Gómez-Pérez, Gómez, and Alvarez, 2015; Gómez et al., 2015). ***ii.*** The physical restrictions over the system's inputs, states, and outputs can be naturally included as part of sets computation leading to a realistic result from the application point of view.

In this work, Srinivasan and Bonvin (2007) output-controllability definition is adopted. Then, to verify the output-controllability of batch processes, the set-theoretic methodology developed by Gómez et al. (2015) is used here as the framework for addressing the output-controllability analysis of a multiscale system. The mentioned methodology includes three main steps: *1.* to compute the reachable sets for each of the i-steps belonging to the finite sequence of N steps; *2.* to compute the controllable set for each of these i-steps; and *3.* to compute the subset called CTS, which is the intersection between both, the reachable and the controllable sets, in each of the i-steps. In this work, the algorithm proposed by Gómez et al. (2015) to estimate the Controllable

Trajectories Set (CTS) is adopted as part of the framework for evaluating the controllability of multiscale systems based on a set-theoretic approach. It is important to notice that computing the controllable trajectory set requires both, the calculation of the reachable and controllable sets. The difficulty of computing these sets for nonlinear systems that are subject to input-output constraints has been an impediment in the successful implementation of the sets-based controllability analysis. The curse of dimensionality is perhaps the major drawback in the computational approximation of the different required sets (Gómez et al., 2015).

Chapter 3

Multiscale model of a free-radical semibatch emulsion polymerization process

Abstract

In this chapter, the micro-, meso- and macro-scopic scales are combined into the framework of PDE/ODEs - kMC multiscale models to simulate the synthesis of core-shell particles by emulsion polymerization. The multiscale model is proposed attempting to keep a good balance between model predictions accuracy and tractability. This model integrates microscopic scale calculations based on kinetic Monte Carlo (kMC) simulations (stochastic). The mesoscopic scale representation of the dispersed media is carried out by the Fokker-Planck Equation (FPE) for describing the stochastic nature of particle growth. The macroscopic-scale (deterministic) is described based on mass and energy balances. The developed model predicts the traditional macro- and mesoscopic variables, along with the average number of free radicals and the secondary nucleation rate at the microscopic scale.

3.1 Derivation of the set of equations for the multiscale dynamical model

The process considered here is a semi-batch surfactant-free emulsion polymerization of a polymer P_2 in the presence of polymer P_1 that is assumed monodisperse, initiated by a water-soluble initiator I. Monodispersity is assumed in order to observe the evolution of the particle size distribution (PSD) from a single particle size. The usefulness of this assumption has been recognized since several decades ago ((Overbeek, 1982; Ugelstad et al., 1985)). The process aims to grow core-shell particles of P_2 in P_1 by the continuous addition of monomer M. Particularly, core-shell systems (and structured polymers in general) are relevant for high-performance applications,

for example in the synthesis of nanocomposites for energy storage and dielectric applications (Huang and Jiang, 2015), catalysts (Mei et al., 2007), and biomedical applications (Sounderya and Zhang, 2008), just to mention a few.

It is assumed that during the polymerization process the kinetic mechanism in Table 3.1 governs the polymer P_2 production. Here, I is the initiator, $R_o^\bullet$ are the primary free-radicals formed by the initiator decomposition, $R_{i,j}^\bullet$ are radical chains, $R_{i+1}^\bullet$ are radical chains plus one monomer unit, M is a monomer unit, P_{i+j} is a dead polymer of chain length $i+j$ as a result of termination by recombination between two growing chains of length i and j, both in the aqueous phase, $R_{j_{max}-1}^\bullet$ is a radical chain formed by $j_{max}-1$ monomer units, $[R_{j_{max}}^\bullet]_p$ is a radical chain formed by j_{max} monomer units which is considered as a new polymer particle, all of them in the aqueous phase. $[R_i^\bullet]_{aq}$ and $[R_i^\bullet]_p$ represents monomeric radical chains, $[M]_{aq}$ and $[M]_p$ represents the monomer units, in each side of the aqueous – polymer interface, respectively. $[R_{i,j}^\bullet]_{p_k}$ are free radical chains, $[R_{i+1}^\bullet]_{p_k}$ are free radical chains plus one monomer unit, $[M]_{p_k}$ is a monomer unit, and $[P_{i+j}]_{p_k}$ is a dead polymer of chain length $i+j$ as a result of termination by recombination between two growing chains of length i and j, both in the polymer phase.

TABLE 3.1: Free-radical polymerization mechanism.

Phase	Step	Mechanism
Aqueous	**Initiator decomposition**	$2\,\mathrm{I} \xrightarrow{k_d} 2\,\mathrm{R}_o^\bullet$
	Propagation	$\mathrm{R}_i^\bullet + \mathrm{M} \xrightarrow{k_p} \mathrm{R}_{i+1}^\bullet$
	Termination	by recombination $\mathrm{R}_i^\bullet + \mathrm{R}_j^\bullet \xrightarrow{k_t} \mathrm{P}_{i+j}$ by disproportionation $\mathrm{R}_i^\bullet + \mathrm{R}_j^\bullet \xrightarrow{k_t} \mathrm{P}_i + \mathrm{P}_j$
	Nucleation	$\mathrm{R}_{j_{max}-1}^\bullet + \mathrm{M} \xrightarrow{k_p} [\mathrm{R}_{j_{max}}^\bullet]_p$
Aqueous-polymer interface	**Radicals Dynamic**	$[\mathrm{R}_i^\bullet]_{\mathrm{aq}} \underset{k_o}{\overset{k_a}{\rightleftharpoons}} [\mathrm{R}_i^\bullet]_p$
	Swelling	$[\mathrm{M}]_{\mathrm{aq}} \overset{K_{eq}=\frac{[M]_p}{[M]_{aq}^{Sat}}}{\rightleftharpoons} [\mathrm{M}]_p$
Polymer	**Propagation**	$[\mathrm{R}_i^\bullet]_{\mathrm{p}_k} + [\mathrm{M}]_{\mathrm{p}_k} \xrightarrow{k_p} [\mathrm{R}_{i+1}^\bullet]_{\mathrm{p}_k}$
	Termination	by recombination $[\mathrm{R}_i^\bullet]_{\mathrm{p}_k} + [\mathrm{R}_j^\bullet]_{\mathrm{p}_k} \xrightarrow{k_t} [\mathrm{P}_{i+j}]_{\mathrm{p}_k}$ by disproportionation $[\mathrm{R}_i^\bullet]_{\mathrm{p}_k} + [\mathrm{R}_j^\bullet]_{\mathrm{p}_k} \xrightarrow{k_t} [\mathrm{P}_i]_{\mathrm{p}_k} + [\mathrm{P}_j]_{\mathrm{p}_k}$

At the beginning of the polymerization process, the reactor is charged with polymer P_1 seeds. Then the reactor is heated up until the reaction temperature T is reached, starting the polymerization reactions. Once the reactor reaches the reaction temperature, it is fed with both I and M until the end of reaction time. Since the polymerization reactions are highly exothermic, the reactor is cooled using a jacket that keeps

its temperature in a bounded interval. It is assumed here that any change in the jacket temperature T_j occurs instantaneously, thus it dynamic evolution is neglected and not model. Both flows, I and M, and the jacket temperature T_j can be used all together or any combination of them as manipulated process inputs to control the outputs.

The multiscale model for describing the dynamic evolution of free-radical polymerization couples macroscopic variables (e.g., input flows and the reactor temperature) with microscopic quantities (e.g., the average number of free-radicals and the secondary nucleation rate). These two microscopic states are critical to satisfactorily obtain structured polymer particles with the desired size and morphology. Macroscopic and microscopic scales are connected through the definition of a mesoscopic scale which represents the evolution in time of PSD inside the reactor.

A very important aspect of the multiscale model is the exchange of information among the different scales. At lower-scales the model requires information about the state of the system (temperature, composition, etc.) which is determined at upper-scales. At the same time, the upper-scales require parametric and structural information of the system, which is obtained at lower-scales. Therefore, top-down and bottom-up information exchange procedures must be clearly defined. Figure 3.1 shows a schematic representation of the scale interactions for the EP process, where the information exchanged among scales is indicated by directional arrows that show the direction in which the information flows.

3.1.1 Macroscopic scale model

The macroscopic model is composed of the traditional mass and energy balances. Assumptions to derive the macroscopic model included: the density and the overall heat transfer coefficient remain constant, the monomer is fed in excess which implies that all monomer eventually goes to the polymer phase (Klein, Kuist, and Stannett, 1973) which implies that:

$$[M]_{aq} = [M]_{aq}^{sat} = 0.607e3 - 91.258e3/T, \tag{3.1}$$

The mass balance for both aqueous and polymer phases and the energy balance are given by:

Mass Balance for water:

$$\frac{d(\rho_w V \Phi_{aq})}{dt} = F_I \rho_w \tag{3.2}$$

Balance for the initiator in the aqueous phase:

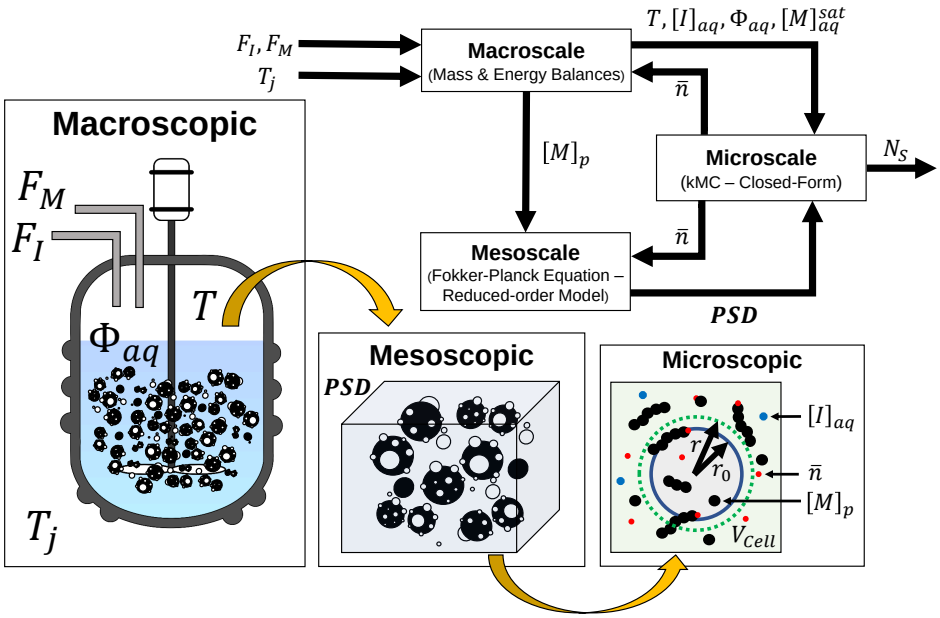

FIGURE 3.1: Scales exchange information scheme of the emulsion polymerization multiscale model. F_M and F_I are the initiator and monomer flows rate, respectively , T and T_j are the temperature of the reactor and the jacket, respectively, $[I]_{aq}$ is the initiator concentration in the aqueous phase, $[M]_p$ is the monomer concentration in the polymer phase, Φ_{aq} is the water volume fraction, $[M]_{aq}^{sat}$ is the saturation concentration of the monomer in the aqueous phase, $\bar{n}$ is the average number of free-radicals, N_s is the secondary nucleation rate, and V_{Cell} is the reference volume of the microscopic scale.

$$\frac{d([I]_{aq}\Phi_{aq}V)}{dt} = F_I[I]_{aq_0} - k_d[I]_{aq}\Phi_{aq}V \tag{3.3}$$

Balance for the monomer in the polymer phase:

$$\frac{d[M]_p}{dt} = \frac{1}{V(1-\Phi_{aq})}\left(F_M[M]_{p_0} - r_pV - (1-\Phi_{aq})[M]_p\frac{dV}{dt} + V[M]_p\frac{d\Phi_{aq}}{dt}\right) \tag{3.4}$$

Total mass balance:

$$\frac{d(\rho V)}{dt} = F_M\rho_M + F_I\rho_w \tag{3.5}$$

Energy balance inside the reactor:

$$\frac{d(\rho C_pVT)}{dt} = F_M\rho_MC_{p_M}T_M + F_I\rho_wC_{p_w}T_I - U\left(\frac{4V}{D_{rd}}\right)(T-T_j) - r_pV\Delta H_r \tag{3.6}$$

where ρ is the mixture density (water, monomer, and polymer P_2), ρ_w is the water density, ρ_M is the monomer M density, C_p is the mixture heat capacity (water, monomer, and polymer P_2), C_{p_M} is the monomer M heat capacity, C_{p_w} is the water heat capacity, k_d is the initiator decomposition rate coefficient, r_p is the polymerization rate, U is the overall heat transfer coefficient, D_{rd} is the reactor diameter (assuming a cylindrical reactor), ΔH_r is the reaction enthalpy, F_I and F_M are the initiator and monomer flows rate, respectively: T_M, T_I, and T_j are the temperature of the monomer stream, initiator stream, and the jacket, respectively. Φ_{aq} is the water volume fraction, $[I]_{aq}$ is the initiator concentration in the aqueous phase, $[M]_p$ is the monomer concentration in the polymer phase, V is the reactor volume, T is the temperature inside the reactor; $[I]_{aq_0}$ is initiator concentration in the feed stream and $[M]_{p_0}$ is concentration of the monomer in the feed stream.

The rate of polymerization r_p is given as follows (Odian, 2004):

$$r_p = \frac{N_p k_p [M]_p}{N_A} \bar{n}(\mathbf{x}) \tag{3.7}$$

with r_p given in mol/cm^3 s and $\mathbf{x} = [V, \Phi_{aq}, [I]_{aq}, [M]_p, T, F_M, F_I, T_j]$, the process variables at the macroscopic scale and

$$N_p = \frac{6(1-\Phi_{aq_0})}{\pi d_{p_0}^3}, \tag{3.8}$$

where N_p is the particle number concentration inside the reactor, k_p is the propagation rate coefficient, N_A is the Avogadro number, d_p is the average polymer particle diameter, and $\bar{n}$ is the average number of free-radicals inside the polymer particles. The latter is computed at the microscopic scale. In practice, the number of particles changes over time, as a result of secondary nucleation and coagulation. However, these effects are neglected here. In other words, this work focuses only on the kinetic behavior and growth of the seed particles.

Although the use of equation (3.7) for determining polymerization rates seems quite straightforward, the average number of radicals per particle in a given polymerization system cannot be measured directly but must be estimated. For this purpose, Smith and Ewart (1948) proposed their famous recursion equation for describing the distribution of the number of radicals inside the polymer particles.

The Smith-Ewart recursion formula can be obtained from the more general Chemical Master Equation (CME) formulation as in equation (3.9) (Hernández, 2008):

$$\begin{aligned} \frac{d\mathbf{N}_n}{dt} &= \frac{\rho}{N_p}(\mathbf{N}_{n-1} - \mathbf{N}) + k_0[(n+1)\mathbf{N}_{n+1} - n\mathbf{N}_n] \\ &\quad + \frac{k_t}{N_A v}[(n+2)(n+1)\mathbf{N}_{n+2} - n(n-1)\mathbf{N}_n] \end{aligned} \tag{3.9}$$

where N_n is the number concentration of particles containing **n** radicals, ρ is the rate of radical capture (s^{-1}), k_0 is the rate of radical desorption (s^{-1}), k_t is the rate of the termination and v is the volume of a polymer particle.

In order to obtain analytical expressions for $\bar{n}$ from the solution of the recursion equation. Smith-Ewart model describes the time evolution of the number of particles containing **n** radicals by considering the kinetic events leading to the free radicals capture and loss within the polymer particles (Smith and Ewart, 1948). The typical Smith-Ewart's conditions are: case 1 ($\bar{n} \ll 1$): chain transfer of radicals to monomers and subsequent desorption from the particles and termination in the aqueous phase is much faster than radical absorption and propagation. Case 2 ($\bar{n} = 0.5$): instantaneous termination when a second radical enters the latex particles already containing a radical instantaneous termination occurs. Case 3 ($\bar{n} \gg 1$): when the pseudo-first-order rate coefficient for bimolecular termination is very small while termination in the aqueous phase and desorption are less important. Examples of cases 1, 2, and 3 are given by Penlidis, MacGregor, and Hamielec (1988), Huo et al. (1988), and Sajjadi and Yianneskis (2003), respectively. However, equation (3.9) has been used as the basis for much more complex analytical and numerical solutions.

3.1.2 Mesoscopic scale model

The mesoscopic scale is associated with the size of the polymer particles inside the reactor, meaning the Particle Size Distribution (PSD). The Fokker-Planck Equation (FPE) is adopted in combination with mass and energy balance equations to simulate the dynamical evolution of the PSD as a stochastic process. The following equation refers to the associated Langevin equation of the stochastic process:

$$G'(r,t) = G(r,t) + K(r,t)\frac{dW_t}{dt} \tag{3.10}$$

The growth rate model is given by:

$$G(r,t) = \frac{dr}{dt} = \frac{k_p M_{wM}}{4\pi r^2 \rho_{Pol} N_A}\bar{n}(\mathbf{x})[M]_p. \tag{3.11}$$

where G and G' are the deterministic and stochastic growth rate kernels, respectively, K is a function which determines the fluctuation of the particles size around their mean value, and dW_t is the differential update of a Wiener process. It should be noticed that equation (3.10) has the form of a standard stochastic differential equation, with G referred to as the drift coefficient, while K is called the diffusion coefficient. The higher the value of K, the higher the effect of the stochastic component in the particle's growing process. This translates into a broader particle size dispersion.

M_{wM} is the monomer molecular weight and ρ_{Pol} is the structured polymer density. The evolution of the population density function ($\eta_r(r,t)$) of the stochastic process in equation (3.10) is represented by the FPE given by (Beers, 2006):

$$\frac{\partial \eta_r(r,t)}{\partial t} = -\frac{\partial (G(r,t)\eta_r)}{\partial r} + \frac{\partial}{\partial r}\left(D(r,t)\frac{\partial \eta_r}{\partial r}\right) \text{ on } \Omega_r \tag{3.12}$$

where $D = 0.5K^2$ and $\Omega_r \in \mathbb{R}$ is the particles size domain. G and D can be interpreted as the advection and diffusion coefficients, respectively. The diffusion coefficient is a main factor that influences the predictive capabilities of the FPE to fit the PSD obtained from experimental results. In general, it is a function of the particle size and time, but following the approach by Hosseini, Bouaswaig, and Engell (2013), it is chosen here as $D = D(r)$, only depending on the particle radius.

The initial condition of the FPE is given by a normal distribution that represents the initial PSD of the seeds inside the reactor, as follows:

$$\eta_r(r, t=0) = \eta_{r_0} = \frac{1}{\sqrt{2\pi}\sigma_{r_0}} \exp\left(-\frac{(r-\bar{r}_0)^2}{2\sigma_{r_0}^2}\right) \tag{3.13}$$

where $\bar{r}_0$ and σ_{r_0} are the mean value and the standard deviation of the PSD of the seeds, respectively. Neumann type boundary conditions are defined at the left and right sides of Ω_r, that is at the boundaries $\partial\Omega_r$, to preserve the total amount of the particles inside the reactor over the whole simulation time, as follows:

$$\frac{\partial \eta_r}{\partial r} = 0 \text{ on } \partial\Omega_r \tag{3.14}$$

3.1.3 Microscopic scale model

In this work, $\bar{n}$ is computed by means of a microscopic model solved via a kMC simulation method instead of approximating it to the typical Smith-Ewart's limiting cases. Thus, equation (3.7) closes the problem of EP kinetics to the determination of the concentration of monomer in the particles ($[M]_p$), the number of polymer particles (N_p) and the average number of radicals per particle ($\bar{n}$), which in turn depends on the processes of radical capture, radical desorption, radical generation, chain transfer and radical termination.

The kMC method was formally presented by Gillespie (1976) as a method for obtaining singular realizations of processes described by the Chemical Master Equation (CME). The full kMC approach repetitively generates two random numbers (r_1 and r_2) with an uniform distribution between 0 and 1 to simulate the chemical reactions stochastically: r_1 governs the time-step between reaction events, denoted as τ; r_2

determines which reaction occurs at the given instant based on the reaction probabilities P_ν. The two random numbers are generated repetitively until the sum of all τ_i ($i = 1, 2, \ldots, N_\tau$) is equal or greater than a desired reaction time N_τ. The reaction events time step is defined as:

$$\tau_i = \frac{1}{a_0(\mathbf{x})} \ln\left(\frac{1}{r_1}\right) \tag{3.15}$$

where a_0 is the total rate defined as $a_0 = \sum_{\nu=1}^{m} a_\nu$ and a_ν is the propensity function, or stochastic rate, of the νth reaction channel. $\mathbf{x}$ refers to the species concentration at the microscopic scale. Moreover, the reaction probabilities are defined as:

$$\sum_{\nu=1}^{\mu-1} P_\nu < r_2 < \sum_{\nu=1}^{\mu} P_\nu \tag{3.16}$$

where $\mu \in [2, m]$ is the index of the selected reaction channel and P_v is the probability of the v-th reaction channel, which is obtained based on the fraction of the total reaction rate as:

$$P_v = \frac{a_\nu}{\sum_{\nu=1}^{m} a_\nu}. \tag{3.17}$$

The kMC simulation calculates the average number of radical per particle $\bar{n}$ in a small reactor volume V_{cell} with k polymer particles and the rate of new formed polymer particles N_s, secondary particle nucleation rate. $k = 1, \ldots, \mathcal{N}_p$, where $\mathcal{N}_p = N_p V_{cell}$ the total number of particles within V_{cell}. Regarding V_{cell}, two assumptions are made: ***(i)*** it is a continuous homogeneous medium, that is, it has uniform properties throughout its volume; and ***(ii)*** it has periodic boundary conditions meaning that each particle escaping through one face of the volume will re-enter through the opposite face (boundary). This is a reasonable assumption since the aim is not to capture spatial variations but to understand the overall reaction kinetics inside the reactor.

The following six competitive events are considered in the kMC simulation (Hernández and Tauer, 2008b): ***(i)*** initiator decomposition in the aqueous phase, ***(ii)*** radical capture by polymer particles, ***(iii)*** propagation and ***(iv)*** termination by recombination reactions in the aqueous phase, ***(v)*** termination in the particle phase, and ***(vi)*** dead polymer absortion. Therefore, the $m = 6$ propensity functions $a_1, \ldots, a_6$ are defined as:

$$\text{Aqueous-phase Initiation:} \quad a_1 = k_d \| C_{[I]_{aq}} V_w N_A \| \tag{3.18}$$

$$\text{Aqueous-phase Propagation:} \quad a_2 = \frac{k_p}{N_A V_w} \| C_{[M]_w} V_w N_A \| \| C_n V_w N_A \| \tag{3.19}$$

$$\text{Aqueous-phase Termination:} \quad a_3 = \frac{k_t}{N_A V_w} \| C_n V_w N_A \| \left(\| C_n V_w N_A \| - 1 \right) \tag{3.20}$$

$$\text{Living polymer absorption:} \quad a_4 = \frac{k_c}{N_p N_A V_w} \| C_n V_w N_A \| N_p \tag{3.21}$$

$$\text{Dead polymer absorption:} \quad a_5 = \frac{k_c}{N_p N_A V_w} \| C_{[P]} V_w N_A \| \tag{3.22}$$

$$\text{Termination in particles:} \quad a_6 = \max \left[0, \frac{6 k_t n (n-1)}{\pi N_A d_p^3} \right] \tag{3.23}$$

where $C_{[I]_{aq}}$, $C_{[M]_w}$, C_n, and $C_{[P]}$ are initiator concentration, monomer concentration, radical concentration, and polymer concentration at the microscopic scale, respectively; $V_w = (1 - \Phi_o) V_{cell}$ is the aqueous phase volume in cm^3; and $\| x \|$ means the nearest integer to x. Regarding equation (3.23), since this is a microscopic approach to the reactions taking place inside a single particle, $\bar{n}$ cannot be used. It is therefore necessary to use the actual number of radicals n in the particle k considered to execute this event. While the microscopic approach differs from the standard macroscopic approach, both of them are equivalent when a large number of individual particles are sampled according to the chemical master equation (Gillespie, 1977). Different research groups working on polymer reaction engineering have already recognized the benefits of implementing stochastic models (such as kinetic Monte Carlo) in emulsion polymerization (Araújo et al., 2001; Butte, Storti, and Morbidelli, 2002; Vale and McKenna, 2005; Sheibat-Othman et al., 2017; Marien et al., 2019; Zetterlund and D'hooge, 2019).

Additionally, the apparent radical absorption coefficient is determined from (Hernández and Tauer, 2007):

$$k_c = 2\pi D_r N_A \left(\frac{17.95 \pi N_p d_p^4}{6} + d_p \right) \tag{3.24}$$

where D_r is the diffusion coefficient of the primary radicals.

It is remarked here that the typical method for describing the apparent radical absorption coefficient employs d_p^2 and d_p dependencies. However, d_p^2 and d_p dependencies are constrained to small changes in particle size and polymer contents (Hernández and Tauer, 2008a). Accordingly, the more general equation (3.24) used in this work captures the evolution of radical capture by changing from the d_p to the d_p^4 behavior as the polymer contents in the dispersion increases.

The event to be executed is determined by introducing the a_ν computed in equations

(3.18) - (3.23) into equations (3.15), (3.16), and (3.17). The event to be executed is given by μ in equation (3.16). Due to the random nature of r_1 and r_2 in equations (3.15) and (3.16), the kMC event execution is completely stochastic.

All the kMC simulation variables must be updated after the event selection. Defining the living **R** and dead **P** polymer chains arrays such that each entry contains the information of a single particle within V_{cell}. Additionally, a new random number $r_3 \sim \mathcal{U}(0,1)$ is generated to pick up the particle in which the event will take place, hence **R** and **P** are updated following the probabilities given by:

$$\text{Termination:} \quad \sum_{j'=1}^{j} R_{j'} > r_3 \sum_{i=1}^{k} R_i \tag{3.25}$$

$$\text{Living polymer absorption:} \quad \left(\sum_{j'=1}^{j} R_{j'} \mathbf{k}_{cR_{j'}} \right) > r_3 \left(\sum_{i=1}^{k} R_i \mathbf{k}_{cR_i} \right) \tag{3.26}$$

$$\text{Dead polymer absorption:} \quad \left(\sum_{j'=1}^{j} P_{j'} \mathbf{k}_{cD_{j'}} \right) > r_3 \left(\sum_{i=1}^{k} P_i \mathbf{k}_{cD_i} \right) \tag{3.27}$$

with

$$\mathbf{k}_{cR_{j',i}} = \mathbf{k}_{cR_{j'-1,i-1}} + k_c \frac{R_{j',i}}{\sum_{j',i=1}^{k} R_{j',i}} \tag{3.28}$$

$$\mathbf{k}_{cD_{j',i}} = \mathbf{k}_{cD_{j'-1,i-1}} + k_c \frac{P_{j',i}}{\sum_{j',i=1}^{k} P_{j',i}} \tag{3.29}$$

where j is the smallest integer that satisfies each of the above conditions.

Two events modify the number of free-radicals inside a particle k at time t, $n_{p_k}^t$, as follows: ***(i)*** if a living polymer absorption event is executed then $n_{p_k}^t = n_{p_k}^{t-\tau_i} + 1$ in the particle where the event occurs; ***(ii)*** if a termination event is executed then $n_{p_k}^t = n_{p_k}^{t-\tau_i} - 2$ in the particle where the event occurs. With τ_i given by equation (3.15). At the end of one kMC execution,

$$\bar{n} = \frac{\sum_{i=1}^{n_{events}} \sum_{k=1}^{\mathcal{N}_p} n_{p_k}^{t_i} \tau_i}{\mathcal{N}_p \sum_{i}^{n_{events}} \tau_i}. \tag{3.30}$$

The secondary nucleation rate N_s is initiated as equal to zero which implies that at the beginning of the polymerization process only P_1 particles are present. Therefore, growing chains of monomer M larger than j_{max} are considered as new polymer particles. Thus, N_s is updated at each kMC execution as follows: $N_s(k) = N_s(k-1) + R_{new}$, where R_{new} is equal to the number of growing monomer chains

that reached a chain length larger than j_{max}. At the end of the kMC execution, N_s is divided by the kMC time-length event.

The nucleation mechanism considered occurs by homogeneous nucleation as it assumes that a new particle is formed when a water-soluble oligomer reaches a critical chain length. This new formed particle becomes insoluble and precipitating as a new particle. Admittedly, heterogeneous nucleation is highly likely to occur in heterophase systems, but it has been shown, e.g., by Ocepek et al. (2017); Rocha-Botello et al. (2019); Wang et al. (2020), that this homogeneous nucleation mechanism based on a critical oligomer solubility is a decent approximation for the nucleation process.

Finally, j_{max} is a critical size for oligomer precipitation (chain collapse) resulting in the formation of a new secondary particles. Since thermal motion contributes with a fluctuating repulsive force, the length at which the chain collapses may vary around the average critical chain length (j_{max}), but for simplicity, it is assumed that all chains collapse at such critical length (Ferguson, Russell, and Gilbert, 2002).

It is highlighted that the purpose of using kMC simulation for estimating $\bar{n}$ is obtaining a more precise estimation of its value, since kMC reflects the true discrete nature of the Chemical Master Equation for scarce entities (such as radicals inside particles). Whereas other estimation methods assume the number of radicals inside a particle as a continuous variable. Furthermore, kMC also allows detecting changes in $\bar{n}$ when the environmental conditions of the particles change. Additionally, the only purpose of performing the kMC simulation is not to estimate $\bar{n}$ but N_s (rate of secondary nucleation). This last one is a microscopic variable that gives information of the quality of the produced polymer and it is hard to track either by using empirical or semiempirical models or via online measurements. By adopting a kMC simulation, a reliable estimation of N_s is obtained and the construction of the data-driven model could spot how this microscopic variable is related to both macroscopic variables and inputs of the polymerization process. This last feature presents remarkable advantages when analyzing, e.g., the process controllability or designing a control strategy to regulate N_s.

3.2 Multiscale model solution strategy

3.2.1 Mesoscopic scale: Finite Element Method

The FPE is an advection-diffusion equation which describes the evolution of a probability distribution function over time. Time-dependent or unsteady advection-diffusion problems combines both parabolic and hyperbolic characteristics of the PDEs. Advection-diffusion type problems possess hyperbolic characteristics due to the appearance of the advection term, which yields a solution traveling into the direction affected by the advection coefficient. If the advection part goes to zero, a pure diffusion equation arises and the problem becomes parabolic, which means

that the solution will not travel but spread in all directions over the spatial domain. Therefore, solution procedures for advection-dominated problems should differ from those of either advection or diffusion dominated nature.

In this work, the Finite Element Method (FEM) is adopted to numerically solve the FPE formulation to describe the PSD of the emulsion polymerization process. The first step is the derivation of the weak form of equation (3.12).

Assuming that $t_f > 0$ is the final simulation time (referred as reaction time as well) and $\eta_{r_0} \in \mathcal{L}^2(\Omega_r)$. Using the standard notation for Sobolev spaces $\mathcal{H}^1(\Omega_r)$, $\mathcal{H}^2(\Omega_r)$, $\mathcal{H}^1((0,t_f);\mathcal{L}^2(\Omega_r))$, $\mathcal{C}^1([0,t_f];\mathcal{L}^2(\Omega_r))$ (see Flotron and Rappaz (2013)), a classical weak formulation of (3.12) consists in looking for

$$\eta_r \in \mathcal{L}^2((0,t_f);\mathcal{H}^1(\Omega_r)) \cap \mathcal{C}^0([0,T];\mathcal{L}^2(\Omega_r)) \tag{3.31}$$

such that:

$$\int_{\Omega_r} w\frac{\partial \eta_r}{\partial t}dr + \int_{\Omega_r} w\left(\frac{\partial\left(G(r,t)\eta_r\right)}{\partial r}\right)dr - \int_{\Omega_r} w\left(\frac{\partial}{\partial r}\left(D(r,t)\frac{\partial \eta_r}{\partial r}\right)\right)dr = 0, \quad \forall w \in \mathcal{V} \tag{3.32}$$

where the test functions w belongs to the space $\mathcal{V}$ of $\mathcal{H}^1(\Omega_r)$ functions and do not depend on time. $\mathcal{V}$ is the space of weighting functions w. The time dependence of η_r can be translated to the trial space $\mathcal{S}_t$, which varies as a function of time. $\mathcal{S}_t$ consists of real-valued functions η_r defined on Ω_r.

Now, integrating by parts the weak form of equation (3.12), the following is obtained:

$$\begin{aligned}\int_{\Omega_r} w\frac{\partial \eta_r}{\partial t}dr + \int_{\Omega_r} w\left(\frac{\partial\left(G(r,t)\eta_r\right)}{\partial r}\right)dr \\ - \int_{\Omega_r}\frac{\partial w}{\partial r}\left(D(r,t)\frac{\partial \eta_r}{\partial r}\right)dr + \int_{\partial\Omega_r} w\left(\frac{\partial \eta_r}{\partial r}\cdot n\right)d\Gamma = 0\end{aligned} \tag{3.33}$$

In a compact notation, equation (3.33) reads:

$$\begin{aligned}(w,\eta_{r_t}) + a(w,\eta_r) + l(w) = 0 \\ (w,\eta_r(r,0)) = (w,\eta_{r_0})\end{aligned} \tag{3.34}$$

with:

$$(w, \eta_{r_t}) = \int_{\Omega_r} w \frac{\partial \eta_r}{\partial t} dr \tag{3.35}$$

$$a(w, \eta_r) = \int_{\Omega_r} w \left(\frac{\partial \left(G(r,t) \eta_r \right)}{\partial r} \right) dr - \int_{\Omega_r} \frac{\partial w}{\partial r} \left(D(r,t) \frac{\partial \eta_r}{\partial r} \right) dr \tag{3.36}$$

$$l(w) = \int_{\partial\Omega_r} w \left(\frac{\partial \eta_r}{\partial r} \cdot n \right) d\Gamma \tag{3.37}$$

The spatial discretization of the unsteady advection-diffusion equation by means of the Galerkin approach consists of defining two finite dimensional spaces $\mathcal{S}^h \in \mathcal{H}^1(\Omega_r)$ and $\mathcal{V}^h \in \mathcal{H}^1(\Omega_r)$ as subsets of $\mathcal{S}$ and $\mathcal{V}$. The so-called semi-discrete Galerkin formulation is obtained by restricting form (3.33) to the above finite dimensional spaces, namely, for any $t \in [0, t_f]$ find $\eta_r^h \in \mathcal{S}_t^h$ such that for all $w^h \in \mathcal{V}^h$,

$$\begin{aligned} &(w^h, \eta_{r_t}^h) + a(w^h, \eta_r^h) - l(w^h) = 0, \quad \forall w^h \in \mathcal{V}^h \\ &(w^h, \eta_r^h(r,0)) = (w^h, \eta_{r_0}) \end{aligned} \tag{3.38}$$

At this point, Ω_r must be seen as discretized into n_{el} elements Ω_r^e, with $1 \leq e \leq n_{el}$. As an index rule, A and B are used to represent global node numbers in the finite element mesh: $1 \leq A, B \leq n_{np}$. The system of ODEs is then obtained. Recall that the time dependence of the solution $\eta_r^h(r,t)$ is taken into account by the time dependency of the nodal values of the unknowns $\eta_{r_A} = \eta_{r_A}(t)$. The approximation $\eta_r^h(t)$ can be written as:

$$\eta_r^h(r,t) = \sum_{A \in \mathcal{N}} N_A(r) \eta_{r\,A}(t) \tag{3.39}$$

where $\mathcal{N} = \{1, 2, \ldots, n_{np}\}$ denotes the set of global node numbers in the finite element mesh and N_A is the shape function (piecewise polynomial) associated with node A. As standard in Galerkin approximation, the arbitrary test functions w are interpolated by the same shape functions.

Finally, the usual assembly process delivers the semi-discrete system of ordinary differential equations (Wriggers, 2008; Zienkiewicz, Taylor, and Zhu, 2013):

$$\mathbf{M}\dot{\boldsymbol{\eta}}_r + (\mathbf{C}(t) + \mathbf{K})\boldsymbol{\eta}_r = \mathbf{0} \tag{3.40}$$

where $\boldsymbol{\eta}_r$ is the vector of the unknowns and $\dot{\boldsymbol{\eta}}_r$ their time derivatives. $\mathbf{M}$, $\mathbf{C}$, and $\mathbf{K}$ are the consistent mass matrix, the advection matrix, and the diffusion matrix, respectively. These matrices are obtained by topological assembly of elements contribution

as follows:

$$\begin{aligned} \mathbf{M} &= \mathop{\mathrm{A}}_{e}\mathbf{M}^{e} & M^{e}_{ab} &= \int_{\Omega^{e}_{r}} N_a N_b dr \\ \mathbf{C}(t) &= \mathop{\mathrm{A}}_{e}\mathbf{C}^{e} & C^{e}_{ab} &= \int_{\Omega^{e}_{r}} N_a (G(r,t)\cdot\nabla N_b) dr \\ \mathbf{K} &= \mathop{\mathrm{A}}_{e}\mathbf{K}^{e} & K^{e}_{ab} &= \int_{\Omega^{e}_{r}} \nabla N_a \cdot (D(r)\nabla N_b) dr \end{aligned} \tag{3.41}$$

where A denotes the assembly operator, $1 \leq a, b \leq n_{en}$ and n_{en} is the number of element nodes.

If the standard Galerkin method is adopted, the time-marching schemes should only involve first time derivatives of the unknowns. One of the most popular methods for time discretization are the so-called Crank-Nicholson scheme (trapezoidal rule) given by:

$$\mathbf{M}\frac{\Delta\boldsymbol{\eta}_r}{\Delta t} + \frac{1}{2}\left[(\mathbf{C}(t+\Delta t)+\mathbf{K})\boldsymbol{\eta}_r(t+\Delta t)\right] + \left(1-\frac{1}{2}\right)\left[(\mathbf{C}(t)+\mathbf{K})\boldsymbol{\eta}_r(t)\right] = 0 \tag{3.42}$$

which is second-order accurate in time.

The Galerkin approximation for solving advection-diffusion problems as the FPE given by equation (3.12) loses its best approximation property when the non-symmetric convection operator ($\mathbf{C}$ in equation (3.40)) dominates the diffusion operator ($\mathbf{K}$ in equation (3.40)) in the transport equation, and, consequently, spurious node-to-node oscillations appear. To avoid this occurrence, the mesh discretization step size should be related to advective-diffusive features of equation (3.12). A practical test for verifying the accurateness of the numerical solution obtained with the Garlerkin approximation is offered by the Péclet number:

$$Pe = \frac{\tilde{G}\Delta r}{\tilde{D}} \tag{3.43}$$

where $\tilde{G}$ and $\tilde{D}$ are measures of $G(r,t)$ and $D(r)$, respectively, and Δr refers to the spatial step size (Donea and Huerta, 2003a). If Pe is large (i.e., $Pe > 1$), the problem becomes advection dominated and the Galerkin approach leads to inaccurate solutions represented by non-physical oscillations.

3.2.2 Macroscopic scale: time-integration of the ODEs set

The macroscopic scale dynamics are governed by the set of ODEs presented in equations (3.2) - (3.6). This set of ODEs have to be solved numerically at each gauss integration point regarding to the FEM spatial discretization in the mesoscale, in which the growth kernel ($G(r,t)$) is evaluated and linked to the macroscopic states.

The set of ODEs from equations (3.2) - (3.6) leads in general to an initial value problem of the form which can be formally written as:

$$\dot{\mathbf{x}}(t) = f(\mathbf{x}, r, \bar{n}, t) \qquad \text{with} \qquad \mathbf{x}(0) = \mathbf{x}_0 \tag{3.44}$$

Adopting as integration scheme a generalized midpoint rule

$$\mathbf{x} = \mathbf{x}_n + \Delta t f(\mathbf{x}_{n+\lambda}) \tag{3.45}$$

yields an equation for the variables $\mathbf{x}$ at time t depending upon quantities at time t_n. Defining $\mathbf{x}_{n+\lambda} = \lambda\mathbf{x} + (1-\lambda)\mathbf{x}_n$, and choosing $\lambda = 1/2$, the trapezoidal rule is obtained.

It is convenient to preserve the local character of the macroscopic states within each element Ω_r^e of the FEM discretization scheme. Then we have here the case of a time-dependent gauss point coupled problem (Wriggers, 2008). This idea of the integration algorithm has been extensively adopted for the solution of general elasto-plastic material deformation problems, see e.g. (Simo, 1998; Souza Neto, Owen, and Periae, 2008). Investigations regarding the consistency, stability, and accuracy of the solution algorithm were already performed, see e.g. (Simo, 1998). Consistency and stability are essential properties for establishing convergence of the numerical solution for arbitrary small time steps. Figure 3.2 shows a schematic description of the algorithm for the global-local iteration. To guarantee the accuracy of the numerical approximation, it is required the convergence of the mesoscopic scale. That is, a global iteration must be performed such that $\|\hat{\eta}_{r_{i+1}} - \hat{\eta}_{r_i}\| < tol$, where $\hat{\eta}_{r_i}$ and $\hat{\eta}_{r_{i+1}}$ are Newton-Raphson approximations of η_r at iteration i and $i+1$, respectively. If $\|\hat{\eta}_{r_{i+1}} - \hat{\eta}_{r_i}\| < tol$, then $\eta_r(t) \approx \hat{\eta}_{r_{i+1}}$ and the time is increased by Δt. $\mathbf{x}_i^g$ and $\hat{\mathbf{x}}_i^g$ are, respectively, the value of the macroscopic and microscopic state variables defined at the gauss point and their numerical approximation at the Newton-Raphson i iteration. It is important to remark that the local-global algorithm presented in Figure 3.2 highlights the element-wise definition of the multiscale problem. That is, the full multiscale problem is solved in each individual element of the discretized domain and then all is assembled to reconstruct the full PSD.

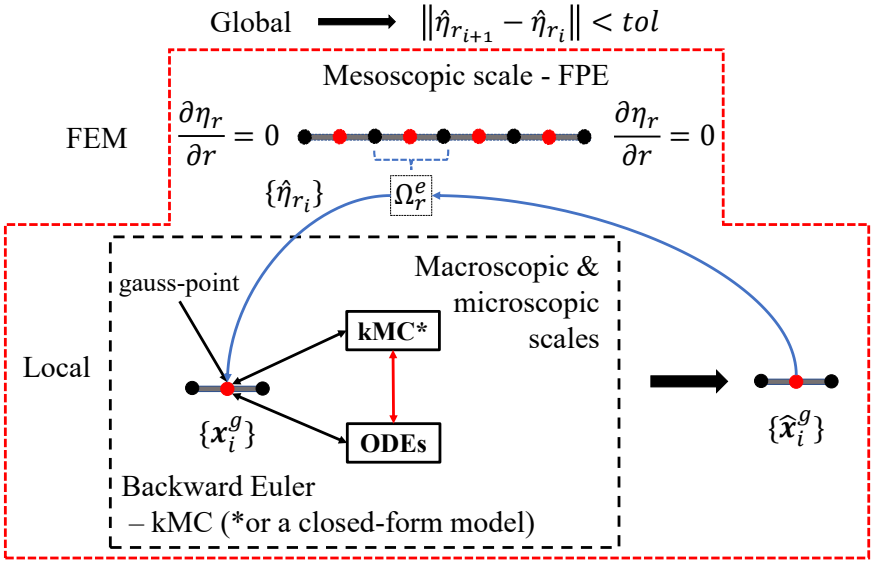

FIGURE 3.2: Algorithm for the local-global integration.

3.2.3 Microscopic scale: kinetic Monte Carlo algorithm

The probability that the system is in a particular state or configuration can be described by the CME given the stochastic nature of processes taking place at fine-scales. While the solution of the CME can be obtained using traditional numerical methods for solving ODEs, the challenge of finding a solution lies on the number of states that need to be evaluated. For systems with even a relatively small size, the CME cannot be solved since the number of possible states is prohibitively large (Gillespie, 2007). This imposes a limitation towards the direct application of the CME to obtain an estimate of system states.

The kMC method, also known as Stochastic Simulation Algorithm (SSA), was formally presented by Gillespie (1976) as a method for obtaining singular realizations of processes described by the Chemical Master Equation (CME). Due to the stochastic nature of the kMC method used to describe the evolution of the microscopic states, the results obtained from the simulations could be different. Particularly if the simulation time at this scale becomes large (up to some seconds). This would induce considerable fluctuations in the system state trajectories. One alternative to reduce such fluctuations is to use the kMC to simulate events in the order of femto to nano seconds. The second alternative is to run the kMC algorithm not only once but several times. Then taking the average among system states realizations until algorithm fluctuations stabilizes. Later approach has been used as an effective technique dealing with kMC stochasticity, see, e.g., Chaffart, Rasoulian, and Ricardez-Sandoval (2016); Kimaev and Ricardez-Sandoval (2017). This averaging process is a kind of coarse-grained methodology in which the information of one microscopic variable is propagated in a bottom-up information exchange procedure to the coarse scale (Chatterjee and Vlachos, 2006). Both approximations were explored to update

coarser scales in the EP process. However, it was the second one that presented convergence results. The number of kMC execution producing acceptable fluctuations is determined iteratively. Thus, at the beginning, the kMC algorithm is executed 5 times each time that the microscopic scale is triggered and the number of iterations is increased by 5 until it reaches 100. Then, both macro- and meso-scales are updated with an average scenario value for both $\bar{n}$ and N_s. It was noticed that up to 40 kMC executions kMC fluctuations have significant effect on the macroscopic states, but after this value that effect is almost neglectable. Consequently, 50 kMC executions are chosen to perform all the multiscale simulations.

Scales updating are determined by two triggers: ***i.*** maximum change of monomer concentration and ***ii.*** maximum change of the particle size. Any of the triggers is activated when the monomer concentration or the mean particle size change more than 5% from one simulation time to another. Then, the kMC simulations are executed. A maximum simulation time is established and a discretization through the simulation time is carried out. The time step is determined by the rate of change of the state variables in both macro- and meso-scales, e.g., if $\Delta x_i = x_i(t) - x_i(t-1) > tol$, time step is equal to δt, otherwise, the time step is equal to $\delta t/10$. Where x_i is a state variable on either macro- or meso-scales. Once macro- and meso-scales are executed, microscopic scale is executed as well and macro- and meso-scales parameters are updated. At the beginning, all process parameters for macro- and meso-scales should be settled at their initial conditions.

One characteristic of the kMC simulation is that it is cumulative in time. That is, if the kMC simulation time is very large, the number of executed events becomes very large too. This imposes a computational limitation and a restriction in the maximum process simulation time that could be simulated with the kMC method. In this work, two-temporal conditions are established, one for the maximum time step in the macro- and meso-scales and another one for the maximum simulation time in the microscopic scale. At the macro- and meso-scales, the maximum allowed time step is 100 s. While, at the microscopic scale, the maximum kMC simulation allowed time is 50 s. Because of the kMC simulation time is fixed in 50 s, the values of $\bar{n}$ and N_s are extrapolated to the total macro- and meso-scales simulation time step.

The flowchart of the kMC algorithm is presented in Figure 3.3. Additionally, it illustrated how each scale takes part in the simulation. In the right hand side of the Figure, the kMC algorithm is detailed.

3.3 Multiscale model simulation results

3.3.1 Kinetic and thermodynamic multiscale model parameters

Parameters values used in the simulation are reported in Tables 3.2 - 3.5. Table 3.2 summarizes the kinetic and thermodynamic parameters related with both macro-

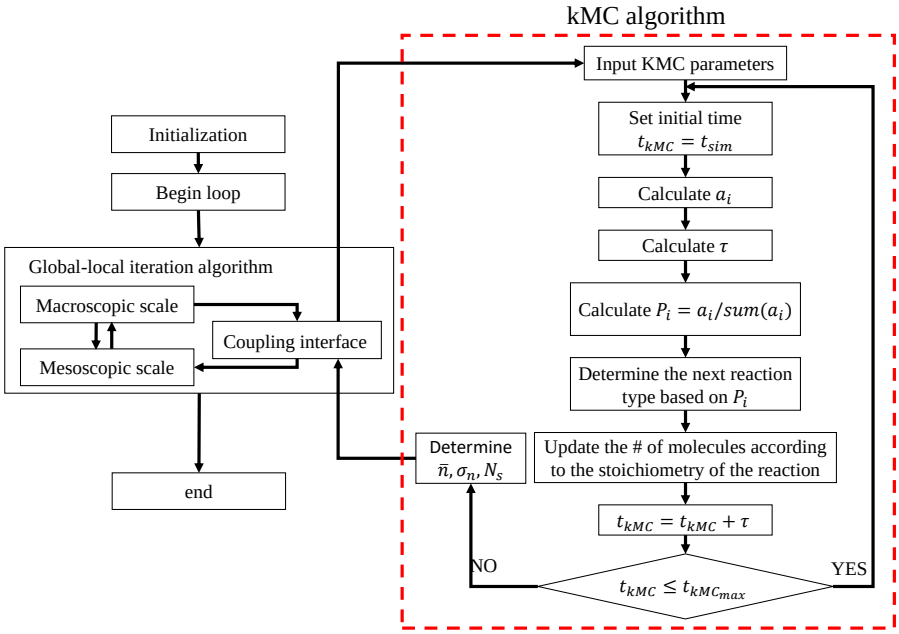

FIGURE 3.3: Flowchart of the kMC algorithm.

and meso-scales. Table 3.3 shows reactor input feed flows. Table 3.4 presents the initial conditions for the state variables at the macroscopic-scale. Table 3.5 shows values for the kinetic and thermodynamic parameters used in the kMC simulation. From Table 3.5, it is noticed that some of the kMC simulation parameters depend on the conditions at the macroscopic-scale coupling these two scales.

TABLE 3.2: Kinetic and thermodynamic parameters at macro-and meso-scales.

Parameter	Value	Units	Parameter	Value	Units
N_A	6.023×10^{23}	molecules/mol	$C_{p_{P_2}}$	1.77	J/g K
ΔH_r	-87500	J/mol	C_{p_M}	1.17	J/g K
D_{rd}	100	cm	$C_{p_{P_1}}$	1.4	J/g K
M_{wM}	86.09	g/mol	d_{p_0}	100×10^{-7}	cm
M_{wI}	270.322	g	f	0.9	
ρ_w	1	g/cm^3	U	0.025	W/cm^2 K
ρ_{P_2}	1.3	g/cm^3	Φ_{Seed}	0.2	
ρ_M	0.8722	g/cm^3	Φ_{aq}	0.8	
ρ_{P_1}	1.06	g/cm^3	k_p	1.29×10^7	cm^3/mol s
C_{p_w}	4.18	J/g K	k_d	8.6×10^{-5}	s^{-1}

TABLE 3.3: Reactor feed conditions.

Parameter	Value	Units	Parameter	Value	Units
F_M	41.6667	cm^3/s	T_M	298.15	K
F_{red}	6.9444	cm^3/s	T_{red}	298.15	K
F_{ox}	6.9444	cm^3/s	T_{ox}	298.15	K

The particles size domain is defined as $\Omega_r \in [20, 150]$ nm. The total reaction time is taken as $t_f = 18000$ s. The values of $\bar{r}_0$ and σ_{r_0} for the initial condition of the PSD

TABLE 3.4: macroscopic-scale initial conditions.

Parameter	Value	Units
V	1×10^6	cm^3
Φ_{aq}	0.8	
$[I]_{aq}$	0	mol/cm^3
$[M]_p$	0	mol/cm^3
T	333.15	K
T_j	333.15	K

TABLE 3.5: Kinetic and thermodynamic parameters at the microscopic scale.

Parameter	Value	Units	Parameter	Value	Units
k_B	1.381×10^{-23}	J/K	k_t	1.13×10^{10}	1/mol s
V_{cell}	1×10^{-14}	l	μ_w	0.355	cP
Φ_p	$1 - \Phi_{aq}$		V_{Mr}	0.046	l/mol
d_{p_0}	d_p	nm	M_{Mr}	96.16	g/mol
$[M]_{aq}$	$[M]_{aq}^{sat}$	mol/l	V_{Mm}	0.075	l/mol
F_M	$F_M \rho_M / M_{wM} V$	mol/l s	M_{Mm}	86.09	g/mol
F_I	$F_I \rho_w / M_{wI} V$		j_{max}	18	
$[I]_0$	$[I]_{aq}$	mol/l	d_r	0.526	nm
$[I]_{Feed}$	1×10^{-3}	mol/l	m_r	0.664	g

were taken as 50 nm and 5 nm, respectively.

3.3.2 Simulation results for the process nominal conditions

The flowchart of the algorithm proposed in this work to solve the multiscale model for the EP process is presented in Figure 3.4.

Simulations were carried out in a 2.50 GHz Intel Core i7 − 3537U with 8GB RAM. Multiscale simulation based on the FPE takes an average of 5 h to simulate the 5 h of the polymerization process.

Figure 3.5 shows the macroscopic-states trajectories. Three simulations were run to show the stochastic effect at the microscopic scale. V, Φ_{aq} and $[I]_{aq}$ match for all three simulations because they are not directly coupled with the microscopic state variables. Figure 3.5 shows the three different trajectories obtained for $[M]_p$ and T. From the Figure, it is observed how every update in $\bar{n}_{\bar{r}}$ implies a jump in both $[M]_p$ and T states trajectories. It is also observed that each simulation follows a different trajectory because of the stochastic evolution of $\bar{n}_{\bar{r}}$.

From Figure 3.5, it is observed that $[M]_p$ stabilizes faster than the other macroscopic state variables, implying that the monomer is consumed at a high rate. Thus, the polymer particles are effectively produced. An evidence for such affirmation is that $[M]_p$ profile does not have large changes and $[M]_p$ values are within a bounded region over the simulation time. The jumps in each $[M]_p$ trajectory are due to the $\bar{n}$ stochastic updating. Another evidence of the polymerization success is the fact that

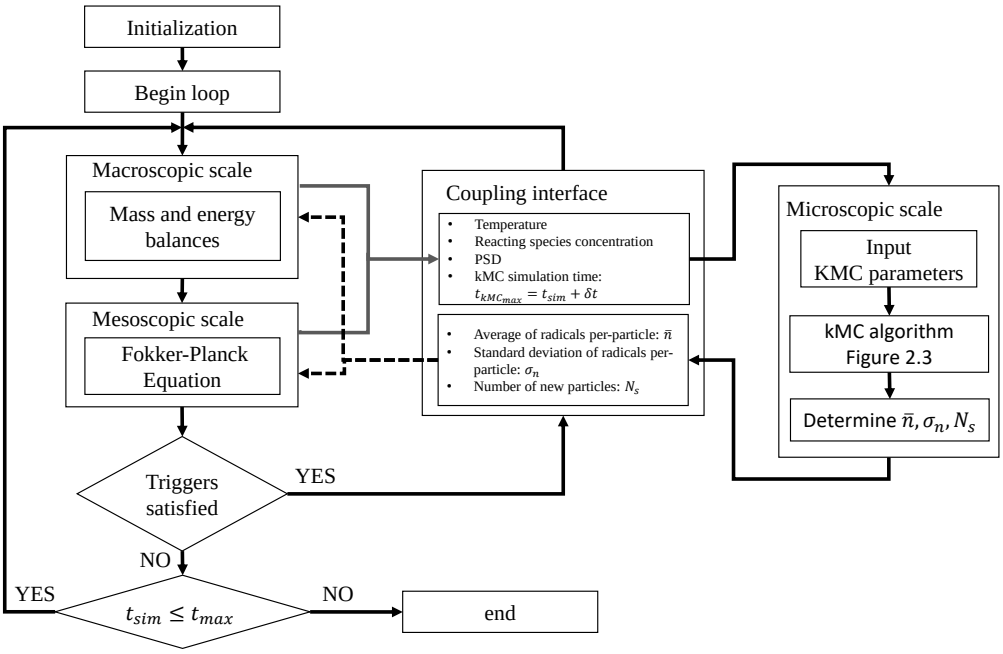

FIGURE 3.4: Multiscale algorithm for the emulsion polymerization model solution.

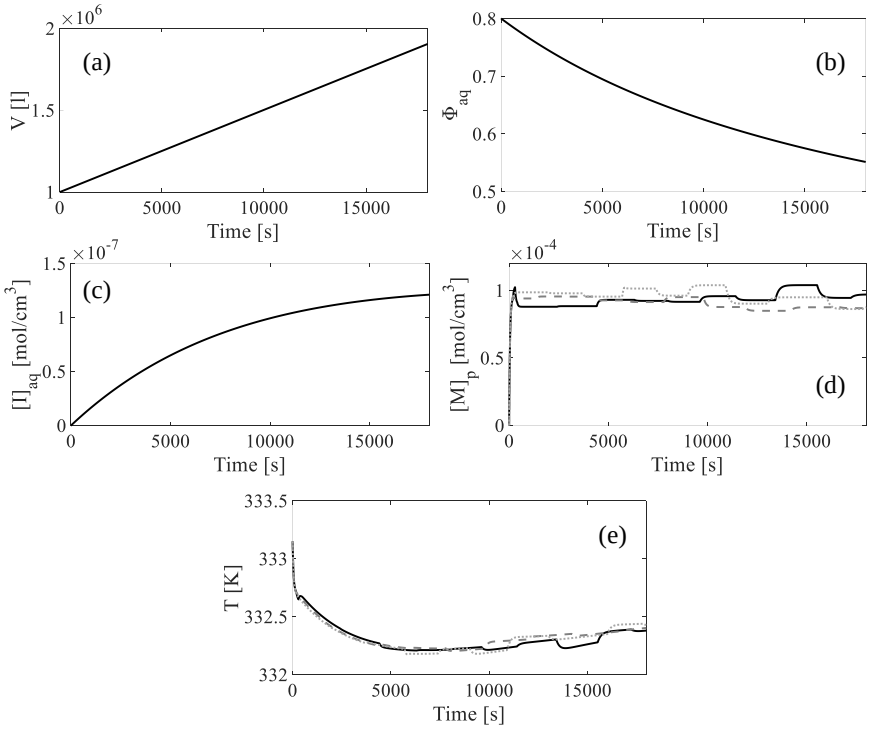

FIGURE 3.5: Macroscopic states trajectories: (a) V the volume of the reactor, (b) Φ_{aq} water volume fraction, (c) $[I]_{aq}$ initiator concentration in the aqueous phase, (d) $[M]_p$ the monomer concentration in the polymer phase, and (e) T the reactor temperature.

the Φ_{aq} is a decreasing function of time which implies that the dissolved medium has been replaced for new polymeric material. Additionally, from Figure 3.5, it is possible to observe that the $[I]_{aq}$ tends to stabilize as time proceeds, which means that the initiator has been consumed as a result of the chemical reaction with the monomer particles.

Figure 3.6 shows the evolution of the microscopic states. From Figure 3.6, it is observed that every $\bar{n}_{\bar{r}}$ update occurs randomly in time. This is because the microscopic state simulation is triggered based on the macro- and meso-scopic scales conditions which are different for every simulation. Notwithstanding the stochastic nature of micro-states evolution, for each of the three simulations the value of $\bar{n}_{\bar{r}}$ remains bounded.

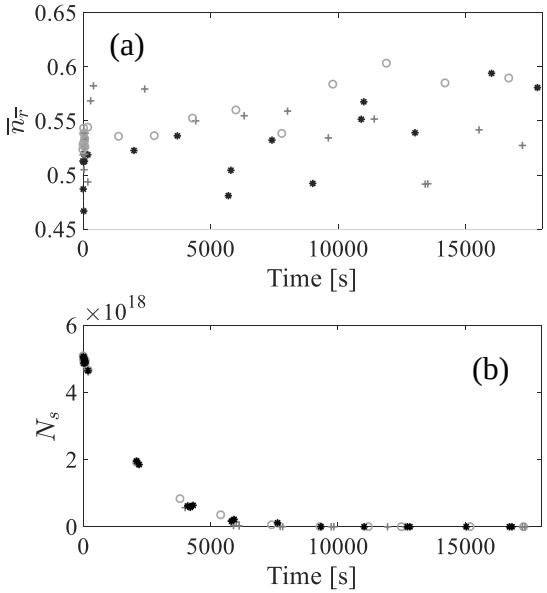

FIGURE 3.6: Microscopic states trajectories: (a) $\bar{n}_r$ the average number of the free-radicals and (b) N_s the secondary nucleation rate.

Something noteworthy from Figure 3.6 is that the process was in a Smith-Ewart II type condition during the considered simulation time due to the fact that the average number of free radicals per particle remained close to 0.5. On the other hand, from Figure 3.6, it is possible to observe that secondary nucleation rate over the first hour and a half of the simulation time. This implies that new polymer particles of the added monomer M appeared, which is not desirable since the final end-product characteristics would deteriorate. However, because of the multiscale model structure, the microscopic scale is linked with the macroscopic scale. Therefore, one could take advantage of this coupling between scales to implement an optimization/control strategy for minimizing the secondary nucleation rate over the whole process trajectory. Precisely, one of the major challenges in the production of structured polymers is minimizing the secondary nucleation, which becomes more critical if the process starts with an adverse condition as it is the case presented here.

Figure 3.7 shows the initial (solid line) and final (dashed line) PSD of the polymer particles. Figure 3.7 shows that if a constant value for D is adopted, the PSD evolution over time preserves the Gaussian distribution shape of the initial condition. That is, the polymer particles size spreads symmetrically with respect to its mean value. From Figure 3.7, it is also seen that the dynamical evolution of the PSD does not present an appreciable sensitivity with respect to the stochastic fluctuations in $\bar{n}$.

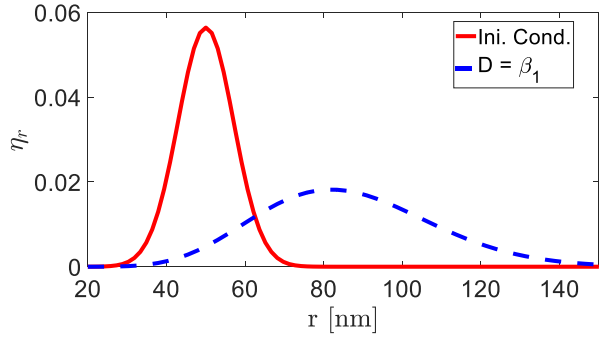

FIGURE 3.7: PSD: initial condition for the FPE (solid line). Final condition for the FPE with $D = 2.5 \times 10^{-10}$ nm^2/s (dashed line).

It is remarked that all above simulations were performed by adopting a constant vale for the diffusion parameter D. However, it is well known that the shape of the final PSD in an emulsion polymerization process tends to be skew-normal rather than gaussian (Hosseini, Bouaswaig, and Engell, 2012). Hosseini, Bouaswaig, and Engell (2013) proposed different dependencies of the diffusion coefficient (linear, quadratic, and exponential) on the particles size to increase the flexibility of the FPE in capturing the shape of the experimental PSD. Here, we will take the same idea and propose the following expression for the diffusion coefficient:

$$D(r) \quad = \quad \beta_j \, r^k \tag{3.46}$$

with $j = 1, 2, 3$ and $k = 0, 2, 4$. It is pointed out here that the choice of the power of $k = 4$ dependency, instead of an exponential expression, is due to the fact that the exponential dependency makes the bigger particles grow too faster. But the real picture is that should exist an upper bound value which limits the particles growing rate. The value of the parameters were adapted such that the diffusion coefficient belongs to the same scale magnitude within the range in which the particles population is concentrated over the whole simulation domain, that is, approximately between 20 nm and 150 nm. Additionally, β_j units must be consistent such that $D(r)$ has units of nm^2/s. The values of the β_j parameters are summarized in Table 3.6.

On the other hand, as was already mentioned, attention must be paid to the stability of the numerical method to consistently solve the FPE. That means, Pe number should remain small (it is suggested lower than 1) to guarantee a good performance

TABLE 3.6: β_j parameters of the diffusion coefficients.

Parameter	Value	Units
β_1	2.5×10^{-10}	nm^2/s
β_2	2.5×10^{-7}	$1/s$
β_3	2.5×10^{-2}	$1/nm^2\ s$

of the numerical scheme. To determine the mesh size as a function of the space coordinates within the spatial domain, the following procedure is adopted: ***i.*** $G(r,t)$ and $D(r)$ are computed offline. It is remarked here that because of the value of $G(r,t)$ and $D(r)$ do not depend on η_r, they can be computed by considering only the set of ODEs at the macroscopic scale coupled with the closed-form at the microscopic scale. ***ii.*** A coarse mesh is created by dividing Ω_r into $e = 100$ uniform elements Ω_r^e. ***iii.*** The characteristic elements size Δr is given as function of both $G(r,t)$ and $D(r)$:

$$\Delta r\Big|_{\Omega_r^e} = \min\left\{\frac{D(r_{e/2})}{G(r_{e/2},t)}\bar{Pe}, 1\right\} \tag{3.47}$$

with $r_{e/2}$ the value of r at the middle point of each element. Therefore, a local remeshing step is performed by establishing a maximum value of Pe equal to $\bar{Pe} = 0.01$.

Figure 3.8 shows the final PSD for the different cases of D dependency of r. It is observed in the Figure that the PSD evolves from a gaussian initial condition to a final gaussian condition when D is taken as a constant value. However, it is possible to observed that the system evolves from a gaussian initial condition towards a skew-normal distribution once D is defined such that a dependency of r is specified. That result matches with the experimental result presented by Hosseini, Bouaswaig, and Engell (2013) in which, at the end of the process time, it is expected to have a larger diffusion for the bigger particles sizes (long right-tale or right-skewness). Furthermore, from Figure 3.8, it is noticed that a longer right-tail is obtained if the order of the D dependency is increased from the power of 2 to the power of 4. In order to make that result more evident, the value of the first three moments of the final PSD are summarized in Table 3.7. It is the value of the skewness that determines in which side of the distribution the tail is larger and how large is compared to a gaussian distribution. In this case the tail is larger at the right hand side of the distribution meaning that at the end of the reaction there are more polymer particles of bigger sizes than polymer particles of smaller sizes.

3.3.3 Growth kernel and diffusion parameter analysis

Regarding the the growth kernel (G), it is remarked that the its rate of change over time is determined by the rate of change of $[M]_p$, which reaches its steady-state value

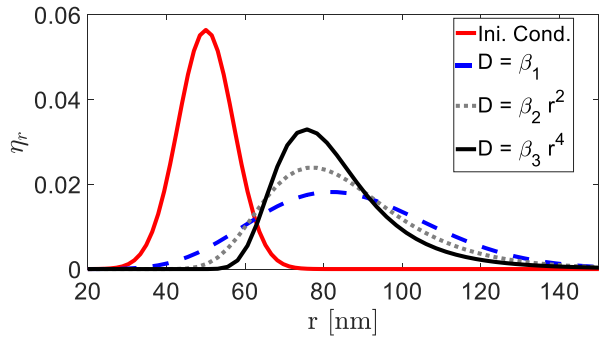

FIGURE 3.8: Final PSD for the different D dependencies of r.

TABLE 3.7: Final PSD statistical moments.

	Statistical moments		
Dependency	**Mean [nm]**	**Std. dev. [nm]**	**Skewness**
β_1	86.2987	21.9055	0
$\beta_2\ r^2$	85.3651	19.0904	1.0515
$\beta_3\ r^4$	83.8233	16.6425	1.8738

in a small time compared to the process simulation time. This causes an imperceptible change of G over time which is not capture by the performed simulations. On the other hand, regarding the particles size domain meshing, when Δr is kept constant, the Pe number is too large for the smallest values of r. This makes the numerical solution unstable and the simulation does not converge. Then any simulation result by keeping Δr constant is reported.

Figure 3.9 shows both the growth kernel (G) and diffusion coefficient (D) values over the spatial domain and the Δr and Pe which determines the numerical scheme stability. Figure 3.9a shows the chance of G over the particles size domain. It is observed that G is higher for the smallest polymer particles than for the biggest ones. This means that the smaller is the size of the polymer particles, the more they grow. In Figure 3.9b, the comparison of D values are plotted for the three proposed dependencies of the particles size. Figure 3.9c shows how the meshing rule change as function of the D values. As expected, a finer mesh is generated in the zone of the spatial domain where the advection dominates over diffusion (the region of the smallest polymer particles) and becomes coarse once the diffusion dominates over advection. Finally, the Pe number is plotted in Figure 3.9d for a constant Δr and for Δr given by equation (3.47). When Δr is kept constant, the Pe number is too large for the smallest values of r (exponential-like curves plotted in the log scale). On the other hand, when Δr varies as in equation (3.47), the Pe number equals 0.01 for the space domain portion in which $\Delta r < 1$ and then is even smaller. Only by varying Δr the numerical stability of the solution is preserved and the adopted method converged as expected.

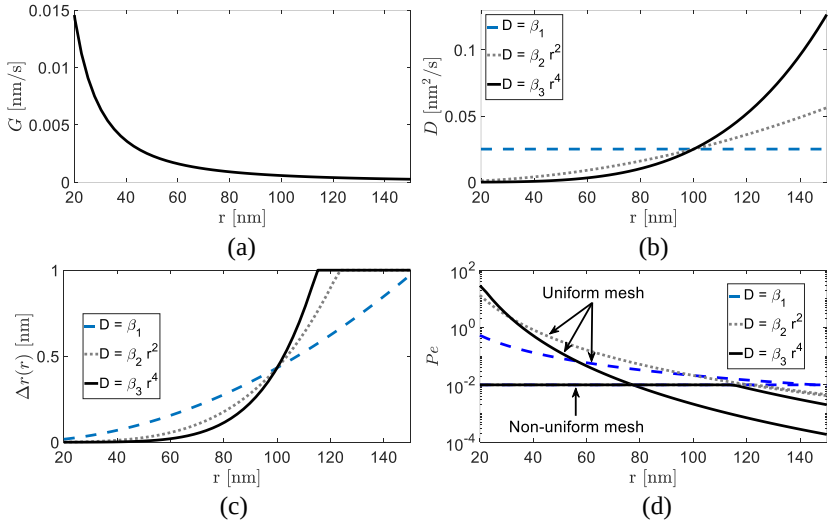

FIGURE 3.9: (a) Growth kernel G, (b) diffusion coefficient D, (c) Δr meshing rule, and (d) Pe number for both uniform and non-uniform meshes, i.e., constant and adaptive Δr, respectively.

3.4 Chapter concluding remarks

A multiscale model for describing the dynamic evolution of free-radical polymerization was successfully derived. The developed multiscale model includes the traditional macroscopic and mesoscopic dynamics of the free-radical polymerization process, and also the average number of free-radicals and secondary nucleation rate (which are important microscopic states). These two microscopic states are critical to satisfactorily obtaining structured polymer particles with the desired size and morphology.

A computational model by the adoption of the FEM was developed. Such a computational model was composed of a set of algebraic nonlinear set of equations and allowed an efficient computation of the nonlinear evolution of the multiscale model. Particularly, by adopting the FEM, it was possible to accurately capture the evolution of the PSD taking several nonlinear expressions for the diffusion coefficient. Additionally, the multiscale problem was defined in an element-wise fashion allowing the solution of both macroscopic and microscopic scales locally within each element. Then, the local solution was assembled in the usual FEM way by saving a lot of effort in the coding procedure. The robustness and versatility of the FEM-based numerical scheme was successfully through several simulations.

Chapter 4

Multiscale model order reduction

Abstract

In this chapter, on the one hand, mesoscopic-scale representation of the dispersed media is carried out by using Variance Algebra concepts for describing the stochastic nature of particle growth. On the other hand, to deal with the curse of dimensionality, the procedure based on the statistical modeling approach introduced by (Hernandez, 2018) is adopted to derive a closed-form model for the microscopic scale. When the obtained reduced-order models at the mesoscopic and at the microscopic scales are assembled with the model at the macroscopic scale, a convenient representation of the system is obtained from the control viewpoint. This because the reduce-order model can be written as a set of ODEs representing a nonlinear dynamical system with a direct realization of the outputs of interest (e.g., the microscopic states). Therefore, the obtained model is suitable for being used in optimization/control tasks. The main novelty of this chapter is the implementation of the tools described above to develop the reduced-order model for the multiscale model presented in Chapter 3.

4.1 Reduced-order model for the mesoscopic scale: Variance Algebra approach

4.1.1 Reduced-order model derivation

The mesoscopic scale refers to the size of polymer particles inside the reactor, described by the Particle Size Distribution (PSD). Frequently, predictions of the distribution of the particle sizes in Emulsion Polymerization (EP) (e.g. for online monitoring, optimization, and control of latex properties) are carried out by formulating Population Balance Equation (PBE) based models (Puschke and Mitsos, 2016; Gil, Vargas, and Corriou, 2016; Tjiam and Gomes, 2014; Hosseini, Oshaghi, and Engell, 2013; Dokucu, Park, and Doyle, 2008b). Typically, a PBE is composed of the following terms: the distribution (also called the population density), which

is a function of the internal coordinates; the growth/dissolution rate, and the creation/depletion rate. Internal coordinates usually are the characteristic length, volume, or mass, but it can also be age, composition, and other characteristics of an entity in a distribution (Gunawan, Fusman, and Braatz, 2004). The creation/depletion rate term in the PBE represents phenomena such as nucleation, aggregation, agglomeration, breakage, attrition, and material leaving or entering the system can be a function of other variables including the distribution. Consequently, a highly nonlinear function of their arguments should be considered, which typically involves integrals. Therefore, the PBE is a hyperbolic-type integrodifferential partial equation. The solution of this type of Partial Differential Equations (PDEs) is expected to be of the shock-wave type imposing the challenge of requiring high-performance numerical resolution schemes for its solution (Bouaswaig and Engell, 2010).

As reported by Hosseini, Bouaswaig, and Engell (2012), classical PBE models of EP are not capable of predicting the evolution of the breadth of the experimental particle size distributions correctly even when a high-resolution discretization method is used to suppress the numerical errors. Also, by re-tuning the model parameters the model predictions did not fit the experimental results which points out a structural inadequacy of the conventional deterministic growth models in describing the experimentally observed broadening phenomenon. To overcome this drawback, Hosseini, Bouaswaig, and Engell (2013) proposed two different approaches for improving the predictive capability of classical PBE. In the first approach, a stochastic extension for the PBE formulation was added to the deterministic growth kernel. This formulation augmented the deterministic particle growth kernel by including the stochastic nature of the particle growth process, resulting in the incorporation of a stochastic differential equation (Langevin equation) for polymer particle growth. Langevin equation evolves over time according to the Fokker-Planck Equation (FPE). In the second approach, the growth kernel was extracted from the characteristics of the transient experimental PSD leading to a semi-empirical growth kernel which relates the states variables of the EP process to the particle size. While the first approach accounted for the inhomogeneities of the growth process, the second one aimed to extract a semi-deterministic growth kernel from the trajectories of the characteristic curves of the transient experimental PSD. Hosseini, Bouaswaig, and Engell (2013) reported that both approaches were effective in overcoming the limitations of the original PBE models of emulsion polymerization to describe experimental results. However, the FPE-based approach resulted to be more convenient of applying when studying the dynamical evolution of a particle distinctive property (e.g., size or shape) of the population, rather than to obtain a detailed mechanistic approach (Grosso et al., 2010). The mentioned FPE-based approach has recently been used by several authors to model the evolution of crystal size distributions (Grosso et al., 2010; Tronci et al., 2011; Grosso et al., 2011; Cogoni et al., 2014).

Notwithstanding the improvements reported, the solution of the FPE is still computationally highly expensive and therefore, coupling it with a kinetic Monte Carlo (kMC) simulation (microscopic scale) could become computationally prohibitive, especially for using it in online applications for optimization and/or process control. Additionally, a rigorous derivation of expression to describe fluctuations of the particle size around the mean value (diffusion coefficient) is still missing. In order to address these two issues, Variance Algebra concepts are applied for obtaining a reduced (lower-order) model for predicting the behavior at the mesoscale. In the following, the derivation of the equations of the so-called reduced-order model for describing the mean and standard deviation of the particle size distribution is presented.

The formulation of the reduced-order model begins with the adoption of the same growth rate kernel of the polymer particles given in equation (3.11) to the FPE construction, as follows:

$$\frac{dr}{dt} = \frac{k_p M_{wM}}{4\pi r^2 \rho_{Pol} N_A} n(\mathbf{x})[M]_p, \tag{4.1}$$

where k_p is the propagation rate coefficient and M_{wM} is the monomer molecular weight, and ρ_{Pol} the structured polymer density. It is possible to assume that n is a random variable with the following properties since the number of radicals varies among particles. That is:

$$E(n) = \bar{n} \tag{4.2}$$

$$V(n) = \sigma_n^2 \tag{4.3}$$

where $E(n)$ and $V(n)$ are the mean value and the variance of n, respectively. Therefore, $\bar{n}$ is the mean value and σ_n is the standard deviation of the number of free-radicals per particle, respectively.

For a pure zero-one kinetics emulsion polymerization system it follows that:

$$\bar{n} = 0.5 \tag{4.4}$$

$$\sigma_n^2 = \frac{1}{4}\frac{N_p}{N_p - 1} \approx \frac{1}{4} \tag{4.5}$$

because N_p is generally a large number. It is also assumed that the variation of monomer concentration inside the particles is negligible.

A particle size could vary among particles, then, r is a random variable. A normal distribution is assumed, as suggested by Hosseini, Bouaswaig, and Engell (2012), as follows:

$$r = \bar{r} + \sigma_r Z_r \tag{4.6}$$

In equation (4.6), $\bar{r}$ is the mean value of a particle size, σ_r is the standard deviation of the particle radius and Z_r is a standard normal random variable ($N \sim (0,1)$) that represents the size variation among different particles, but remains constant in time for each specific particle. Therefore, the following equations are obtained:

$$r^2 = \bar{r}^2 + 2\bar{r}\sigma_r Z_r + \sigma_r^2 Z_r^2 \tag{4.7}$$

$$\frac{dr}{dt} = \frac{d\bar{r}}{dt} + \sigma_r \frac{dZ_r}{dt} + Z_r \frac{d\sigma_r}{dt} \tag{4.8}$$

Equations (4.2)-(4.8) can be grouped in a single equation as follows:

$$4\pi \left(\bar{r}^2 + 2\bar{r}\sigma_r Z_r + \sigma_r^2 Z_r^2\right) \left(\frac{d\bar{r}}{dt} + \sigma_r \frac{dZ_r}{dt} + Z_r \frac{d\sigma_r}{dt}\right) = \frac{k_p M_{wM} [M]_p}{\rho_{Pol} N_A} n \tag{4.9}$$

From equation (4.9), it is possible to take the expected value and the variance, then, by assuming that $\sigma_r \ll \bar{r}$, the dynamical evolution of the expected value of a polymer particle size is given by equation (4.10):

$$\frac{d\bar{r}}{dt} = \frac{k_p M_{wM} [M]_p}{4\pi\rho_{Pol} N_A \left(\bar{r}^2 + \sigma_r^2\right)} \bar{n} - \frac{2\bar{r}\sigma_r}{\left(\bar{r}^2 + \sigma_r^2\right)} \frac{d\sigma_r}{dt} \tag{4.10}$$

If instead of the expected value we take the variance, the following equation is obtained:

$$\begin{aligned} &2{\sigma_r}^2 \left(2\bar{r}^2 + {\sigma_r}^2\right) \left(\frac{d\bar{r}}{dt}\right)^2 + 4\bar{r}\sigma_r \left(\bar{r}^2 + 4{\sigma_r}^2\right) \frac{d\bar{r}}{dt} \frac{d\sigma_r}{dt} \\ &+ \left(\bar{r}^4 + 14\bar{r}^2{\sigma_r}^2 + 15{\sigma_r}^4\right) \left(\frac{d\sigma_r}{dt}\right)^2 = \left(\frac{k_p M w_M \left[M\right]_p \sigma_n}{4\pi\rho_{Pol} N_A}\right)^2 \end{aligned} \tag{4.11}$$

Replacing equation (4.10) and performing some additional maths, equation (4.12) is obtained which describes the dynamical evolution of the standard deviation of a polymer particle size:

$$\begin{aligned}\frac{d\sigma_r}{dt} &= -\frac{2\bar{r}\sigma_r}{\bar{r}^2+{\sigma_r}^2}\left(\bar{r}^2+2{\sigma_r}^2\left(1-\frac{\bar{r}^2}{\bar{r}^2+{\sigma_r}^2}\right)\right)\left(\frac{k_p M w_M [M]_p}{4\pi\rho_{Pol}N_A}\right)\frac{\bar{n}}{\Pi} \\ &+\left(\frac{k_p M w_M [M]_p}{4\pi\rho_{Pol}N_A}\right)\frac{\sqrt{\Psi}}{\Pi}\end{aligned} \tag{4.12}$$

with Π

$$\begin{aligned}\Pi &= \bar{r}^4+14\bar{r}^2{\sigma_r}^2+15{\sigma_r}^4+8{\sigma_r}^4\left(\frac{\bar{r}^2}{\bar{r}^2+{\sigma_r}^2}\right)\left(1+\frac{\bar{r}^2}{\bar{r}^2+{\sigma_r}^2}\right) \\ &-8{\sigma_r}^2\left(\bar{r}^2+4{\sigma_r}^2\right)\left(\frac{\bar{r}^2}{\bar{r}^2+{\sigma_r}^2}\right)\end{aligned} \tag{4.13}$$

where Ψ is given by:

$$\begin{aligned}\Psi &= \left(\frac{2\bar{r}\sigma_r}{\bar{r}^2+{\sigma_r}^2}\left(\bar{r}^2+2{\sigma_r}^2\left(1-\frac{\bar{r}^2}{\bar{r}^2+{\sigma_r}^2}\right)\right)\bar{n}\right)^2 \\ &-\left[\begin{array}{r}\bar{r}^4+14\bar{r}^2{\sigma_r}^2+15{\sigma_r}^4+8{\sigma_r}^4\left(\frac{\bar{r}^2}{\bar{r}^2+{\sigma_r}^2}\right)\left(1+\frac{\bar{r}^2}{\bar{r}^2+{\sigma_r}^2}\right) \\ -8{\sigma_r}^2\left(\bar{r}^2+4{\sigma_r}^2\right)\left(\frac{\bar{r}^2}{\bar{r}^2+{\sigma_r}^2}\right)\end{array}\right] \\ &\left(2\frac{{\sigma_r}^2}{\bar{r}^2+{\sigma_r}^2}\left(1+\frac{\bar{r}^2}{\bar{r}^2+{\sigma_r}^2}\right)\bar{n}^2-{\sigma_n}^2\right)\end{aligned} \tag{4.14}$$

Equation (4.12) can be simplified by assuming that $\sigma_r^4 \ll \bar{r}^4$, as follows:

$$\frac{d\sigma_r}{dt} \approx \frac{\left(\frac{k_p M w_M [M]_p}{4\pi\rho_{Pol}N_A\bar{r}}\right)}{\bar{r}^2+6{\sigma_r}^2}\left(\sqrt{\Xi}-\frac{2\sigma_r}{\bar{r}^2+{\sigma_r}^2}\left(\bar{r}^2+2{\sigma_r}^2\left(1-\frac{\bar{r}^2}{\bar{r}^2+{\sigma_r}^2}\right)\right)\bar{n}\right) \tag{4.15}$$

where Ξ is given by:

$$\Xi = {\sigma_n}^2\left(\bar{r}^2+6{\sigma_r}^2\right)-\Upsilon{\sigma_r}^2\bar{n}^2$$

with

$$Y = \left(1+\frac{1}{1+\frac{{\sigma_r}^2}{\bar{r}^2}}\right)\left(\frac{1+6\frac{{\sigma_r}^2}{\bar{r}^2}}{1+\frac{{\sigma_r}^2}{\bar{r}^2}}\right) - 4\left(1-\frac{\frac{{\sigma_r}^2}{\bar{r}^2}}{1+\frac{{\sigma_r}^2}{\bar{r}^2}}\left(\frac{2}{1+\frac{{\sigma_r}^2}{\bar{r}^2}}-1\right)\right)^2$$

It could be possible that under some conditions equation (4.15) has an imaginary part. The condition to obtain such imaginary part is given by the following inequality:

$$\frac{{\sigma_n}^2}{\bar{n}^2} < Y\frac{\frac{{\sigma_r}^2}{\bar{r}^2}}{\left(1+6\frac{{\sigma_r}^2}{\bar{r}^2}\right)} \tag{4.16}$$

Figure 4.1 shows a graphical representation of the condition given by equation (4.16), which corresponds to the feasible zone. The solid line represents the condition for which the right hand side of equation (4.16) equals its left hand side. Meanwhile, the unfeasible zone corresponds to the case where the right hand side of equation (4.16) lower than its left hand side. From Figure (4.1), it is possible to observe that the most critical value occurs when the ratio $sigma_r/\bar{r}$ is equal to 87%, giving a value of $\sigma_n^2/\bar{n}^2 = 0.2$. Even for this condition, if the number of free-radicals follows a binomial distribution, $\sigma_n^2/\bar{n}^2 = 0.3333$, meaning that equation (4.16) still does not have any imaginary part. Moreover, since in this work is assumed that r is normal, $\sigma_r/\bar{r} \ll 1/3$ (otherwise, it would describe particles with a negative size) and, $\sigma_r^2/\bar{r}^2 \ll 1/9$, then $\sigma_n^2/\bar{n}^2$ should be negative in order to obtain imaginary results. Therefore, the right hand side of equation (4.16) is always positive and results in real values for a normal distribution of r (i.e. lying on the feasible zone).

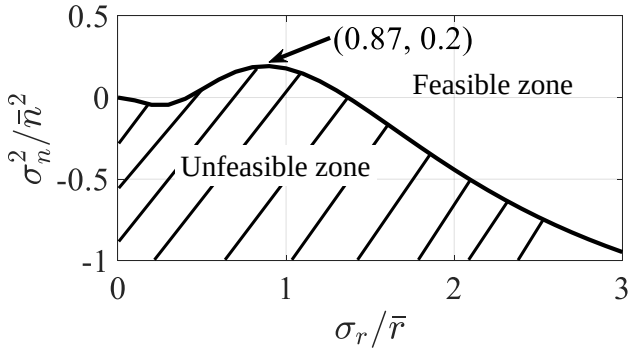

FIGURE 4.1: Graphical representation of the feasible condition given by equation 4.16 (feasible zone).

Assuming that the EP process evolves from a polydisperse condition, equations (4.10) and (4.15) are enough to describe both the mean and standard deviation of the PSD of the process. Accordingly, the developed reduced-order model at the

mesoscopic scale is composed of only two ordinary differential equations representing the mean and the standard deviation of the PSD. The main feature of this model is that it can be coupled with the macro- and micro-scopic models for obtaining a multiscale process representation.

4.1.2 Simulation results based on the reduced-order model

It is noteworthy that the first term in the right-hand side of the equation (4.10) is quite similar with the deterministic growth rate kernel given in equation (3.11); the difference is σ_r^2 in the denominator. Consequently, it is possible to appreciate that equation (4.10) describes the growth of the particle radius similar as in equation (3.10), where the second term in the right-hand side of the equation (4.10) takes into account the stochastic fluctuations in the particle growth process.

In this work, equation (4.12) is contrasted with the diffusion coefficient in equation (3.12). It is known from equations (3.10) and (3.12) that $K^2 = 2D$, where K is in units of nm$/\sqrt{s}$, while, equation (4.12) is in units of nm/s. Hence, $K^2 \approx (d\sigma_r/dt)^2 \tau_{\mathcal{M}} = 2\mathcal{D}$, where $\tau_{\mathcal{M}}$ is a characteristic time of the mesoscopic-scale and it is in units of s. Thus, equations (4.17) and (4.18) refer to the growth kernel and an expression for the dispersion coefficient in the reduced-order model, respectively.

$$\mathcal{G} = \frac{k_p M_{wM}[M]_p}{4\pi\rho_p N_A \left(\bar{r}^2 + \sigma_r^2\right)}\bar{n} - \frac{2\bar{r}\sigma_r}{\left(\bar{r}^2 + \sigma_r^2\right)}\frac{d\sigma_r}{dt} \tag{4.17}$$

$$\mathcal{D} \approx \frac{\tau_{\mathcal{M}}}{2}\left(\frac{d\sigma_r}{dt}\right)^2 \left[\frac{nm^2}{s}\right] \tag{4.18}$$

Figure 4.2 shows the dynamical evolution of both $\mathcal{G}$ and $\mathcal{D}$ for the reduced-order model. In Figure 4.2a, $\mathcal{G}$ and G, the growth kernel dynamical evolution for both the reduced-order model (solid line) and the FPE (dotted line) models are compared. From Figure 4.2a, it is seen that for both models the growth kernel is very similar, which is an expected result because the only difference in the growth kernel for both models are the σ_r^2 correction term that appears in the first term in right-hand side of equation (4.10). On the other hand, Figure 4.2b shows the dynamical evolution of the dispersion coefficient $\mathcal{D}$ for the reduced-order model (solid line) and the dispersion coefficient D for the FPE based model (dotted line), which is assumed to be constant. For the reduced-order model, the maximum value of $\mathcal{D}$ corresponds to the initial condition of the simulation which is $\mathcal{D} = 5.107 \times 10^{-5}$ nm^2/s and the minimum value of $\mathcal{D}$ corresponds to the final condition of the simulation which is $\mathcal{D} = 4.286 \times 10^{-6}$ nm^2/s. The range in which $\mathcal{D}$ varies for the reduced-order based model is about the same order of magnitude of the value that D takes in the FPE simulation for yielding similar final mean and standard deviation in particle size distribution ($D = 2.5 \times 10^{-5}$ nm^2/s). However, it is important to remark that for the reduced-order model case, $\mathcal{D}$ is a parameter that depends on a characteristic time $\tau_{\mathcal{M}}$, that

was taken as $\tau_{\mathcal{M}} = 100$ s in these simulation results which is a representative time scale of the phenomena occurring at the mesoscopic-scale.

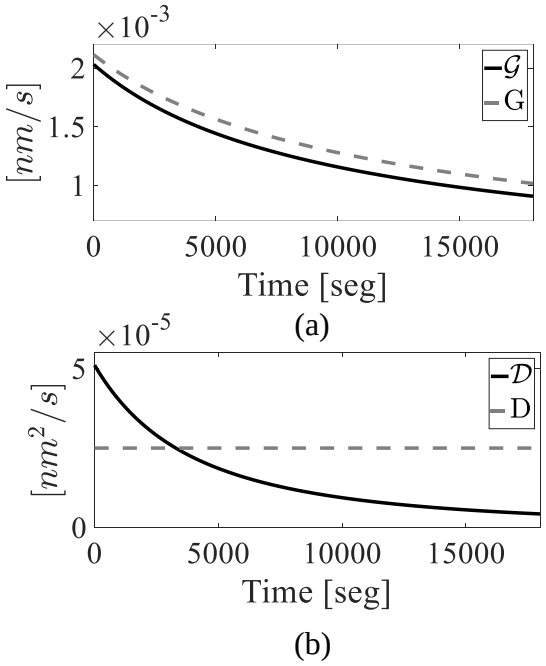

FIGURE 4.2: *(a)* Growth kernel and *(b)* dispersion coefficient: the reduced-order model (solid line), FPE (dotted line).

It is important to notice that Variance Algebra based approach might also be used to describe the dynamics of other relevant distributions in the EP system, such as molecular weight distribution, particle shape distribution, particle morphology distribution and even particle composition distribution. For the particular case of particle shape distribution for example, Tauer and Hernandez (2010) have shown that a certain shape parameter can be defined to described a wide range of particles from perfect spheres to discs to needle-like particles. The distribution of the shape parameter could be described by a mean and a standard deviation whose evolution can be tracked using two ordinary differential equations derived from Variance Algebra, using a similar approach as the one presented in this work. This would be an important contribution to the model, because radical dynamics is significantly influenced by particle shape and not only particle diameter.

Figure 4.3 shows the dynamical evolution of $\bar{r}$ (asterisk) and $\bar{r} \pm \sigma_{\bar{r}}$ (circle). $\bar{r}$ and $\bar{r} \pm \sigma_{\bar{r}}$ were overlapped with the probability density function (p.d.f.) (solid line) constructed assuming a Gaussian distribution for the polymer PSD. From Figure 4.3, it is seen that the dynamical evolution of the PSD does not present an appreciable sensitivity to the stochastic oscillation in $\bar{n}_{\bar{r}}$, i.e., there is not any visible jump neither over $\bar{r}$ nor $\sigma_{\bar{r}}$ trajectories.

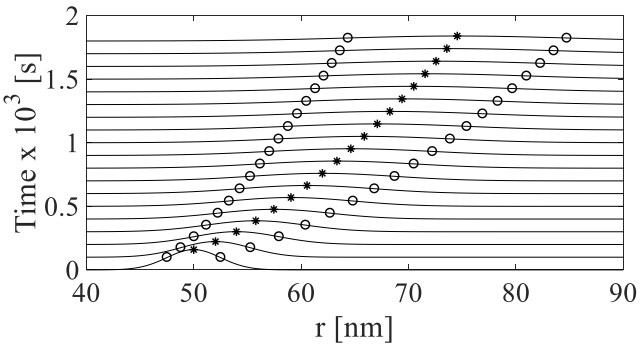

FIGURE 4.3: The reduced-order model PSD dynamical evolution: $\bar{r}$ (asterisk), $\bar{r} \pm \sigma_{\bar{r}}$ (circle) and p.d.f. (solid line).

4.2 Closed-form model for the microscopic-scale: statistical modeling approach

4.2.1 Closed-form model derivation

In this chapter, the procedure based on the statistical modeling approach introduced by Hernandez (2018) is adopted to derive a closed-form model for the microscopic scale. Compared to the traditional methods as the Analysis of Variance (ANOVA), the main advantages of this procedure are: ***i.*** no particular distribution is assumed over the data, which facilitates its application; ***ii.*** the parameters estimation can be made independently using a standard parameter identification method, and ***iii.*** the method incorporates the effect of the extreme values or outliers.

The main assumption to compute the closed-form model for the microscopic scale is that the stochastic fluctuations of the microscopic states to be approximated do not have a significant impact over the solution of the coarse scales. In other words, it is enough to take a regularized function of the microscopic states coupled with the coarse scales to describe the evolution of the system without affecting the reliability of the model.

To find a closed-form model of the microscopic states $\bar{n}$ and N_s, it is required to generate a suitable database from the kMC simulation. This database must contain as much as possible of the different conditions in which the EP process could evolve at the microscopic scale. Additionally, it is necessary to apply step by step the procedure for the statistical modeling presented by Hernandez (2018), namely: ***i.*** the transformation and standardization of the response variables and the definition of the predictor functions; ***ii.*** the selection of the next most promising factor; ***iii.*** the test of the significance of the next most promising factor; ***iv.*** the computation of the coefficient of the next most promising factor; ***v.*** the update of the standardized response variable to remove the effect of the predictor function; ***vi.*** the computation of the original model coefficients; and ***vii.*** the calculation of the performance of the model.

The closed-form model must relate the microscopic states with the macro-, mesoscopic scales or even with the system inputs which allows the employment of the model for optimization/control tasks. The method proposed by Hernandez (2018) is based on the following general statistical model used for describing a certain random response variable $\mathbf{Y}$ (e.g., $\bar{n}$ or N_s) as a function of a set of random predictor variables $\mathbf{X}$ (e.g., F_M, F_I, T, T_j, $[I]_{aq}$, $[M]_p$, Φ_{aq}):

$$q(\mathbf{Y}) = b_0 + \sum_{i=1}^{n} b_i m_i(\mathbf{X}) + \varepsilon \tag{4.19}$$

The function q represents any linear or nonlinear transformation of the response variable, b_0 is an independent coefficient, b_i represents the coefficients of the i-th predictor function m_i for each of the $i = 1, \ldots, N_{m_i}$ predictor functions considered, and ε is the random error of the model, namely:

$$\varepsilon(\mathbf{b}) = q(\mathbf{Y}) - b_0 - \sum_{i=1}^{n} b_i m_i(\mathbf{X}) \tag{4.20}$$

with $\mathbf{b} = [b_0, \ldots, b_n]$. The predictor function m_i may represents any general nonlinear function involving one or more random predictor variables X_i from the set of random predictor variables $\mathbf{X}$.

In principle, the best statistical model describing the response variable $\mathbf{Y}$ should provide the minimum error variance $Var(\cdot)$ while being unbiased and parsimonious. That is, the best model should provide a solution to the following multi-objective optimization problem:

$$\begin{aligned} \underset{\mathbf{b},\mathbf{X}}{\textbf{minimize}} \quad & \{Var(\varepsilon(\mathbf{b})), m_i(\mathbf{X})\} \\ \textbf{s.t.} \quad & E(\varepsilon(\mathbf{b})) = 0 \end{aligned} \tag{4.21}$$

where $E(\cdot)$ is the expected value operator.

The first step is the transformation and standardization of the variables. Firstly, the transformation function of the response variable $q(\mathbf{Y})$ to be used are defined by:

$$q(\mathbf{Y}) = q\begin{pmatrix} Y_{\bar{n}} \\ Y_{N_s} \end{pmatrix} = \begin{bmatrix} \ln(\bar{n}) \\ N_s \end{bmatrix} \tag{4.22}$$

Secondly, the standardized transformed response variable is obtained as follows:

$$\mathbf{Y}^* = \frac{q(\mathbf{Y}) - \langle q(\mathbf{Y}) \rangle}{\max(q(\mathbf{Y})) - \min(q(\mathbf{Y}))} \tag{4.23}$$

Next, it is necessary to define the predictor functions to be considered in the analysis: $m_i(\mathbf{X})$. The number of predictor functions that can be considered is unlimited, independently of the number of experiments, unlike modeling based on degrees of freedom. However, the closed-form model will depend on the number of the experiments despite the number of significant factors resulting. This because significance is more difficult to prove in smaller samples. For this work the predictor functions are defined as follows:

$$\begin{aligned} \mathbf{Y}^* = {} & b_0 + b_1\mathbf{t} + b_2\mathbf{V} + b_3\mathbf{\Phi_{aq}} + b_4[\mathbf{I}]_{\mathbf{aq}} + b_5[\mathbf{M}]_{\mathbf{p}} + b_6\mathbf{T} \\ & + b_7\bar{\mathbf{r}} + b_8\boldsymbol{\sigma_r} + b_9\mathbf{F_M} + b_{10}\mathbf{F_I} + b_{11}\mathbf{T_j} \end{aligned} \tag{4.24}$$

Variables in equation (4.24) were selected because they relate the process input vectors ($\mathbf{F_M}$, $\mathbf{F_I}$, $\mathbf{T_j}$) to the macroscopic and mesoscopic states vectors ($\mathbf{V}$, $\mathbf{\Phi_{aq}}$, $[\mathbf{I}]_{\mathbf{aq}}$, $[\mathbf{M}]_{\mathbf{p}}$, $\mathbf{T}$, $\bar{\mathbf{r}}$, $\boldsymbol{\sigma_r}$) to predict the evolution of the microscopic states ($\bar{n}$ and N_s). $\mathbf{V}$, $\mathbf{\Phi_{aq}}$, $[\mathbf{I}]_{\mathbf{aq}}$, $[\mathbf{M}]_{\mathbf{p}}$, $\mathbf{T}$, $\bar{\mathbf{r}}$, and $\boldsymbol{\sigma_r}$ vectors collect values of the macroscopic and mesoscopic states in the inputs ($\mathbf{F_M}$, $\mathbf{F_I}$, $\mathbf{T_j}$) space. It is important to remark that the time vector $\mathbf{t}$ is included here because there exists the possibility that external factors not considered in the analysis are affecting the results. $\mathbf{t}$ can be used to test the independence.

Then, the standardized transformed factor for each predictor function is obtained as follows:

$$X_j^* = \frac{m_j(\mathbf{X}) - \langle m_j(\mathbf{X}) \rangle}{\max(m_j(\mathbf{X})) - \min(m_j(\mathbf{X}))} \tag{4.25}$$

The second step is the selection of the next most promising factor. Therefore, the correlation coefficients between $\mathbf{Y}^*$ and each $\mathbf{X}_i^*$ are computed and the standardized transformed factor with the largest absolute correlation coefficient $\mathbf{X}_m^*$ is identified.

The third step is to test the significance of the next most promising factor. Consequently, the best probability model describing the overall behavior of $\mathbf{Y}^*$ should be identified. Next, both positive and negative subgroups of experiments must be determined. The positive and negative subgroups are those for which $m_j(\mathbf{X}) \geq \langle m_j(\mathbf{X}) \rangle$ and $m_j(\mathbf{X}) \leq \langle m_j(\mathbf{X}) \rangle$, respectively. Then, the smaller subgroup must be identified (for critical resolution). Finally, the validity of the overall model using the smaller subgroup data is tested. If the alternative hypothesis cannot be rejected, then the coefficient b_m^* is significant.

Before performing the hypothesis test a certain relative tolerance can be used as a filter. By default, the value of the tolerance is set at 0.05, purposely chosen similar to the conventional value used for the significance value. The hypothesis test is only performed if the difference between the mean values of both subgroups is larger than the tolerance.

The fourth step is to calculate the coefficient of the most promising factor. That is, if the coefficient b_m^* is significant, then:

$$b_m^* = \frac{Cov(\mathbf{Y}^*, \mathbf{X}_m^*)}{Var(\mathbf{X}_m^*)}. \tag{4.26}$$

Otherwise, if b_m^* is not found significant, or if $|b_m^*|$ is below the relative tolerance 0.05, then $b_m^* = 0$. The significance of b_m^* is determined by a statistical test. Such a test determines whether the b_m^* value is significantly different from zero or not.

The fifth step is updating the data. The standardized response variable must be updated to remove the effect of the predictor function $\mathbf{X}_m^*$ already included in the model, as follows:

$$\mathbf{Y}^* = \mathbf{Y}^* - b_m^* \mathbf{X}_m^* \tag{4.27}$$

The predictor function $\mathbf{X}_m^*$ is removed from the list of the factors available. The procedure must be repeated from the second step if the list of factors is not empty. Otherwise, it is possible to proceed with the following step.

The sixth step is to calculate the original model coefficients. The values of the coefficient in the original model, equation (4.19), and the independent coefficient can be computed by using equations (4.28) and (4.29).

$$b_0 = \langle q(\mathbf{Y}) \rangle - \sum_{i=1}^{n} b_i \langle m_i(\mathbf{X}) \rangle \tag{4.28}$$

$$b_i = b_i^* \frac{\max(q(\mathbf{Y})) - \min(q(\mathbf{Y}))}{\max(m_i(\mathbf{X})) - \min(m_i(\mathbf{X}))} \tag{4.29}$$

The seventh step is to calculate the performance of the model. Calculate the residuals of the original model by using equation (4.30).

$$\varepsilon = \varepsilon^* (\max(q(\mathbf{Y})) - \min(q(\mathbf{Y}))) \tag{4.30}$$

Consequently, identify the best probability model describing the behavior of the residuals using a standard parameter identification method. Thus, determine the variance of the residuals $(Var(\varepsilon))$ for the best probability model identified. Finally, the R^2 goodness-of-fit could be computed as:

$$R^2 = 1 - \frac{\sum \varepsilon^2}{\sum \left(q(\mathbf{Y}) - \langle q(\mathbf{Y}) \rangle\right)^2} \tag{4.31}$$

and the adjusted R^2 goodness-of-fit as:

$$R^2_{adj} = 1 - \frac{Var(\varepsilon)}{\langle \left(q(\mathbf{Y}) - \langle q(\mathbf{Y}) \rangle\right)^2 \rangle} \tag{4.32}$$

An implementation of the method in R language can be found in the supplementary information in (Hernandez, 2018), where also several application examples were included.

The required database to obtain the close-form models of the microscopic scales is generated by running the kMC simulation iteratively over the whole domain of the microscopic input parameters. That is: $V \in [1 \times 10^6, 2.5 \times 10^6]$ cm^3, $\Phi_{aq} \in [0.45, 0.8]$, $[I]_{aq} \in [0, 1.8 \times 10^{-7}]$ mol/cm^3, $[M]_p \in [0, 1.8 \times 10^{-4}]$ mol/cm^3, $T \in [328.15, 348.15]$ K, $\bar{r} \in [50, 90]$ nm, $\sigma_r \in [5, 25]$ nm, $F_M \in [20.83, 62.50]$ cm^3/s, $F_I \in [6.94, 20.83]$ cm^3/s, and $T_j \in [323.15, 353.15]$ K. Such an iteration is performed by adopting a Monte Carlo method where an uniform distribution was assuming for the input parameters. The closed-form models are given by:

$$\begin{aligned} \ln(Y_{\bar{n}}) &= -2.5416 - 5.6020 \times 10^3 [M]_p + 1.5313 \times 10^{-2} F_M \\ &\quad + 7.3867 \times 10^{-2} T_j + 0.3220\varepsilon \end{aligned} \tag{4.33}$$

$$Y_{N_s} = 7.7269 \times 10^{17} - 4.3564 \times 10^{25} [I]_{aq} + 2.7490 \times 10^{17} F_I + 4.2516 \times 10^{17} \varepsilon \tag{4.34}$$

They fit with $R^2 = 53.4429\%$ and $R^2_{adj} = 63.0253\%$ for $Y_{\bar{n}}$ and $R^2 = 82.9849\%$ and $R^2_{adj} = 96.6499\%$ for Y_{N_s}, respectively. Additionally, equations (4.33) and (4.34) are independent of $\mathbf{t}$.

4.2.2 Simulation results based on the closed-form

For the sake of comparison, the same simulation performed to generate the database is executed again but, instead of the kMC model, the closed-form of the microscopic scale states is used. Figure 4.4 shows the comparison between the generated database with the kMC simulation and the results obtained by using the closed-form of the models. In Figure 4.4, it is possible to appreciate that the closed-form models

(black vertical lines) are able to capture with a good extent the results of the kMC simulations (blue dots).

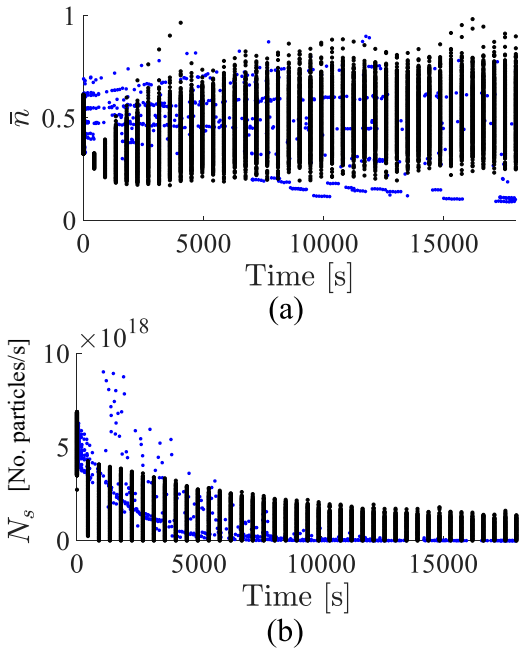

FIGURE 4.4: Microscopic states evolution comparison between the full-multiscale (blue dots) and closed-form models (black vertical lines) for all the combined F_I and F_M values: (a) free-radicals inside the polymer particles and (b) rate of secondary nucleation.

Figure 4.5 shows the dynamical evolution of macroscopic states. From the Figure, it is noticed that the total reactor volume increase over time due to the fact that both the initiator and the monomer are added at a constant rate from the beginning to the end of the batch time. Additionally, from the Figure, it is observed that $[M]_p$ stabilizes really fast (after about 500 s), which is really fast with respect to $[I]_{aq}$, who tend to stabilize once at the end of the reaction time. On the other hand, Φ_{aq} is always decreasing. This means that $[I]_{aq}$ as well as $[M]_p$ are effectively consumed to form new monomer chains. The fact that the T variation remains bounded and small benefits the reaction conditions in such a way that the reaction rate does not decrease significantly to slow down the particles growing process allowing to reach the desired particles size at the of the batch time.

Figure 4.6 shows the dynamical evolution of the PSD by considering only the power of 4 dependency of D, that is for $D = 2.5 \times 10^{-2} r^4$. From Figure 4.6, it can be seen that the full particles population shifts in the increasing direction of the particles size. This occurs in agreement with the nonlinear form of D, which establishes that the bigger polymer particles grow faster than the smallest one causing the observed asymmetry in the PSD. Additionally, from Figure 4.6, the polymer particles growth appears to decrease over time. This can be observed from the fact that although snapshots of the PSD dynamical evolution were taken every 6000 s, the peak value of the plotted PSDs are not equidistant. This is consistent with the definition of the

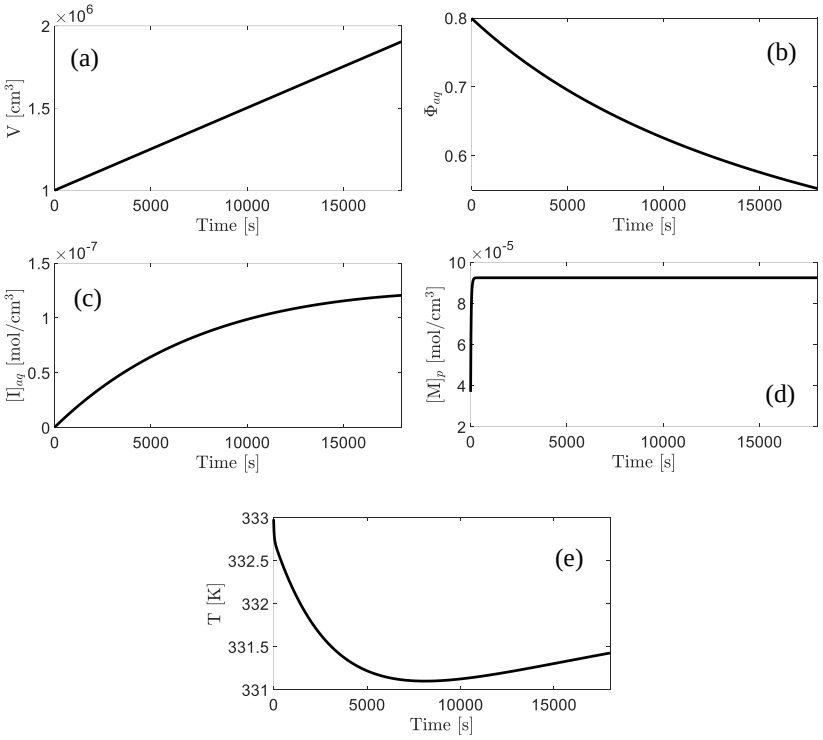

FIGURE 4.5: Macroscopic states trajectories: (a) V the volume of the reactor, (b) Φ_{aq} water volume fraction, (c) $[I]_{aq}$ initiator concentration in the aqueous phase, (d) $[M]_p$ the monomer concentration in the polymer phase, and (e) T the reactor temperature.

growth kernel due to the fact that the advection effect in the FPE presents a nonlinear decreasing behavior in the positive direction of the particles size.

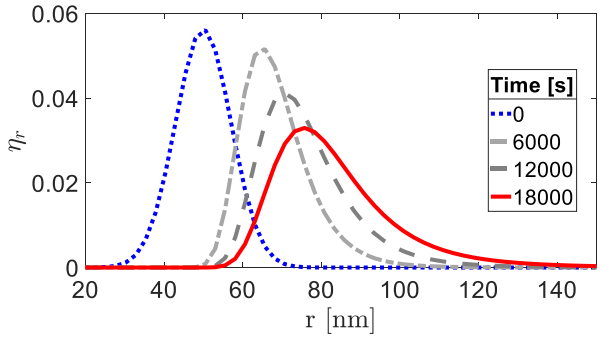

FIGURE 4.6: Dynamical evolution of the particle size distribution (PSD).

Figure 4.7 shows the dynamical evolution of microscopic states adopting the closed-form given by equations (4.33) and (4.34), respectively. From Figure 4.7a, it is observed that at the beginning of the simulation $\bar{n}$ takes the overall highest value. However, a value close to 0.55 is reached very fast and then $\bar{n}$ remains close to that value during the remaining reaction time. This result is consistent with the result presented in Figure 3.6a in Chapter 3 where the value of $\bar{n}$ also fluctuates around

a value of 0.55. On the other hand, Figure 4.7b shows the evolution the secondary nucleation rate N_s. From Figure 4.7b, it is seen that neither the initial value of N_s nor the time at which N_s reached a value equal to zero are accurately captured by the closed-form model (see Figure 3.6b). This evidences the difficulties of capturing the nonlinear behavior of this microscopic state. However, it is remarked here that the general decreasing trend of N_s is captured by the closed-form model while drastically reducing the computational cost of solving the full multiscale model. Admittedly, even though not perfect, simulations adopting this closed-form model are much less computationally expensive than those based on the kMC method, and therefore might be much more suitable for optimization and control purposes.

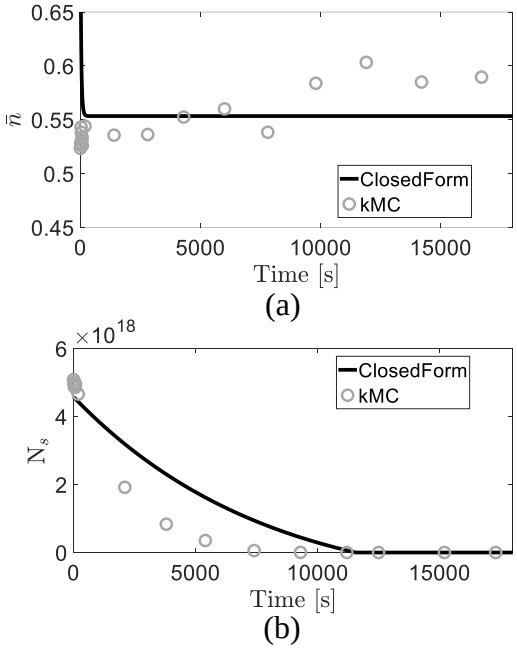

FIGURE 4.7: Microscopic states trajectories: (a) $\bar{n}$ the average number of the free-radicals and (b) N_s the secondary nucleation rate.

4.3 Computational cost analysis: comparison between the full multiscale model v.s. the reduced-order based models

For the sake of comparison between different model approaches, namely, ***i.*** the full-multiscale model (FEM-kMC), ***ii.*** the multiscale model by adopting the closed-form model for the microscopic scale (FEM-ClosedForm), ***iii.*** the reduced-order model presented in (Urrea-Quintero, Ochoa, and Hernández, 2019) (RO-kMC), and ***iv.*** the reduced-order model coupled with the closed-form model for the microscopic scale (RO-ClosedForm), some simulations are performed in a a 2.50 GHz Intel Core i7 − 7700 with 32GB RAM.

The FEM-kMC model is taken as a reference as the true solution of the multiscale problem. Mean value (Mean), standard deviation (Std. dev.), and skewness (Skw)

TABLE 4.1: Comparison between the full-multiscale model and its order-reduction approximations.

	Statistical moment				
Model	**Mean [nm]**	**Std. dev. [nm]**	**Skw**	D_B	**Relative Sim. time [%]**
FEM-kMC	82.3581	17.0904	1.7515	0	100
FEM-ClosedForm	82.8233	16.6425	1.7938	0.0918	2.15
RO-kMC	79.7492	20.9364	0	0.2673	13.15
RO-ClosedForm	81.2847	21.5284	0	0.3077	0.01

are taken for each of the four final PSDs to have an idea of how much they vary among them. Additionally, the Bhattacharyya distance (D_B) was computed for the four cases to measure the closeness between each of the final PSD being considered and the true solution.

Let η_{r_p} and η_{r_q} represent two probability distributions over the same domain Ω_r, the Bhattacharyya distance is defined as

$$D_B(\eta_{r_p}, \eta_{r_q}) = \sqrt{1 - \int_{\Omega_r} \sqrt{\eta_{r_p}^T \eta_{r_q}} dr}. \tag{4.35}$$

The Bhattacharyya distance $D_B(> 0)$ is directly proportional to the degree of dissimilarity of different probability distribution functions, being equal to 0 for two full overlapped probability distribution functions (Aherne, Thacker, and Rockett, 1998).

The four considered approaches evolved towards a comparable final PSD which are however endowed by remarkable differences. From Table 4.1, it is observed that both FEM-kMC and FEM-ClosedForm models capture the skewness of the final PSD, i.e., its nonlinear evolution. In contrast, the limitation of both RO-kMC and RO-ClosedForm is that the gaussian shape of the PSD is preserved in time. Moreover, the most expensive simulation corresponds to the FEM-kMC model as expected (see Table 4.1). Nevertheless, no significant differences can be noted in terms of the mean value and the standard deviation. This fact is reflected in small Bhattacharyya distances. The adoption of the closed-form model for the microscopic scale represents the main computational load reduction. The FEM-ClosedForm model is the best candidate if a trade-off between computational cost and accuracy is desired. On the other hand, the RO-kMC is the most appropriate approach to preserve the stochastic nature of the microscopic scale in terms of the average of free-radicals and rate of secondary nucleation (only mean $\pm$ std. dev. of the PSD are computed), while saving some computational time (0.01% w.r.t. the full FEM-kMC model).

It is remarked that because of the computational cost, the most appropriate representations to be used on optimization/control tasks are the two adopting the closed-form model of the microscopic scale. However, the FEM-ClosedForm imposes an additional challenge with respect to the RO-ClosedForm model, namely, the solution of the FPE. From the control viewpoint, the FEM-ClosedForm model requires the adoption of a specialized framework for the control of nonlinear distributed process systems. Such frameworks, by the way, typically leads to the adoption of model-order reduction techniques because of the high computational cost of determining the control actions (see Christofides (2001) and Meurer (2017) for more details). Consequently, the RO-ClosedForm model seems to be the most appropriate representation to being adopted in optimization/control tasks. By using this model most of the traditional control theory could be applied.

4.4 Sensitivity analysis

In terms of industrial applications, it is important to understand (among others), two main aspects: ***i.*** the effect of both monomer and initiator flows as manipulable inputs over the final PSD. Since the inputs might determine the shape of the final PSD, they can be used to drive the process towards a desired final PSD such that a final-end product quality is attained. ***ii.*** The effect of the uncertainty of the PSD at the beginning (η_{r_0}) of the polymerization process. If η_{r_0} has a significant impact over the final PSD, it could be not possible to reach the final desired PSD, which implies a deterioration on the final end-product quality.

Regarding the effect of both the monomer and the initiator flows as manipulable inputs over the final PSD, a sensitivity analysis of the flows at the input over the final PSD is performed. To perform such an analysis a Monte Carlo simulation is designed to iteratively solve the FEM-ClosedForm model and evaluate 250 combinations of for both the monomer flow $F_M \in [20.83, 62.50]$ cm^3/s and the initiator flow $F_I \in [6.94, 20.83]$ cm^3/s. Both input flows are varied adopting an uniform distribution discretized within the defined inputs range.

Figure 4.8 shows the three first statistical moments of the final PSD and the Bhattacharyya distance (B_D) with respect to the final PSD obtained by adopting the nominal values of the flows at the input. From Figures 4.8a,b, and c, it is possible to observe that the monomer flow has a significant impact over the shape of the final PSD. In contrast, the initiator flow does not have almost any effect (Figure 4.8d). However, because of the high correlation among the statistical moments and F_M, explained by their monotonic increasing or decreasing behavior, it is possible to conclude that the three moments can not be determined independently, instead the full final PSD can be. That result is expected due to the fact that the diffusion coefficient is neither directly nor indirectly coupled with the inputs.

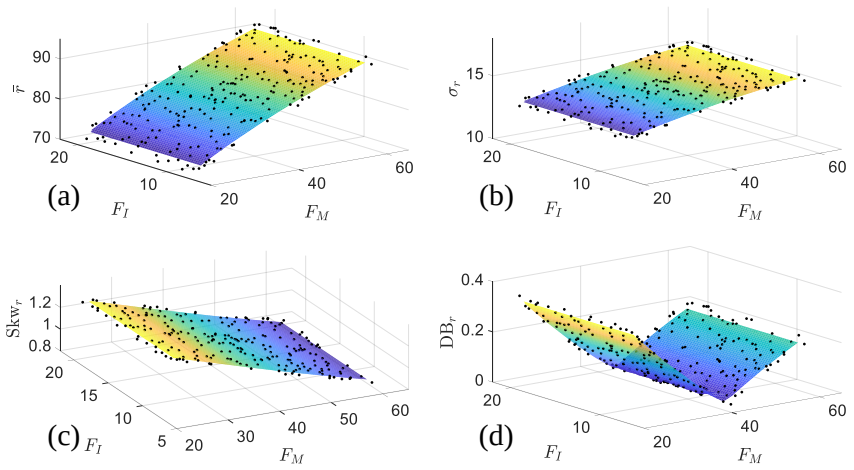

FIGURE 4.8: Impact of the input flows over the final PSD: (a) $\bar{r}$, (b) σ_r, and (c) Skw., the mean value, the standard deviation, and the skewness of the PSD, respectively, (d) B_D, the Bhattacharyya distance.

The fact that F_I does not have any significant effect over the final PSD (see Figures 4.8a, b, and c) is advantageous since the rate of the secondary nucleation is directly related to this input flow (see equation (4.34)). Consequently, F_M can be used to tune the final PSD while F_I can be used to control the rate of the secondary particle nucleation. This strategy can be exploited to improve the quality of the final polymeric material.

Regarding the effect of the uncertainty of η_{r_0} of the polymerization process, a sensitivity analysis of the $\bar{r}_0$ and σ_{r_0} over the final PSD is performed. To perform such an analysis a Monte Carlo simulation is designed, as in the flows case, to iteratively solve the FEM-ClosedForm model and evaluate several combinations of values of $\bar{r}_0 \in [40, 60]$ nm and $\sigma_{r_0} \in [1, 12.5]$ nm. Both $\bar{r}_0$ and σ_{r_0} are varied using an uniform distribution discretized with 250 samples.

Figure 4.9 shows the three first statistical moments of the final PSD and the Bhattacharyya distance with respect to the final PSD obtained by adopting the nominal values of both $\bar{r}_0$ and σ_{r_0}. From Figures 4.9a,b, and c, it is possible to observe that both $\bar{r}_0$ and σ_{r_0} indeed have an impact over the shape of the final PSD. From Figure 4.9d, it is possible to observe that the final PSD changes with the variation of η_{r_0}. That means, a high uncertainty on η_{r_0} can influence the prediction capabilities of the multiscale model.

It is remarked here the fact that, by comparing Figures 4.8a,b,c and 4.9a,b,c, it is possible to observe that the variation in the monomer flow has a higher impact over the final mean value and skewness of the final PSD, while the uncertainty about η_{r_0} has major impact over the standard deviation of the final PSD. Finally, if we compare Figures 4.8d and 4.9d, it is possible to notice that the monomer flow has a higher overall impact over the shape of the final PSD than η_{r_0}. For instance, $\max(D_B) =$

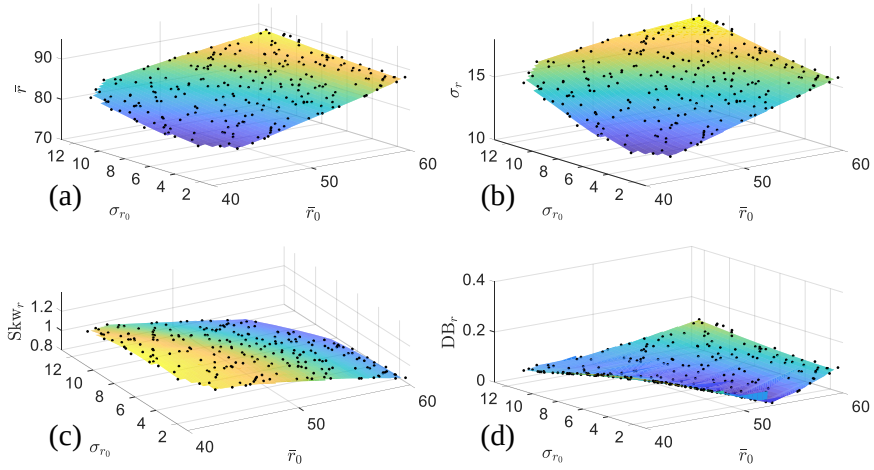

FIGURE 4.9: Impact of the PSD initial condition over the final PSD: (a) $\bar{r}$, (b) σ_r, and (c) Skw., the mean value, the standard deviation, and the skewness of the PSD, respectively, (d) B_D, the Bhattacharyya distance.

0.3714 for the F_M variation case, while $\max(D_B) = 0.1676$ for the η_{r_0} variation case.

4.5 Chapter concluding remarks

In this chapter, the mesoscopic-scale representation of dispersed media was carried out by using Variance Algebra concepts for describing the stochastic nature of particle growth. This was the first step towards the construction of a control-oriented model. The reduced-order model was proposed for describing the mean and standard deviation of the particle size distribution by means of only two ODEs at the mesoscopic-scale. On the other hand, the closed-form model derivation at the microscopic scale was treated as a statistical modeling problem which made the problem only dependent on the quality of the dataset used to build the regression. That is, if the closed-form model prediction wants to be improved, only more kMC simulations are required to increase the size and diversity of database. The closed-form model derivation is the second step in the development of the control-oriented model. The combination of the reduced-order model at the mesoscopic scale with the macroscopic scale model leads to a model composed only of ODEs. The microscopic states could be taken as system outputs and their evolution can be obtained from the numerical integration of the set of ODEs using any standard numerical method as the Runge-Kutta 4th order method.

Chapter 5

Set-theoretic output-controllability analysis

Abstract

This work presents a framework for evaluating the controllability of multiscale systems based on a set-theoretic approach. Calculation of the Controllable Trajectories Set is the core of the set-theoretic approach. From a multi-scale perspective, such calculation is a computationally- intractable problem. Therefore, to overcome the intrinsic curse of dimensionality of the problem, Variance Algebra concepts and a statistical modeling approach are combined to obtain a closed-form allowing to perform an output-controllability analysis for a multiscale system. A semi-batch emulsion polymerization process is adopted as a case study. Results have shown that both, the final Particle Size Distribution (mesoscopic variable) and the secondary particle nucleation rate (microscopic variable) are output-controllable. Evaluating the controllability of lower-scale variables (i.e. below macroscopic) could both, mitigate the dependency of the current control strategies of on-line measurements at the lower scales and help to better understand the process capabilities of achieving the desired product quality specifications.

5.1 Set-theoretic based batch output-controllability analysis

5.1.1 Batch output-controllability from the multiscale perpective

We will focus on processes which could be described through a multiscale dynamical model composed of lumped and spatially distributed states as follows:

$$\frac{d\mathbf{x}_l}{dt} = \mathcal{F}(\mathbf{x},\mathbf{u},\boldsymbol{\theta}), \quad \mathbf{x}_l(t=0)=\mathbf{x}_{l0}, \quad \text{on} \quad \Omega_1 \tag{5.1}$$

$$\frac{\partial \mathbf{x}_d}{\partial t} = \mathcal{A}(\mathbf{x}) + g(\mathbf{x},\mathbf{u},\boldsymbol{\theta}), \quad \mathbf{x}_d(\mathbf{e},t=0)=\mathbf{x}_{d0}(\mathbf{e}), \quad \text{on} \quad \Omega_2 \tag{5.2}$$

$$\mathbf{x}_m(t_i) = \Pi(\delta t, \mathbf{x}(\gamma,t_i),\mathbf{u},\boldsymbol{\theta}), \quad \text{on} \quad \Omega_3 \tag{5.3}$$

$$\mathbf{y} = H(\mathbf{x},\mathbf{u},\boldsymbol{\theta}) \tag{5.4}$$

$$\delta t = t + \Delta t_m \tag{5.5}$$

$$h\left(\mathbf{x}, \frac{d\mathbf{x}}{d\eta}, \mathbf{u}, \bar{\mathbf{x}}\right) = 0, \quad \text{on} \quad \Gamma \tag{5.6}$$

$$\bar{\mathbf{x}} = \mathcal{L}(\mathbf{x}_m) \tag{5.7}$$

Equations (5.1), (5.2), and (5.3) represent the macroscopic, mesoscopic, and microscopic descriptions of the system over the respective domains Ω_1, Ω_2, and Ω_3.

It is assumed that Ω_1, Ω_2, and Ω_3 overlap only at their common interface $\gamma(\subseteq \Gamma) = \Omega_1 \cap \Omega_2 \cap \Omega_3$, where $\Omega = \Omega_1 \cup \Omega_2 \cup \Omega_3$ spans the whole process domain. $\mathbf{x} = \mathbf{x}_l(t) \cup \mathbf{x}_d(\mathbf{e},t) \cup \mathbf{x}_m(t_i) \in \mathcal{X} \subseteq \mathbb{R}^n$ is the state-space vector; $\mathbf{x}_l(t) \in \mathbb{R}^l$ denotes the vector of macroscopic state variables described by a set of Ordinary Differential Equations (ODEs); and $\mathbf{x}_d(\mathbf{e},t) \in \mathbb{R}^d$ denotes the vector of mesoscopic state variables described by a set of Partial Differential Equations (PDEs). For instance, $\mathbf{e} = [e_1, e_2, e_3] \in \Omega_2 \subseteq \mathbb{R}^3$ is the vector of internal coordinates. $\mathbf{y} \in \mathcal{Y} \subseteq \mathbb{R}^m$ is the vector of the outputs which corresponds to a subset of $\mathbf{x}$ ($\mathcal{Y} \subseteq \mathcal{X}$), $\mathbf{y}$ can be composed by some of the states or any combination among them. $t \in [0, t_f]$ is the time (t_f is the batch end-time). $\mathcal{A}(\mathbf{x})$ is a dissipative, possibly nonlinear, spatial differential operator which includes up to second-order spatial differential derivatives. This means the spatial differential operator represents the most common physical phenomena, namely, advection, diffusion or advection-diffusion type problems. $\mathcal{F}(\mathbf{x},\mathbf{u},\boldsymbol{\theta})$, $H(\mathbf{x},\mathbf{u},\boldsymbol{\theta})$, and $g(\mathbf{x},\mathbf{u},\boldsymbol{\theta})$ are nonlinear, possibly time-varying, vector functions which are assumed to be sufficiently smooth with respect to its arguments. $\mathbf{u}(t) \in \mathcal{U} \subseteq \mathbb{R}^p$ is the vector of the input variables which are assumed to be piecewise continuous functions of time, $\boldsymbol{\theta}(t) \in \mathbb{R}^q$ is the vector of the system parameters which are common to all scales and could be updated at any time within the batch time, $\mathbf{x}_{l0}$ is the vector of initial conditions for the macroscale model, and $\mathbf{x}_{d0}$ is a smooth vector function of $\mathbf{e}$.

Function Π is a time-stepper function which describes the system at microscopic scale. This function interacts via an input/output structure and may be unavailable in a closed-form. It uses $\mathbf{x}_m(t_{i-1})$ and macroscopic, mesoscopic or both state vectors at the interface γ as input, evolves over the time-interval δt, and produces states $\mathbf{x}_m(t_i)$. The vector function $h\left(\mathbf{x}, (d\mathbf{x}/d\eta), \mathbf{u}, \bar{\mathbf{x}}\right)$ represents the boundary conditions which depend upon $\bar{\mathbf{x}}$, the coarse realization of the microscopic states, linking the macroscopic with the microscopic states. Coarse variables are defined through the

restriction operator denoted as $\mathcal{L}(\cdot)$. Typically, they are lower order statistical moments of microscopic states selected such that the coarse-dynamics are observable.

Equations (5.1), (5.2), and (5.3), as a whole, describe the dynamical evolution of a dispersed-phase process or a process containing particles as a dispersed-phase system. For instance, crystallization and precipitation, dissolution, deposition (e.g., chemical vapor deposition), polymerization, fermentation, cell growth, division differentiation, and death, among others (Ramkrishna and Singh, 2014). The macroscopic model could be derived from the mass and energy balances whereas the mesoscopic model can be derived from the Population Balance Equations (PBEs) framework. The microscopic model accounts for the simulation of a well-stirred chemically reacting system by stepping in time to successive molecular reaction events in exact accord with the premises of the Chemical Master Equation (CME) (Gillespie, 2007).

Batch processes are processes that by nature have some irreversible states (Gómez et al., 2015). Therefore, it is expected at least one of the macroscopic variables represented by equation (5.1) to be irreversible (Haddad, Chellaboina, and Nersesov, 2008). This means the following condition must be satisfied: for some $i = 1, 2, \ldots, n$, and $\forall t = [t_1, t_2, \ldots, t_{i-1}, t_i, t_{i+1}, \ldots, t_f]$, it follows that $x_l^{(i)}(t_{i-1}) \geq x_l^{(i)}(t_i) \geq x_l^{(i)}(t_{i+1})$ or $x_l^{(i)}(t_{i-1}) \leq x_l^{(i)}(t_i) \leq x_l^{(i)}(t_{i+1})$; e.i., $\mathbf{x}_l$ is a function that increases or decreases monotonically $\forall \mathbf{x}_l \in \Omega_1$ and $\mathbf{u} \in \mathcal{U}$.

The following definition introduced by Srinivasan and Bonvin (2007) is rewritten here for the batch output-controllability, as follows:

Definition 1 (Batch Output-Controllablity)**.** Let $\mathbf{y}$ be the vector of the system outputs (eq. (5.4)) to be controlled. System (5.1) - (5.3) is locally **batch-output controllable** from t_0 on, if it is possible to construct a set of admissible control actions sequence $\mathbf{u}_i \in \mathcal{U}$, $i = 1, \ldots, N$, such that, for every initial condition $\mathbf{x}_{t_0} \in \Omega_0$ and $\mathbf{y}_{t_0} \in \mathcal{Y}_0$, the convergence of the system to a final bounded region $\mathbf{x}_{t_f} \in \Omega_f$ is guaranteed while $\mathbf{y}$ is driven to the given final desired run-end specification $\mathcal{Y}_f$ in both a finite time t_f and a finite sequence of N steps.

Remark 1. With the above definition two issues are addressed simultaneously: ***i.*** the existence of the run-time trajectories that must be followed to reach the end-time specification; ***ii.*** the feasibility of the end-batch specification due to the existence of at least one trajectory such that with the available control actions the system can be driven from the initial condition to the desired final one.

5.1.2 Sets definition

To better understand the concept of the CTS, the following definitions are re-called here that were given by Gómez et al. (2015) and Gómez-Pérez, Gómez, and Alvarez (2015).

Consider a nonlinear dynamical system such that:

$$\begin{aligned} \dot{\mathbf{x}} &= F(\mathbf{x}, \mathbf{u}, \boldsymbol{\theta}) \\ \mathbf{y} &= H(\mathbf{x}, \mathbf{u}, \boldsymbol{\theta}) \end{aligned} \tag{5.8}$$

with $\mathbf{u}(t) \in \mathcal{U} \subseteq \mathbb{R}^p$ the admissible control actions vector, $\mathbf{x}(t) \in \mathcal{X} \subseteq \mathbb{R}^n$ is the states vector, $F(\cdot, \cdot)$ is defined in the $\mathcal{X} \times \mathcal{U}$ space, $\mathbf{y}(t) \in \mathcal{Y} \subseteq \mathbb{R}^m$ is the outputs vector, and $H(\cdot, \cdot)$ is defined in the $\mathcal{Y} \times \mathcal{U}$ space.

Definition 2 (Reachable Set in time t)**.** Given a set Ω_τ, the Reachable set $\mathcal{R}_t(\Omega_\tau)$ from Ω_τ in a time $t > \tau$ is the set of all states vector $\mathbf{x}$ for which exists a $\mathbf{x}(\tau) \in \Omega_\tau \in \mathcal{X}$ and $\mathbf{u}(\cdot) \in \mathcal{U}$ such that $\mathbf{x}(t) = \mathbf{x}$:

$$\mathcal{R}_t(\Omega_\tau) = \{\mathbf{z} \in \mathcal{X} | \exists \mathbf{x} \in \Omega_\tau \wedge \mathbf{u} \in \mathcal{U} : \mathbf{z} = \varphi(t, \tau, \mathbf{x}, \mathbf{u})\}, \tag{5.9}$$

where $\mathbf{z}$ is the final state to be reached. This means, $\mathcal{R}_t(\Omega_\tau)$ is the set of all state-space vectors that can be reached by the system evolution from Ω_τ in a time t by means of the admissible control actions.

Remark 2. The information provided by the reachable set at the batch time $t = t_f$ could be used in two different ways: *(a)* to verify the feasibility of the end-batch specifications if their are chosen a priori or *(b)* to define the end-batch specifications such that they belong to the interior of the reachable set at t_f.

Definition 3 (Controllable Set in time t)**.** Given a set Ω_τ, the Controllable set $\mathcal{C}_t(\Omega_\tau)$ to Ω_τ in a time $t < \tau$ is the set of all states vector $\mathbf{x}$ for which exists a $\mathbf{x}(\tau) \in \Omega_\tau \in \mathcal{X}$ and $\mathbf{u}(\cdot) \in \mathcal{U}$ such that if $\mathbf{x}(t) = \mathbf{x}$ then $\mathbf{x}(\tau) \in \Omega_\tau$:

$$\mathcal{C}_t(\Omega_\tau) = \{\mathbf{z} \in \mathcal{X} | \exists \mathbf{u} \in \mathcal{U} : \varphi(t, \tau, \mathbf{x}, \mathbf{u}) \in \Omega_\tau\}. \tag{5.10}$$

This means, $\mathcal{C}_t(\Omega_\tau)$ is the set of all state-space vectors from which, given the admissible control actions, it is possible to arrive to the set Ω_τ.

Remark 3. $\mathcal{C}_t(\Omega_\tau)$ must not be a single state-space point but a small state-space region. This because the probability of driving the system to a single point is equal to zero. The size of $\mathcal{C}_t(\Omega_\tau)$ could be thought as a controller accuracy constraint. That is, if $\mathcal{C}_t(\Omega_\tau)$ is almost a point in the state-space, a very precise control strategy must be implemented to drive the system inside $\mathcal{C}_t(\Omega_\tau)$. In contrast, if $\mathcal{C}_t(\Omega_\tau)$ is a small state-space region, a more flexible control strategy could be adopted.

Definition 4 (Controllable Trajectories Set from Ω_0 to Ω_f in time t)**.** Given the sets Ω_0 and Ω_f, the Controllable Trajectories Set (CTS) $\tau_t(\Omega_0, \Omega_f)$ from Ω_0 to Ω_f in a time t is the set of all state vectors that belongs to the Reachable set $\mathcal{R}_t(\Omega_0)$ and the Controllable set $\mathcal{C}_t(\Omega_t)$ in a time t:

$$\tau_t(\Omega_0, \Omega_t) \quad = \quad \{\mathbf{x} \in \mathcal{X} | \exists \mathbf{x} \in \mathcal{R}_t(\Omega_0) \wedge \mathbf{x} \in \mathcal{C}_t(\Omega_t)\}. \tag{5.11}$$

This means, $\tau_t(\Omega_0, \Omega_f)$ is the intersection in the state-space between $\mathcal{R}_t(\Omega_0)$ and $\mathcal{C}_t(\Omega_t)$ that determines the states in which an admissible control action exists such that the states can be driven from an initial condition Ω_0 to the final desired ones Ω_f in the batch time t_f.

Remark 4. If the interior of the CTS is not empty, it is said that the batch process is output-controllable to the selected end-batch specification Ω_f. However, once the process is running, to effectively reach the end-batch specifications, the system must be driven from the batch initial conditions to the final ones through the interior of the CTS during the whole batch time. If the process reaches a state outside the CTS in any time, the states would not converge to the desired final condition. Consequently, the ideal situation is that the CTS occupies the biggest portion of the state-space such that more state variables can converge to the end-batch conditions (Gómez-Pérez, Gómez, and Alvarez, 2015). The main reason why the process would not be driven through the interior of the CTS are process parameter uncertainties, model mismatches, and disturbances.

According to the above definitions, the existence of a non-empty CTS guarantees the existence of a possible trajectory to be followed to meet the end-batch specifications. Moreover, if it is assured that the system is driven through the CTS, then, it is expected that the run-end specifications are indeed fulfilled.

As the batch output-controllability analysis based on the sets theory is a procedure to compute the entire state-space domain which the system can evolve within, it would be possible to use the sets information in the three following ways: first to verify whether a predefined end-batch specifications belong to the CTS; second to compute the reachable set at the last step N and select feasible values for the end-batch specification such that they belong to the interior of this set. This second option is more related to a process design approach, but it is a suitable option in which the system is designed such that its controllability is already guaranteed. The last option, that could be considered as the more practical one from the engineering viewpoint, is to establish upper and lower constraints for each of the controlled outputs, not a fixed end-batch criterion (as it is the usual approach). This option can be seen as related to the so-called zone-control approaches (González and Odloak, 2009), in which rather

than to forcing the system to be driven to a fixed small state-space region, the control objective specification is relaxed to a bounded zone.

In summary, the batch output-controllability framework described above allows verifying through the computation of the CTS: ***i.*** if the system outputs are controllable to an end-batch specification in a finite time t_f and ***ii.*** if the states of the system converge to a bounded final space Ω_f in both a finite time t_f and a finite sequence of N steps. Both conditions are verified through the computation of the CTS.

5.1.3 Sets approximation by a randomized algorithm

Many problems in theory control that have a considerable computational complexity have been solved using randomized algorithms. These algorithms are simple and efficient, e.g., in the analysis and design of robust control systems (Calafiore, Dabbene, and Tempo, 2003; Tempo, Calafiore, and Dabbene, 2005). Applications such as aerospace control, control of hard disk drives, congestion control of high-speed networks, the controllability/reachability analysis of discrete-time piecewise affine systems and the nonlinear model predictive control have been successfully tackled by using randomized algorithms as well (See Tempo, Calafiore, and Dabbene (2013) for a more detailed review of the applications).

A randomized algorithm was introduced by Gómez et al. (2015) for the computational estimation of the reachable, controllable, and controllable trajectories sets for nonlinear systems that are subject to constrains within a polynomial calculation time. The algorithm presented by Gómez et al. (2015) allowed the authors to obtain reliable approximations of the sets with both a bounded error and a risk failure quantification. The same algorithm was adopted by Gómez-Pérez, Gómez, and Alvarez (2015) for the controllability analysis and reference trajectories design of some semi-batch reactors. Here the randomized algorithm introduced by Gómez et al. (2015) to compute both the reachable and the controllable sets is summarized below.

Algorithm 1: Reachable set computation. *Given:* An initial condition set Ω_0, an error and a fail risk (ε and δ), a state constrain set $\mathcal{X} \subseteq \mathbb{R}^n$, and a control variable constraint set $\mathcal{U} \subseteq \mathbb{R}^p$.

(1) Find the sample size by the Chernoff inequality $N \geq (1/2\varepsilon^2)\log(2/\delta)$.

(2) Get N samples $\mathbf{x} \backsim \text{Uniform}(\mathcal{X})$ and $\mathbf{u} \backsim \text{Uniform}(\mathcal{U})$.

(3) Obtain the prediction $\mathbf{x}(t + \Delta t)$ in accordance with equation (5.8).

(4) Return an estimation of the reachable set $\mathcal{R}(\Omega_0)$ such that,

$$P^N \left\{ \mathbf{x} \in \mathcal{X}^N \mid P(\mathcal{R}(\Omega_0)) - \hat{P}(\mathcal{R}(\Omega_0); \mathbf{x}) > \varepsilon \right\} \leq 2\exp(-2N\varepsilon^2)$$

Algorithm 2: Controllable set computation For the computation of the controllable set, the **algorithm 1** applies in the same way. The only difference is that in step (3), the system given by equation (5.8) must be solved in reverse time, that is for $\mathbf{x}(t - \Delta t)$.

Algorithm 3: Controllable trajectories set computation *Given:* An initial condition set $\mathcal{Q}_\prime$, a final condition set $\mathcal{Q}_\mathcal{N}$, and N.

(1) Find N reachable sets in i-steps ($i = 1, 2, \ldots, N$) to $\mathcal{Q}_0$, that is:

$$\mathcal{R}_1(\mathcal{Q}_\prime), \mathcal{R}_2(\mathcal{Q}_\prime), \ldots, \mathcal{R}_N(\mathcal{Q}_\prime).$$

(2) Find N controllable sets in i-steps ($i = 1, 2, \ldots, N$) to $\mathcal{Q}_N$, that is:

$$\mathcal{C}_1(\mathcal{Q}_\mathcal{N}), \mathcal{C}_2(\mathcal{Q}_\mathcal{N}), \ldots, \mathcal{C}_N(\mathcal{Q}_\mathcal{N}).$$

(3) Calculate each of the controllable trajectories set using the intercepts between the i reachable set $\mathcal{R}_i(\mathcal{Q}_0)$ and the $(N - i)$ controllable set $\mathcal{C}_{N-i}$, for every ($i = 1, 2, \ldots, N$), as follows:

$$\begin{aligned}
\mathcal{Q}^{0,N}(\mathcal{Q}_0, \mathcal{Q}_N) &= \mathcal{Q}_0 \\
\mathcal{Q}^{1,N-1}(\mathcal{Q}_0, \mathcal{Q}_N) &= \mathcal{R}_1(\mathcal{Q}_0) \cap \mathcal{C}_{N-1}(\mathcal{Q}_N) = \mathcal{Q}_1 \\
\mathcal{Q}^{2,N-2}(\mathcal{Q}_0, \mathcal{Q}_N) &= \mathcal{R}_2(\mathcal{Q}_0) \cap \mathcal{C}_{N-2}(\mathcal{Q}_N) = \mathcal{Q}_2 \\
\ldots &= \ldots \\
\mathcal{Q}^{N-1,1}(\mathcal{Q}_0, \mathcal{Q}_N) &= \mathcal{R}_{N-1}(\mathcal{Q}_0) \cap \mathcal{C}_1(\mathcal{Q}_N) = \mathcal{Q}_{N-1} \\
\mathcal{Q}^{N,0}(\mathcal{Q}_0, \mathcal{Q}_N) &= \mathcal{Q}_N
\end{aligned}$$

Thus, the controllable trajectories set for N-steps from $\mathcal{Q}_0$ to $\mathcal{Q}_N$ is the sequence:

$$\text{CTS} = \{\mathcal{Q}_0, \mathcal{Q}_1, \mathcal{Q}_2, \ldots, \mathcal{Q}_{N-1}, \mathcal{Q}_N\}.$$

5.1.4 Multiscale model order reduction

The multiscale model described by equations (5.1), (5.2), and (5.3) is a high dimensional one because of the spatial differential operator $\mathcal{A}$ in equation (5.2) and because of function Π in equation (5.3), which is stochastic by nature, lacks from a closed-form mathematical representation. Therefore, from the set-theoretic viewpoint, verifying the system output-controllability from a multiscale perpective is almost impossible without applying a suitable model order reduction technique. In

this work, a procedure to reduce the model dimension is proposed, although other approaches could be adopted as well (see, e.g., Varshney and Armaou (2008)). The proposed procedure to obtain the reduced order model is based on the ideas previously introduced in Chapter 4, which have shown to be effective in a free-radical polymerization process. The aim of the model order reduction procedure proposed here is to obtain a low-order computationally-tractable representation of the multiscale system which allows performing the batch output-controllability analysis by the computation of the CTS.

Set-theoretic based output-controllability analyses possess a computational challenge since the computation of the required sets is classified as a NP-hard problem (Blanchini, 1999; Kerrigan, 2001). For the batch output-controllability analysis, a convenient representation of the multiscale model is through a set of ODEs assembled as the system in equation (5.8). Such an ODEs system should comprise all the information of the dynamical evolution of both macroscopic and mesoscopic scales as state variables and the evolution of the microscopic scale as either system states or outputs such that they could be a function of the macroscopic and mesoscopic states as well as the inputs. A reduced order model in the form of equation (5.8) can be solved through efficient standard algorithms for ODEs integration reducing the sets computational cost.

From the problem definition, the macroscopic scale is already represented by a set of ODEs that describes the dynamical evolution of the macroscopic state variables (see equation (5.1)). On the other hand, the mesoscale corresponds to a PDE which represents the evolution of the dispersed phase of the system (see equation (5.2)). In this case, different spatial discretization methods can be applied to obtain a set of ODEs from the PDE. For the PBE type models, there is a plethora of spatial discretization methods that could be implemented such as finite volume or finite elements methods (See Gunawan, Fusman, and Braatz (2004), Bouaswaig and Engell (2010), John and Suciu (2014), and Mohammadi and Borzì (2015) for some approaches). However, most of those discretization techniques lead to a set of tens to hundreds of ODEs usually depending on the number of selected spatial points in which the spatial differential operator $\mathcal{A}$ is approximated. Such selected spatial points could be determined either by the particularities of $\mathcal{A}$ (e.g., $\mathcal{A}$ representing an advection-diffusion problem) or could be defined by the geometry of the spatial domain (it can be defined as a line, a square, or even as an irregular more complex geometry). Consequently, the mentioned discretization techniques could lead to computational expensive numerical schemes to solve the multiscale model, that might make the output-controllability analysis no viable because of the dimension of the mesoscopic state-space.

Another alternative is applying the method of moments which has shown to be effective in some cases to derive a set of ODEs composed by a small number of equations from a PDE (e.g., see Vafa, Shahrokhi, and Abedini (2013) and Bajcinca et

al. (2015)). The method of moments leads to a set of reduced number of ODEs. However, the limitation is that the stochastic nature of the defined internal coordinates of the PBE could not be accurately captured (Hosseini, Bouaswaig, and Engell, 2012). One solution to the above drawback could be the adoption of a stochastic version for the internal coordinates kernel as was proposed by Hosseini, Bouaswaig, and Engell (2013). The result is the Fokker-Planck Equation (FPE) which also presents several issues regarding the required numerical scheme and computational cost for solving it: ***i.*** the lower-order numerical schemes might suffer from instability and loss of accuracy of the probability density function (p.d.f.) in the tail regions (Kumar and Narayanan, 2006), ***ii.*** higher-order numerical schemes result again in a set of a larger number of ODEs requiring considerable computational effort, which, at the same time, limits the use of the model into optimization or control tasks (Kumar and Narayanan, 2006; Lötstedt and Ferm, 2006; Gathungu and Borzì, 2017).

Therefore, in this work, it is proposed a different approximation to obtain a reducer order model of the mesoscopic scale: the Variance Algebra approach applied to dynamical systems introduced by (Hernandez, 2016). The Variance Algebra is particularly powerful because it can be used for modeling the effect of random variables in nonlinear systems. The Variance Algebra is used for describing fluctuations of the state variables around their mean value with a simple mathematical representation that describes the dynamical evolution of the first statistical moments. This approach can be seen as a model-order reduction technique for the PDE that represents the dispersed phase (Urrea-Quintero, Ochoa, and Hernández, 2019). With the adoption of the Variance Algebra, it is possible to build a lower-order model which captures both the mean and the standard deviation of the states variables at the mesoscopic scale taking as a reference a stochastic kernel for their dynamical evolution.

Regarding to the microscopic model, represented by a kMC simulation and which requires a computationally intensive solution, the main concern is that it lacks of a closed mathematical form. In this work, a general procedure applying statistical modeling and analysis of experiments previously presented by Hernandez (2018) is proposed to obtain a closed-form model of the microscopic scale. Based on such a procedure, the problem of fitting a model based on a dataset generated by some kMC simulations performed from the multiscale model solution given by equations (5.1) - (5.3) can be addressed. The advantages of adopting this procedure, compared to other approaches, are: ***i.*** the problem of the closed-form development is handled as a general regression problem without any further assumption about the states and inputs system relation (e.g., linear, quadratic, exponential, etc.); ***ii.*** no prior distribution is assumed over the data obtained through the kMC simulation which is particularly convenient in this case because the kMC method approximates the Chemical Master Equation without assuming any prior distribution of the system evolution (Gillespie, 2007); and ***iii.*** the statistical modeling method successfully incorporates

the effect of the extreme values, usually representing the system high non-linearities. All the procedure to obtain a closed-form model from the kMC dataset in a free-radical emulsion polymerization process was already presented in chapter 4. The obtained closed-form model for the free-radical polymerization process relates the microscopic states variables with the macroscopic scale and the system inputs allowing the use of the model for the output-controllability analysis.

5.2 Application to the batch output-controllability analysis to a free-radical emulsion polymerization process

5.2.1 Control-oriented multiscale-based dynamical model

At this point, for the sake of clearness, it is remarked that equations (3.2)-(3.6), (3.12), and the kMC simulation represent the multiscale model in the form of equations (5.1), (5.2), and (5.3), which corresponds to a PDE/ODEs - kMC multiscale system. In contrast, equations (3.2)-(3.6), (4.10), (4.15), (4.33), and (4.34) represent the multiscale model in the form of equation (5.8), which is a suitable control-oriented representation, the so-called RO-ClosedForm model, to perform the batch output-controllability analysis based on the set-theoretic approach proposed here. Consequently, henceforth this RO-ClosedForm model representation of the emulsion polymerization process is adopted as the model to perform the set-theoretic based batch output-controllability analysis procedure discussed in Section 5.1.

5.2.2 Output-controllability analysis

In this case study, the verification of the end-point feasibility of the mesoscopic states means verifying whether it is possible or not to control the process towards a final PSD shape to guarantee the end-product quality. From the reachable sets analysis viewpoint, all the final achievable mean and standard deviation values of PSD are evaluated by means of the inputs manipulation, given the states initial condition Ω_0. From the CTS viewpoint, the feasibility of reaching an end-condition $\mathcal{Y}_f$ is evaluated, given a set of admissible inputs and an initial state condition Ω_0.

The total batch time to produce the structured polymer particles is expected to be 5 h. However, it is required a minimum time for the processes to be started. Thus, in this case, the starting time is 0.5 h –the required time to $[M]_p$ be stabilized– and the values of the states at that time are taken as the initial set Ω_0 to compute the reachable and controllable sets. Consequently, the simulated batch time to compute all the sets is 4.5 h.

For the computation of the sets based on the proposed randomized algorithm, the critical parameter determining the accuracy of the sets estimation is the taken number of samples of the states variables and the inputs over their admissible sets $\mathcal{X}$ and $\mathcal{U}$, respectively. The Chernoff inequality is a good first estimator of the number

of samples to be taken. For example, if an error $\varepsilon = 0.01$ and a fail risk $\delta = 0.02$ are desired, then the number of samples should be taken is $N \geq 46 \times 10^3$. In this work, for the computation of the reachable sets, it was tested that for $N > 50 \times 10^3$ no improvement over the approximation of sets was obtained. Thus, $N = 50 \times 10^3$ was selected as the number of samples for the state variables and the inputs for the computation of all the reported simulations regarded to the reachable sets. On the other hand, for a good estimation of the controllable sets, it was necessary to choose a different number of samples for the states variables and for the inputs. This is justified due to the fact that during the computation of the controllable sets a percentage of the computed trajectories could not belong to the set of the end-product quality specifications. Then causing the lost of several of those computed trajectories. Consequently, to obtain a good estimation of the controllable sets, it was necessary to take ten times more samples of the inputs than the state variables. That was, $N = 50 \times 10^3$ for the state variables and $N = 500 \times 10^3$ for the inputs. Then, every state initial condition was combined with ten different inputs values. It is remarked here that an additionally simulation was performed where the same number of samples ($N = 50 \times 10^3$) were taken for both the states variables and inputs. However, no difference in the estimation of the controllable sets was observed, but combining an initial condition with different inputs values was more efficient. Table 5.1 summarizes the simulation parameters for the computation of both the reachable and the controllable sets.

Controllable sets computation

From the product quality viewpoint, end-use properties of latexes obtained by the emulsion polymerization are highly correlated with the final PSD of the latex (Sheibat-Othman et al., 2017). Therefore, it is very common in emulsion polymerization applications to establish the final shape of the PSD as the primary controlled output (Crowley et al., 2000; Dokucu, Park, and Doyle, 2008b; Puschke and Mitsos, 2016). Regarding the final shape of the PSD, either of the following two different control objectives can be established to control the process such that both final value of the average and final value of the standard deviation of the PSD are: ***1.*** attained or ***2.*** kept inside some defined lower and upper bounds. The first objective forces to control the process to a specific narrow $\mathcal{Y}_f$ set, for instance, only a predefined final PSD shape is allowed. The second objective gives a more flexible alternative due to the fact the system is operated such that not a specific PSD must be obtained but only its mean value and standard deviation must be bounded. Besides, the secondary particle nucleation rate N_s also plays an important role in the end-use properties of structured latexes. If a very high number of new polymer particles of the monomer M are formed, the polymer quality would be deteriorated and the final PSD becomes affected (Ferguson, Russell, and Gilbert, 2002). Therefore, an additional restriction for the process operation could be defined such that N_s is kept as lower as possible

TABLE 5.1: Simulation parameters for the computation of the reachable and the controllable sets.

Initial conditions for the reachable sets computation		
State	**Value**	**Units**
V	1.1743×10^6	cm^3
Φ_{aq}	0.7223	
$[I]_{aq}$	4.9149×10^{-8}	mol/cm^3
$[M]_p$	1.0229×10^{-4}	mol/cm^3
T	332.2694	K
$\bar{r}$	55.8228	nm
σ_r	5.8907	nm
Initial conditions set for the controllable sets computation		
State	**Interval**	**Units**
V	$[1 \times 10^6, 2.5 \times 10^6$	cm^3
Φ_{aq}	$[0.45, 0.75]$	
$[I]_{aq}$	$[4.2 \times 10^{-8}, 1.7 \times 10^{-7}]$	mol/cm^3
$[M]_p$	$[0, 1.8 \times 10^{-4}]$	mol/cm^3
T	$[328.15, 348.15]$	K
$\bar{r}$	$[53, 90]$	nm
σ_r	$[5, 15]$	nm
Admissible inputs set		
Input	**Interval**	**Units**
F_M	$[21, 62.5]$	cm^3/s
F_I	$[7, 21]$	cm^3/s
T_j	$[323.15, 353.15]$	K

during the whole batch time. Furthermore, the advantage of the multiscale modeling approach of the EP process over traditional modeling approaches is the possibility of verifying whether it would exist a feasible trajectory to control the process by keeping N_s as low as possible, ideally close to zero. That is a trajectory that could minimize the rate of secondary nucleation along the batch time.

As secondary controlled outputs, relevant process states can be selected and end-batch constrains specified. For the adopted EP process, those relevant states are V, $[M]_p$, and T. Constraints as maximum monomer concentration inside the polymer particles $[M]_p$ and maximum final volume of the reactor V could be taken into account as well as maximum and minimum allowed reactor temperatures T, which is the key process variable operation for keeping the free-radical associated reactions activated. The primary controlled output and all the additional states constraints should be met taking into account the physical limitations of the process inputs such as the maximum and minimum flow rates or the maximum cooling jacket capacity, to be taken into account in the definition of the admissible inputs (Hosseini, Oshaghi, and Engell, 2013; Gil, Vargas, and Corriou, 2016).

Figures 5.1a,b show the reachable sets for ten different equidistant moments in time of both average and standard deviation of the PSD, respectively. From Figures 5.1a,b, it is observed how both the mean and standard deviation of the PSD can evolve

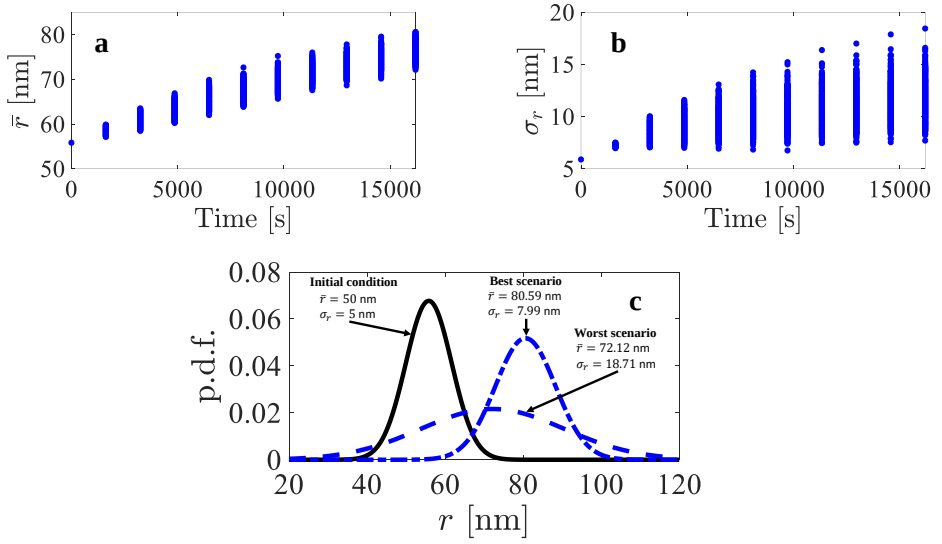

FIGURE 5.1: Feasible PSD shapes based on the reachable sets. **a** $\bar{r}$ reachable sets. **b** σ_r reachable sets. **c** PSD worse and best scenarios.

given the set of admissible inputs. By taking the maximum and minimum values of $\bar{r}$ and σ_r at the final time, the PSDs in Figure 5.1c are obtained. Figure 5.1c shows the initial condition as well as both worst and best scenarios of the reachable PSD at the end of the batch time. The worst scenario is composed by the minimum $\bar{r}$ and the maximum σ_r, which represents the lowest batch reactor yield and highest particles size dispersion. On the other hand, the best scenario is composed by the maximum $\bar{r}$ and the minimum σ_r, which represents the highest batch rector yield with the lowest particles size dispersion. The remarkable fact here is that, establishing as control objective the case **2.**, where both the final value of the average and the final value of the standard deviation of the PSD are kept inside a defined upper and lower bounds, any PSD shape within the worst and the best scenarios can be selected.

Figure 5.2 also shows the reachable sets computed for N_s by means of equation (4.34), the closed-form model of the secondary nucleation rate. From Figure 5.2, it is possible to observe that even if the initial condition of N_s is different from zero, it could be possible to reach the condition $N_s = 0$ at time $t = 0.45$ h and that condition could be hold during the remaining batch time. However, Figure 5.2 shows as well that under some conditions N_s could never be equal to zero through the whole batch time.

Figure 5.3 shows reachable sets for the macroscopic state variables. Results reported in Figure 5.3 allows identifying which are the realistic values that can be chosen as end-batch constraints. From Figures 5.3b,c, it is verified the boundedness of the states that are not taken as controlled outputs, namely, Φ_{aq}, and $[I]_{aq}$, which indeed remain bounded over the whole batch time. Additionally, from Figure 5.3a, it is possible to see that the reachable set of V at the final simulated time belongs to the interval $[1.85 \times 10^6, 2.21 \times 10^6]$ cm^3; from Figure 5.3d, it is possible to observe that

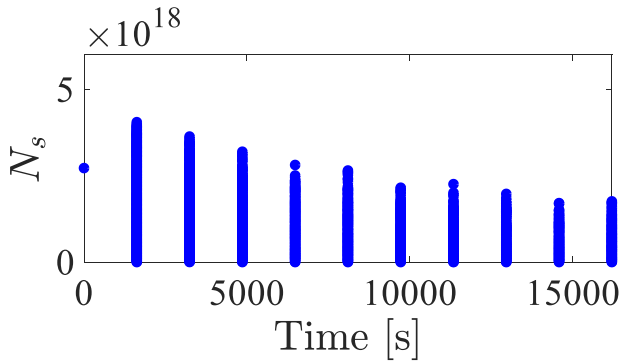

FIGURE 5.2: Reachable N_s set.

the reachable set of $[M]_p$ at the final simulated time belongs to the interval $[0.27 \times 10^{-4}, 1.66 \times 10^{-4}]$ mol/cm^3; and, from Figure 5.3e, it is possible to observe that the reachable set of T at the final simulated time belongs to the interval $[328.5, 347.2]$ K. Therefore, the end-batch constraints for V, $[M]_p$, and T should be established within those intervals.

In summary, from the reachable sets analysis, the following boundaries were found from the reachable sets for the primary controlled outputs at time t_f: $\bar{r} = [72.12, 80.59]$ nm, $\sigma_r = [7.99, 18.71]$ nm, $N_s = [0, 1.76 \times 10^{18}]$ No. of new formed particles/V, and the following boundaries were found from the reachable sets for the secondary controlled outputs at time t_f: $V = [1.85 \times 10^6, 2.21 \times 10^6]$ cm^3, $[M]_p = [0.27 \times 10^{-4}, 1.66 \times 10^{-4}]$ mol/cm^3, and $T = [328.5, 347.2]$ K.

Computation of the Controllable Trajectories Set

Three simulation cases are considered to check the existence of a non-empty CTS. The following three different scenarios are established by considering the reachable sets obtained at the end of the batch time, t_f. In scenario ***1***, the control objective is selected such that narrow end-batch specifications are defined and the outputs are constrained to be inside the reachable set at time t_f. Examples dealing with this type of scenario include the works by Liotta, Georgakis, and El-Aasser (1997); Immanuel and III (2002); Doyle, Harrison, and Crowley (2003); Dokucu, Park, and Doyle (2008a). In scenario **2**, the control objective is defined such that the output constraints fulfill certain upper or lower final end-product quality specifications but are not restricted to a specific value or small region. Those constraints are defined so that the final end-product quality specifications belong to the interior of reachable sets at time t_f, but are flexible enough to easily control the process into them. This type of scenario have has been addressed in the works by Semino and Ray (1995); Liotta et al. (1997); Crowley et al. (2000); Flores-Cerrillo and MacGregor (2002); Immanuel, Wang, and Bianco (2008). Finally, in scenario **3**, the control objective is defined as in the scenario 2, but the upper and lower constraints are shifted up such that the controllable sets at time t_f could be shrunk. Therefore, not only the probability of

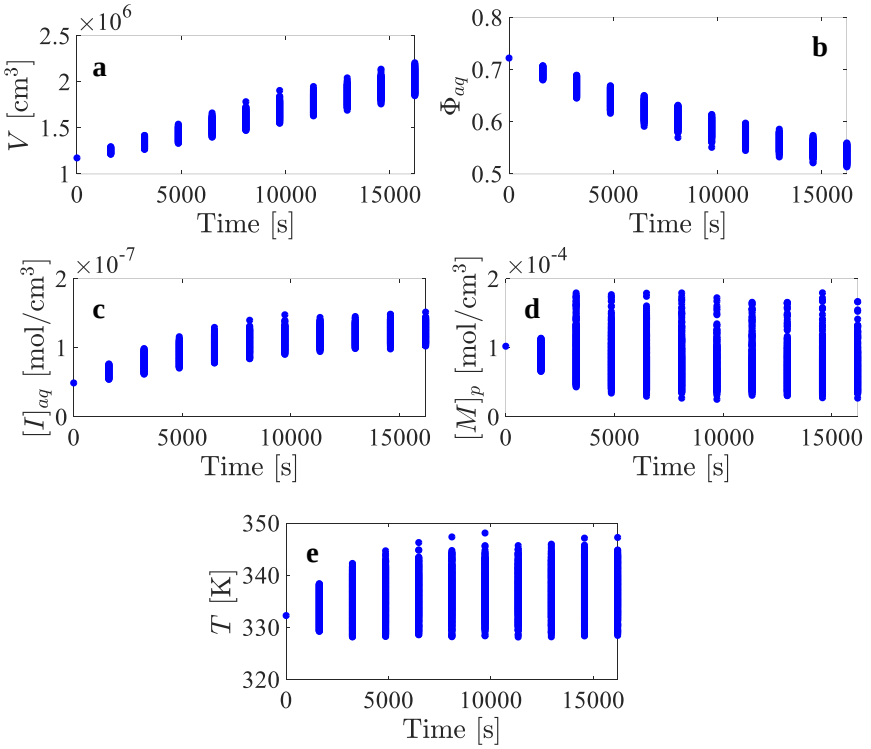

FIGURE 5.3: Reachable macroscopic states sets: **a.** V cm^3, **b.** Φ_{aq}, **c.** $[I]_{aq}$ mol/cm^3, **d.** $[M]_p$ mol/cm^3, **e.** T [K].

reaching the end-batch specifications diminishes but the control action availability to reject any external disturbance at the end of the batch time could decrease as well (Gómez-Pérez, Gómez, and Alvarez, 2015), resulting in a reduction in the size of the CTS. Some published works dealing with this scenario type are the works by Gentric et al. (1999); Vicente, Leiza, and Asua (2003); Zeaiter, Romagnoli, and Gomes (2006).

The purpose of formulating the scenario **2** is to show the effectiveness of the batch output-controllability analysis for engineering applications where it is not required to meet too conservative but minimum yield specifications. Once those minimum yield requirements are met, all the remaining constraints can be relaxed. The aim of formulating scenario ***3*** is to show that if the end-batch specifications are settled such that the process yield is maximized (i.e. to produce polymer particles as higher as possible with a small dispersion, as the best scenario shown in Figure 5.1), the CTS size is shrunk over the whole batch time. This could imply a diminishing process capacity to deal with the uncertainties and disturbances or, in other words, the system control capacity decreases.

Table 5.2 summarizes the output bounds which define the sets of the end-batch specifications for the computation of both the controllable set and the CTS for scenario ***1***, scenario **2**, and scenario ***3***, respectively.

It is remarked from Table 5.2 that the most restrictive condition in scenario ***1*** is for $\bar{r}$, which corresponds to a tolerance of 5% for that output. In the N_s case, the tolerance

TABLE 5.2: Output bounds for the sets of the end-batch specifications for the computation of both the controllable set and the CTS for scenario ***1***, scenario **2**, and scenario ***3***.

	Scenario		
Outputs	$\mathcal{Y}_{f_{sc1}}$	$\mathcal{Y}_{f_{sc2}}$	$\mathcal{Y}_{f_{sc3}}$
V	$[1.90 \times 10^6, 2.20 \times 10^6]$	$[1.90 \times 10^6, --]$	$[1.97 \times 10^6, --]$
$[M]_p$	$[0.36 \times 10^{-4}, 0.72 \times 10^{-4}]$	$[--, 0.72 \times 10^{-4}]$	$[--, 0.54 \times 10^{-4}]$
$\bar{r}$	$[75.20, 77.05]$	$[75.20, --]$	$[78.90, --]$
σ_r	$[8.00, 10.00]$	$[--, 11.00]$	$[--, 9.50]$
N_s	$[0, 0.59 \times 10^{18}]$	$[--, 0.59 \times 10^{18}]$	$[--, 0.38 \times 10^{18}]$

is of 10%, while for V, $[M]_p$, and σ_r tolerance are 20%, 20%, and 15%, respectively. It is also remarked that for scenario ***2*** and scenario ***3*** only upper or lower restrictions are established for each of the outputs, which implies a relaxation of the control objectives.

Figure 5.4 shows both the controllable and the controllable trajectories sets for scenario ***1***. From Figure 5.4, it is possible to observe that indeed is possible to drive the system from the initial condition Ω_0 to the final desired condition $\mathcal{Y}_f$. In particular, it is possible to see that $\bar{r}$ is successfully driven to a narrow final condition, while, at the same time, σ_r is restricted to be inside a particular interval. Another important observed result is that there exists a set of possible trajectories to follow such that the polymer particles can be produced with the desired size while keeping N_s close to zero. Finally, from Figure 5.4, it is possible to observe that the imposed restrictions to V and $[M]_p$ are met. In conclusion, because the control objective in scenario ***1*** can be fulfilled and all the constraints are met, the output-controllability for that scenario is successfully verified, which means that the process can be controlled to those selected end-batch specifications.

Figure 5.5a shows the controllable sets for scenario **2**. Figure 5.5b shows the controllable sets for scenario ***3***. Figure 5.5c shows the overlapping of the CTS for scenarios **2** and ***3***. From Figure 5.5a, it is possible to observe that the results for scenario **2** are quiet similar to the results for scenario ***1*** (see Figure 5.4a). The most evident differences are the sizes in the controllable sets for both $\bar{r}$ and σ_r at time t_f, these are bigger for scenario **2** because of the relaxation in the end-batch specifications. On the other hand, by comparing the controllable sets between scenario **2** and scenario ***3*** (see Figure 5.5a and Figure 5.5b, respectively), it is possible to observe a difference in their size, time by time, in each of the controllable sets, for every output. This is due to the fact that the end-batch specifications in scenario ***3*** are more restrictive than those defined in scenario **2**. The end-batch specifications in scenario ***3*** cause that all the controllable sets shrank. Finally, Figure 5.5c compares the CTS for scenario **2** and scenario ***3***. There, it is possible to observe that, time by time, all the CTS related to scenario **2** have a bigger size compared to the CTS related to scenario ***3***. Again, this is the result of the different end-batch specifications defined for each scenario.

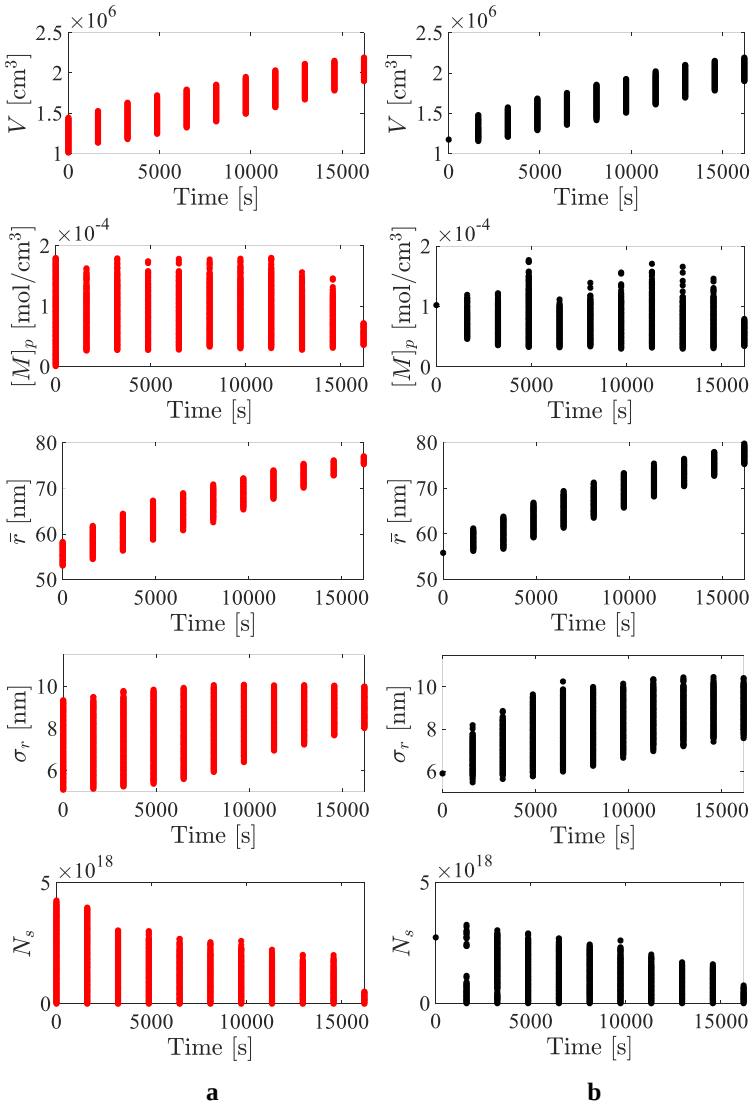

FIGURE 5.4: Controllable sets and CTS for scenario **1**.

Scenario ***2*** takes into account a wide end-batch specification in comparison to the narrow end-batch specification for scenario ***3***.

In conclusion, because the control objectives are fulfilled and all the constraints are met, the batch output-controllability has been successfully verified for both, scenario ***2*** and scenario ***3***, meaning that the process can be controlled to the selected end-batch specifications. The remarkable difference between scenario ***2*** and scenario ***3*** is that the CTS is smaller for scenario ***3*** than the CTS for scenario **2**, which could imply a decrease in the capacity of the system to reject disturbances. Additionally, it is remarked that by means of a batch output-controllability analysis applied to multiscale systems as the case study showed here, trial and error approaches, often adopted at industry to design materials with microscopic specifications, could be replaced for a more systematic approach where the manipulation of the events occurring at the fine scales can be linked to the dynamics at the coarse scales. Then

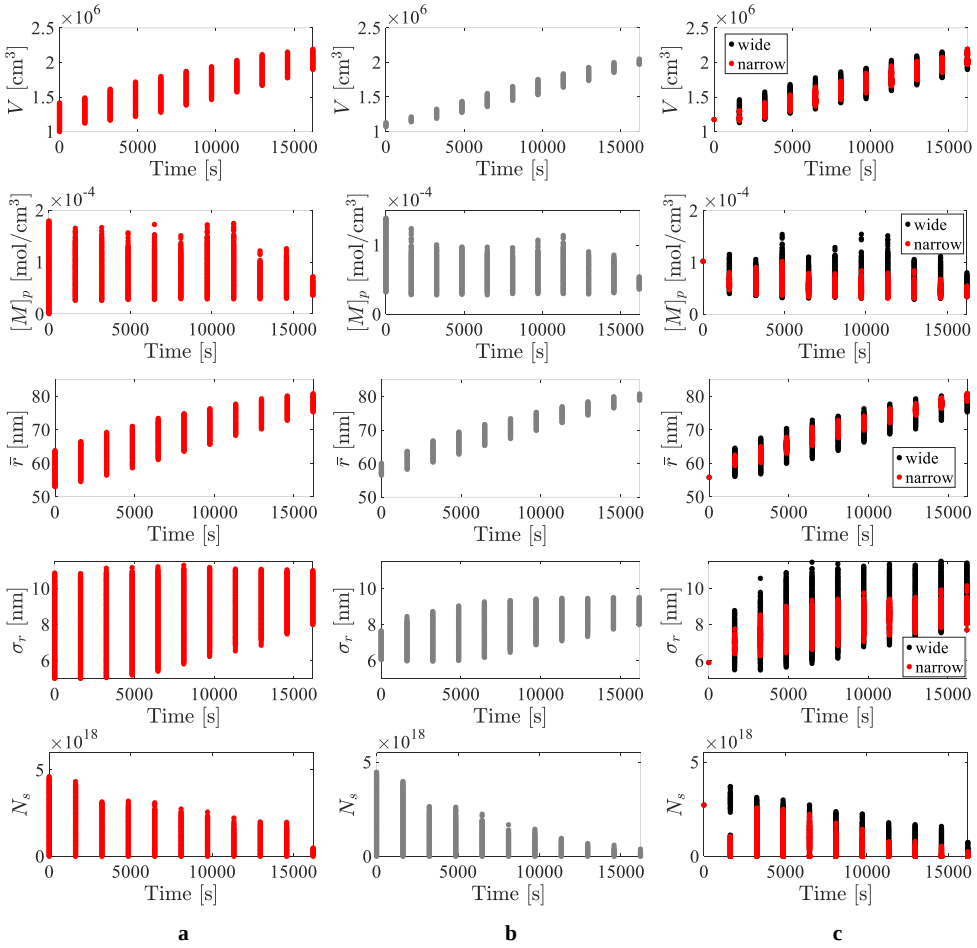

FIGURE 5.5: Controllable sets and CTS for scenarios *2* and *3*.

such finer scales can be controlled through the manipulation of the process inputs to improve the overall product quality.

5.3 Chapter concluding remarks

The batch output-controllability was applied to a semi-batch emulsion polymerization process where three different scenarios were simulated. In the first scenario was demonstrated that if the end-product quality specifications belongs to the inside of reachable set at the end-batch time, then indeed exist a non-empty set of controllable trajectories through the system can be driven to fulfill the end-batch product quality specifications. Scenarios two and three were designed to show that the size of the CTS can be affected by the selection of the end-batch specifications. Very restrictive end-batch specifications shrunk the CTS and could make the system more susceptible to the external disturbances or model uncertainties. Therefore, it was evidenced that not only the final end-product quality specification but the size of the CTS should take into account to successfully operate the process. The advantage of performing the batch output-controllability based on the set-theoretic approach

is that the sets information could be used to determine the multiscale process performance limitations and to better design a robust control strategy which not only accounts for macroscopic control objectives but for mesoscopic and microscopic as well.

Chapter 6

Conclusions and future work

6.1 General Conclusions

A framework for obtaining a control-oriented model from a multiscale perspective which describes the dynamic evolution of a free-radical emulsion polymerization process was successfully implemented. The developed multiscale model includes the traditional macroscopic and mesoscopic dynamics of the free-radical emulsion polymerization process, and also the average number of free-radicals and secondary nucleation rate. These two microscopic states are critical to satisfactorily obtaining structured polymer particles with the desired size and morphology. Results of the multiscale model simulation showed consistency with respect to experimental results reported in the literature.

Two contributions were done regarding the computational efficiency of the full free-radical emulsion polymerization multiscale model. The first contribution was the solution of the Fokker-Planck Equation (FPE) by using a Finite Element Method (FEM) which allowed to accurately capture the nonlinear evolution of Particle Size Distribution (PSD). Additionally, the multiscale problem was defined in an element-wise fashion allowing the solution of both macroscopic and microscopic scales locally within each element. Then, the local solution was assembled in the usual FEM way which saved a lot of effort in the coding procedure and allowed the implementation of an efficient computational solution. The second contribution was the development of a closed-form model of the kinetic Monte Carlo (kMC) simulation. The closed-form model derivation was treated as a statistical modeling problem which made the problem only dependent on the quality of the dataset used to build the regression. That is, if the closed-form model prediction wants to be improved, only more kMC simulations are required to increase the size and diversity of database. By using this closed-form model, the computational time required to solve the FPE-based multiscale model was dramatically reduced requiring only 2.15% of the computational time with respect to the FPE-kMC model and with a low impact over the accuracy of the solution. Furthermore, the required computational time to solve the model combining the mesoscale reduced-order approach and the closed-form for the microscopic scale required 0.01% of the computational time with respect to the

full multiscale model (FPE-kMC representation). Because of the development of the closed-form model of the microscopic scale and the computational cost reduction on the model solution, this multiscale approximation could be used when implementing, e.g., a real-time optimization of the process to control the product quality at the microscopic scale which is the final aim of the application.

Bhattacharyya distance was adopted to measure the similarities between the final PSDs obtained by considering four different model configurations, namely, FEM-kMC (or the full multiscale model), FEM-ClosedForm, RO-kMC, and RO-ClosedForm (the full reduced-order model). It was showed that the four considered model configurations evolved towards a similar PSD. Moreover, different simulations were performed to test that the closed-form model of the microscopic scale was able to successfully capture the main dynamics of the kMC simulation. Because of the good trade-off between predictability and simplicity, and the overall low computational cost, the RO-ClosedForm model appears as a suitable tool to be used when implementing optimization/control strategies to achieve the desired process yield.

A batch output-controllability analysis for a multiscale system was successfully applied by using the RO-ClosedForm model. Three different scenarios were simulated to verify the batch output-controllability analysis. In the first scenario was demonstrated that if the end-product quality specifications belongs to the inside of reachable set at the end-batch time, then indeed exist a non-empty set of controllable trajectories through the system can be driven to fulfill the end-batch product quality specifications. Scenarios two and three were designed to show that the size of the CTS can be affected by the selection of the end-batch specifications. Very restrictive end-batch specifications shrunk the CTS and could make the system more susceptible to the external disturbances or model uncertainties. Therefore, it was evidenced that not only the final end-product quality specification but the size of the CTS should be taken into account to successfully operate the process. The advantage of performing the batch output-controllability based on the set-theoretic approach is that the sets information could be used to determine the multiscale process performance limitations and to better design a robust control strategy which not only accounts for macroscopic control objectives but for mesoscopic and microscopic as well.

It is worthy to remark that, by using the framework presented in this work, it is possible to develop a control-oriented models from a multiscale perspective capturing information of the process from different length scales and combining both a good accuracy in the representation and low computational cost to its numerical solution. On the other hand, by means of the batch output-controllability analysis applied to the multiscale system, trial and error approaches (often adopted at industry to design materials and devices with microscopic specifications), could be replaced for a more systematic approach where the manipulation of the events occurring at the finer scales would be linked to the dynamics at the coarse scales. This link among

scales can be exploited to control the process fulfilling some microscopic product quality specifications. A common requirement within the specialized chemical industry.

6.2 Future work

The current research can potentially be extended in different ways as follows:

Multiscale modeling of the free-radical emulsion polymerization process: The main goal during the the development of the model representing the emulsion polymerization process was the integration of the macro-, meso, and micro-scopic scales in a consistent framework. The key aspect for doing so was the understanding about the required information by the kMC simulation such that the right information was propagated up and down among the scales. Consequently, both the macro- and meso-scopic scales models were kept as simple as possible and the main effort was put on the kMC simulation. Based on this, as future work, both the macro- and meso-scpic scales models can be improved. Some ideas to improve the model at the macroscopic scale are: ***i.*** some impurities on both the initiator and monomer feeds can be incorporated in their respective balances; ***ii.*** the shrinkage phenomena of the polymer particles can be incorporated on the volume balance; and ***iii.*** the polymerization kinetics considering the reactions occurring in the aqueous phase can be added to the polymerization reaction taking into account only the reaction on the polymer phase. Some ideas to improve the model at the mesoscopic scale are: ***i.*** to incorporate the nucleation and coagulation phenomena of the polymerization process as a source term in the Fokker-Planck Equation; ***ii.*** to link the secondary nucleation rate with the Fokker-Planck Equation such that the population new formed particles appears on this scale giving a bimodal particle size distribution; ***iii.*** to define the polymer particles morphology as an additional internal variable for the derivation of a multidimensional Fokker-Planck Equation which represents not only the particles size but their morphology as a set of couple partial differential equations.

Order reduction of the multiscale model: In this work, the Variance Algebra approach was adopted to derive a reduced-order model for the mesoscopic scale. The reduced-order model was able to successfully capture the two first statistical moments of the particle size distribution under the assumption that the polymer particles grow following a Gaussian distribution and it holds during the whole polymerization reaction time. However, it was evidenced from the Fokker-Planck Equation solution that the particle size distribution evolves from a Gaussian distribution towards a skew-like Gaussian distribution. To overcome this limitation of the Variance Algebra approach, one alternative could be to include additional statistical moments in the reduced-order model derivation or to assume a log-normal distribution of the polymer particles and to derive the same two statistical moments from the same

Variance Algebra methodology but capturing the skew-like Gaussian distribution at the end of the polymerization time. Another alternative could be to apply a model-order reduction technique such as the well-known Proper Orthogonal Decomposition framework directly over the Fokker-Planck Equation and to obtain a suitable set of basis functions able to capture its nonlinear evolution. However, the main limitation of this approach might be the requirement of a representative dataset of the solution of the full multiscale model to build the basis functions of the reduced-order model. This because to obtain a representative dataset of the full multiscale model would requires high computational resources.

Regarding the closed-form of the microscopic scale, a good option to improve its prediction capabilities could be the adoption of a so-called Gaussian Process Model. This kind of approach has shown to be a robust regression tool, also suitable for classification, and reinforcement learning tasks. Approaches based on Gaussian Process Models could be useful to clearly identify such conditions which minimize the secondary nucleation rate. In order to mitigate the computational cost could cause the construction of a Gaussian Process Model, some adaptive sampling techniques can be tested, where samples from the kMC simulation would be added to an existing dataset in an iterative procedure. A so-called surrogate model is then generated from available information with an intrinsic lack of knowledge, which in turn can be investigated and next used to obtain further observations. This iterative process can be guided to be performed in an optimal manner enlarging the dataset with only new relevant information and always trying to increase the closed-form model prediction capabilities.

Numerical solution of the multiscale model: The Finite Element Method formulation was kept as simple as possible meaning that none stabilization term was added for the convective part of the Fokker-Planck Equation. This was possible only by using a non-uniform mesh such that the Péclet number remained small. However, if the problem becomes highly advection dominated or the dimension of the problem becomes larger, the Discontinouos Galerkin method is suggested instead of the standard Galerkin method. The reason is that this method is naturally stable for advection-diffusion problems and locally conservative. The main drawback would be the complexity in the coding procedure. Some stabilization techniques based of the addition of an artificial diffusion would be first explored if they are required.

Control related tasks: In this work, a set-theoretic approach was adopted to verify whether a set of end-product quality specifications can be achieved by considering the process states and inputs constraints. The natural next step is the implementation of a control structure which effectively allows to reach such end-product quality specifications. However, some additional control related tasks could be performed as well using the sets information. A first task might be to maximize the process controllability. This can be achieved by computing the Controllable Trajectories Sets size and then defining an optimization problem where the cost function takes this

size information and then tries to maximize their size by varying some design parameter as the reactor volume, the heat transfer area between the reactor and the jacket, among others. Higher Controllable Trajectories Sets means improved process controllability. Another option would be the optimization of the process initial conditions such that the overall process controllability could be maximized. Last, but not least, the Controllable Trajectories Set information would be used as the constraints in an dynamical optimization problem to optimize the process performance, by implementing for example, a non-linear model predictive controller.

Bibliography

Aherne, Frank J, Neil A Thacker, and Peter I Rockett (1998). "The Bhattacharyya metric as an absolute similarity measure for frequency coded data". In: *Kybernetika* 34(4), pp. 363–368. URL: https://dml.cz/handle/10338.dmlcz/135216.

Araújo, Pedro Henrique Hermes et al. (2001). "Modeling Particle Size Distribution (PSD) in Emulsion Copolymerization Reactions in a Continuous Loop Reactor". In: *Macromolecular Theory and Simulations* 10(8), pp. 769–779. DOI: 10.1002/1521-3919(20011001)10:8<769::AID-MATS769>3.0.CO;2-Z. URL: https://onlinelibrary.wiley.com/doi/abs/10.1002/1521-3919(20011001)10:8<769::AID-MATS769>3.0.CO;2-Z.

Aumi, Siam and Prashant Mhaskar (2009). "Safe-steering of batch process systems". In: *AIChE Journal* 55(11), pp. 2861–2872. DOI: 10.1002/aic.11920. eprint: https://aiche.onlinelibrary.wiley.com/doi/pdf/10.1002/aic.11920. URL: https://aiche.onlinelibrary.wiley.com/doi/abs/10.1002/aic.11920.

Bajcinca, Naim et al. (2015). "Approximate ODE models for population balance systems". In: *Computers & Chemical Engineering* 74, pp. 158–168. DOI: https://doi.org/10.1016/j.compchemeng.2014.12.015. URL: https://www.sciencedirect.com/science/article/pii/S0098135414003445.

Beers, Kenneth J (2006). *Numerical methods for chemical engineering: applications in Matlab*. Cambridge University Press. DOI: 10.1017/CBO9780511812194. URL: https://doi.org/10.1017/CBO9780511812194.

Bertin, Diego et al. (2016). "Population balance discretization for growth, attrition, aggregation, breakage and nucleation". In: *Computers & Chemical Engineering* 84, pp. 132 –150. ISSN: 0098-1354. DOI: https://doi.org/10.1016/j.compchemeng.2015.08.011. URL: http://www.sciencedirect.com/science/article/pii/S0098135415002720.

Blanchini, F. (1999). "Set invariance in control". In: *Automatica* 35(11), pp. 1747 –1767. ISSN: 0005-1098. DOI: https://doi.org/10.1016/S0005-1098(99)00113-2. URL: http://www.sciencedirect.com/science/article/pii/S0005109899001132.

Bouaswaig, Ala Eldin and Sebastian Engell (2010). "Comparison of High Resolution Schemes for Solving Population Balances". In: *Industrial & Engineering Chemistry Research* 49(12), pp. 5911–5924. DOI: 10.1021/ie9020057. eprint: https://doi.org/10.1021/ie9020057. URL: https://doi.org/10.1021/ie9020057.

Braatz, RD et al. (2006). "Perspectives on the design and control of multiscale systems". In: *Journal of Process Control* 16(3), pp. 193–204. DOI: https://doi.org/

10.1016/j.jprocont.2005.06.001. URL: https://www.sciencedirect.com/science/article/pii/S0959152405000612.

Butte, Alessandro, Giuseppe Storti, and Massimo Morbidelli (2002). "Emulsion polymerization: radical segregation and its role in controlled polymerization". In: *Macromolecular Symposia* 182(1), pp. 181–194. DOI: 10.1002/1521-3900(200206)182:1<181::AID-MASY181>3.0.CO;2-T.

Calafiore, G., F. Dabbene, and R. Tempo (2003). "Randomized algorithms in robust control". In: *42nd IEEE International Conference on Decision and Control (IEEE Cat. No.03CH37475)*. Vol. 2, 1908–1913 Vol.2. DOI: 10.1109/CDC.2003.1272894.

Chaffart, Donovan, Shabnam Rasoulian, and Luis A Ricardez-Sandoval (2016). "Distributional uncertainty analysis and robust optimization in spatially heterogeneous multiscale process systems". In: *AIChE Journal* 62(7), pp. 2374–2390. DOI: https://doi.org/10.1002/aic.15215. URL: https://aiche.onlinelibrary.wiley.com/doi/full/10.1002/aic.15215.

Chaffart, Donovan and Luis A Ricardez-Sandoval (2017). "Robust dynamic optimization in heterogeneous multiscale catalytic flow reactors using polynomial chaos expansion". In: *Journal of Process Control* 60, pp. 128–140. DOI: https://doi.org/10.1016/j.jprocont.2017.07.002. URL: https://www.sciencedirect.com/science/article/pii/S0959152417301439.

Chaffart, Donovan and Luis A Ricardez-Sandoval (2018a). "Optimization and control of a thin film growth process: A hybrid first principles/artificial neural network based multiscale modelling approach". In: *Computers & Chemical Engineering* 119, pp. 465–479. DOI: https://doi.org/10.1016/j.compchemeng.2018.08.029. URL: https://www.sciencedirect.com/science/article/pii/S0098135418306379.

Chaffart, Donovan and Luis A Ricardez-Sandoval (2018b). "Robust optimization of a multiscale heterogeneous catalytic reactor system with spatially-varying uncertainty descriptions using polynomial chaos expansions". In: *The Canadian Journal of Chemical Engineering* 96(1), pp. 113–131. DOI: https://doi.org/10.1002/cjce.22912. URL: https://doi.org/10.1002/cjce.22912.

Chatterjee, Abhijit and Dionisios G. Vlachos (2006). "Multiscale spatial Monte Carlo simulations: Multigriding, computational singular perturbation, and hierarchical stochastic closures". In: *The Journal of Chemical Physics* 124(6), p. 064110. DOI: 10.1063/1.2166380. eprint: http://dx.doi.org/10.1063/1.2166380. URL: http://dx.doi.org/10.1063/1.2166380.

Chen, Junghui and Rong-Guey Sheui (2003). "Optimal batch trajectory design based on an intelligent data-driven method". In: *Industrial & engineering chemistry research* 42(7), pp. 1363–1378. DOI: 10.1021/ie020480y. URL: https://doi.org/10.1021/ie020480y.

Christofides, Panagiotis D. (2001). "Control of nonlinear distributed process systems: Recent developments and challenges". In: *AIChE Journal* 47(3), pp. 514–518. ISSN: 1547-5905. DOI: 10.1002/aic.690470302. URL: http://dx.doi.org/10.1002/aic.690470302.

Christofides, Panagiotis D. and Antonios Armaou (2006). "Control and optimization of multiscale process systems". In: *Computers & Chemical Engineering* 30(10). Papers form Chemical Process Control VII, pp. 1670 –1686. ISSN: 0098-1354. DOI: https://doi.org/10.1016/j.compchemeng.2006.05.025. URL: http://www.sciencedirect.com/science/article/pii/S0098135406001323.

Cogoni, Giuseppe et al. (2014). "A qualitative comparison between population balances and stochastic models for non-isothermal antisolvent crystallization processes". In: *Computers & Chemical Engineering* 63, pp. 82–90. DOI: 10.1016/j.compchemeng.2014.01.001. URL: http://www.sciencedirect.com/science/article/pii/S0098135414000039.

Crose, Marquis et al. (2015). "Multiscale modeling and operation of {PECVD} of thin film solar cells". In: *Chemical Engineering Science* 136. Control and Optimization of Smart Plant Operations, pp. 50 –61. ISSN: 0009-2509. DOI: https://doi.org/10.1016/j.ces.2015.02.027. URL: http://www.sciencedirect.com/science/article/pii/S0009250915001426.

Crose, Marquis et al. (2017). "Multiscale modeling and run-to-run control of {PECVD} of thin film solar cells". In: *Renewable Energy* 100. Special Issue: Control and Optimization of Renewable Energy Systems, pp. 129 –140. ISSN: 0960-1481. DOI: https://doi.org/10.1016/j.renene.2016.06.065. URL: http://www.sciencedirect.com/science/article/pii/S0960148116305961.

Crowley, Timothy J. et al. (2000). "Control of particle size distribution described by a population balance model of semibatch emulsion polymerization". In: *Journal of Process Control* 10(5), pp. 419 –432. ISSN: 0959-1524. DOI: https://doi.org/10.1016/S0959-1524(00)00017-2. URL: http://www.sciencedirect.com/science/article/pii/S0959152400000172.

D'hooge, Dagmar R. et al. (2016). "The strength of multi-scale modeling to unveil the complexity of radical polymerization". In: *Progress in Polymer Science* 58(Supplement C). Topical Volume Polymer Chemistry, pp. 59 –89. ISSN: 0079-6700. DOI: https://doi.org/10.1016/j.progpolymsci.2016.04.002. URL: http://www.sciencedirect.com/science/article/pii/S0079670016300053.

Dimitratos, John, Guillermo Elicabe, and Christos Georgakis (1994). "Control of emulsion polymerization reactors". In: *AIChE Journal* 40(12), pp. 1993–2021. ISSN: 1547-5905. DOI: 10.1002/aic.690401210. URL: http://dx.doi.org/10.1002/aic.690401210.

Dokucu, Mustafa T., Myung-June Park, and Francis J. Doyle (2008a). "Multi-rate model predictive control of particle size distribution in a semibatch emulsion copolymerization reactor". In: *Journal of Process Control* 18(1), pp. 105 –120. ISSN: 0959-1524. DOI: https://doi.org/10.1016/j.jprocont.2007.04.002. URL: http://www.sciencedirect.com/science/article/pii/S0959152407000753.

Dokucu, Mustafa T., Myung-June Park, and Francis J. Doyle (2008b). "Reduced-order methodologies for feedback control of particle size distribution in semibatch emulsion copolymerization". In: *Chemical Engineering Science* 63(5). Control

of Particulate Processes, pp. 1230 –1245. ISSN: 0009-2509. DOI: https://doi.org/10.1016/j.ces.2007.07.021. URL: http://www.sciencedirect.com/science/article/pii/S0009250907005155.

Donea, Jean and Antonio Huerta (2003a). "Steady Transport Problems". In: *Finite Element Methods for Flow Problems*. John Wiley & Sons, Ltd. Chap. 2, pp. 33–78. ISBN: 9780470013823. DOI: 10.1002/0470013826.ch2. eprint: https://onlinelibrary.wiley.com/doi/pdf/10.1002/0470013826.ch2. URL: https://onlinelibrary.wiley.com/doi/abs/10.1002/0470013826.ch2.

Donea, Jean and Antonio Huerta (2003b). "Unsteady Convection-Diffusion Problems". In: *Finite Element Methods for Flow Problems*. John Wiley & Sons, Ltd. Chap. 5, pp. 209–264. ISBN: 9780470013823. DOI: 10.1002/0470013826.ch5. eprint: https://onlinelibrary.wiley.com/doi/pdf/10.1002/0470013826.ch5. URL: https://onlinelibrary.wiley.com/doi/abs/10.1002/0470013826.ch5.

Doyle, Francis J., Christopher A. Harrison, and Timothy J. Crowley (2003). "Hybrid model-based approach to batch-to-batch control of particle size distribution in emulsion polymerization". In: *Computers & Chemical Engineering* 27(8). 2nd Pan American Workshop in Process Systems Engineering, pp. 1153 –1163. ISSN: 0098-1354. DOI: https://doi.org/10.1016/S0098-1354(03)00043-7. URL: http://www.sciencedirect.com/science/article/pii/S0098135403000437.

Evans, R David and Luis A Ricardez-Sandoval (2014). "Multi-scenario modelling of uncertainty in stochastic chemical systems". In: *Journal of Computational Physics* 273, pp. 374–392. DOI: 10.1016/j.jcp.2014.05.028. URL: https://www.sciencedirect.com/science/article/pii/S002199911400374X.

Ferguson, Christopher J., Gregory T. Russell, and Robert G. Gilbert (2002). "Modelling secondary particle formation in emulsion polymerisation: application to making core-shell morphologies". In: *Polymer* 43(17), pp. 4557 –4570. ISSN: 0032-3861. DOI: https://doi.org/10.1016/S0032-3861(02)00311-7. URL: http://www.sciencedirect.com/science/article/pii/S0032386102003117.

Finlayson, B. (2013). *The Method of Weighted Residuals and Variational Principles*. Society for Industrial and Applied Mathematics: Philadelphia, PA. DOI: 10.1137/1.9781611973242. eprint: https://epubs.siam.org/doi/pdf/10.1137/1.9781611973242. URL: https://epubs.siam.org/doi/abs/10.1137/1.9781611973242.

Flores-Cerrillo, Jesus and John F. MacGregor (2002). "Control of Particle Size Distributions in Emulsion Semibatch Polymerization Using Mid-Course Correction Policies". In: *Industrial & Engineering Chemistry Research* 41(7), pp. 1805–1814. DOI: 10.1021/ie010500g. eprint: https://doi.org/10.1021/ie010500g. URL: https://doi.org/10.1021/ie010500g.

Flotron, Stéphane and Jacques Rappaz (2013). "Conservation schemes for convection-diffusion equations with Robin boundary conditions". In: *ESAIM: Mathematical Modelling and Numerical Analysis* 47(6), pp. 1765–1781. DOI: 10.1051/m2an/2013087. URL: https://doi.org/10.1051/m2an/2013087.

Gathungu, Duncan Kioi and Alfio Borzì (2017). "A multigrid scheme for solving convection–diffusion-integral optimal control problems". In: *Computing and Visualization in Science*, pp. 1–13. DOI: https://doi.org/10.1007/s00791-017-0285-7. URL: https://link.springer.com/article/10.1007/s00791-017-0285-7.

Gentric, C. et al. (1999). "Optimization and non-linear control of a batch emulsion polymerization reactor". In: *Chemical Engineering Journal* 75(1), pp. 31 –46. ISSN: 1385-8947. DOI: https://doi.org/10.1016/S1385-8947(98)00116-8. URL: http://www.sciencedirect.com/science/article/pii/S1385894798001168.

Gil, I.D., J.C. Vargas, and J.P. Corriou (2016). "Optimal nonlinear control of an industrial emulsion polymerization reactor". In: *Chemical Engineering Research and Design* 111(Supplement C), pp. 63 –82. ISSN: 0263-8762. DOI: https://doi.org/10.1016/j.cherd.2016.04.016. URL: http://www.sciencedirect.com/science/article/pii/S0263876216300764.

Gillespie, Daniel T (1976). "A general method for numerically simulating the stochastic time evolution of coupled chemical reactions". In: *Journal of Computational Physics* 22(4), pp. 403 –434. ISSN: 0021-9991. DOI: https://doi.org/10.1016/0021-9991(76)90041-3. URL: http://www.sciencedirect.com/science/article/pii/0021999176900413.

Gillespie, Daniel T. (1977). "Exact stochastic simulation of coupled chemical reactions". In: *The Journal of Physical Chemistry* 81(25), pp. 2340–2361. DOI: 10.1021/j100540a008. URL: https://doi.org/10.1021/j100540a008.

Gillespie, Daniel T. (2007). "Stochastic Simulation of Chemical Kinetics". In: *Annual Review of Physical Chemistry* 58(1). PMID: 17037977, pp. 35–55. DOI: 10.1146/annurev.physchem.58.032806.104637. eprint: https://doi.org/10.1146/annurev.physchem.58.032806.104637. URL: https://doi.org/10.1146/annurev.physchem.58.032806.104637.

Gómez, César A, Lina M Gómez, and Hernán D Alvarez (2010). "An approach to stability and controllability analysis in batch processes using set theory methods". In: *ANDESCON, 2010 IEEE*. IEEE, pp. 1–6. DOI: 10.1109/ANDESCON.2010.5633227. URL: https://ieeexplore.ieee.org/document/5633227.

Gómez, LM et al. (2015). "State Controllability Analysis for Irreversible Systems Using Set Theory". In: *Revista Iberoamericana de Automática e Informática Industrial RIAI* 12(2), pp. 145–153. DOI: https://doi.org/10.1016/j.riai.2015.02.002. URL: https://www.sciencedirect.com/science/article/pii/S1697791215000047.

Gómez-Pérez, C. A., L. M. Gómez, and Hernan Alvarez (2015). "Reference Trajectory Design Using State Controllability for Batch Processes". In: *Industrial & Engineering Chemistry Research* 54(15), pp. 3893–3903. DOI: 10.1021/ie504809x. eprint: https://doi.org/10.1021/ie504809x. URL: https://doi.org/10.1021/ie504809x.

González, Alejandro H and Darci Odloak (2009). "A stable MPC with zone control". In: *Journal of Process Control* 19(1), pp. 110–122. DOI: https://doi.org/10.1016/

j.jprocont.2008.01.003. URL: https://www.sciencedirect.com/science/article/pii/S0959152408000097.

Gooneie, Ali, Stephan Schuschnigg, and Clemens Holzer (2017). "A Review of Multiscale Computational Methods in Polymeric Materials". In: *Polymers* 9(1). ISSN: 2073-4360. DOI: 10.3390/polym9010016. URL: http://www.mdpi.com/2073-4360/9/1/16.

Grosso, Massimiliano et al. (2010). "A stochastic formulation for the description of the crystal size distribution in antisolvent crystallization processes". In: *AIChE journal* 56(8), pp. 2077–2087. DOI: 10.1002/aic.12130. URL: https://aiche.onlinelibrary.wiley.com/doi/abs/10.1002/aic.12130.

Grosso, Massimiliano et al. (2011). "Stochastic approach for the prediction of PSD in crystallization processes: Formulation and comparative assessment of different stochastic models". In: *Industrial & Engineering Chemistry Research* 50(4), pp. 2133–2143. DOI: 10.1021/ie1010299. URL: https://doi.org/10.1021/ie1010299.

Gunawan, Rudiyanto, Irene Fusman, and Richard D. Braatz (2004). "High resolution algorithms for multidimensional population balance equations". In: *AIChE Journal* 50(11), pp. 2738–2749. DOI: 10.1002/aic.10228. eprint: https://onlinelibrary.wiley.com/doi/pdf/10.1002/aic.10228. URL: https://onlinelibrary.wiley.com/doi/abs/10.1002/aic.10228.

Haddad, Wassim M., VijaySekhar Chellaboina, and Sergey G. Nersesov (2008). "Time-reversal symmetry, Poincaré recurrence, irreversibility, and the entropic arrow of time: From mechanics to system thermodynamics". In: *Nonlinear Analysis: Real World Applications* 9(2), pp. 250 –271. ISSN: 1468-1218. DOI: https://doi.org/10.1016/j.nonrwa.2006.10.002. URL: http://www.sciencedirect.com/science/article/pii/S1468121806001313.

Hernandez, H (2016). "Variance algebra applied to dynamical systems". In: *ForsChem Research Reports* 2. DOI: 10.13140/RG.2.2.36507.26403. URL: https://www.researchgate.net/publication/311706912_Variance_algebra_applied_to_dynamical_systems.

Hernández, Hugo (2008). "Multiscale simulation of heterophase polymerization". PhD thesis. Max Planck Institute of Colloids and Interfaces. URL: https://publishup.uni-potsdam.de/frontdoor/index/index/docId/2370.

Hernandez, Hugo (May 2018). "Statistical Modeling and Analysis of Experiments without ANOVA". In: *ForsChem Research Reports* 5. DOI: 10.13140/RG.2.2.21499.00803. URL: https://www.researchgate.net/publication/325348729_Statistical_Modeling_and_Analysis_of_Experiments_without_ANOVA?channel=doi&linkId=5b0742634585157f8711701b&showFulltext=true.

Hernández, Hugo and Klaus Tauer (2007). "Brownian Dynamics Simulation of the Capture of Primary Radicals in Dispersions of Colloidal Polymer Particles". In: *Industrial & Engineering Chemistry Research* 46(13), pp. 4480–4485. DOI: 10.1021/ie070115c. eprint: http://dx.doi.org/10.1021/ie070115c. URL: http://dx.doi.org/10.1021/ie070115c.

Hernández, Hugo and Klaus Tauer (2008a). "Brownian dynamics and kinetic Monte Carlo simulation in emulsion polymerization". In: *18th European Symposium on Computer Aided Process Engineering*. Ed. by Bertrand Braunschweig and Xavier Joulia. Vol. 25. Computer Aided Chemical Engineering Supplement C. Elsevier, pp. 769 –774. DOI: https://doi.org/10.1016/S1570-7946(08)80134-4. URL: http://www.sciencedirect.com/science/article/pii/S1570794608801344.

Hernández, Hugo Fernando and Klaus Tauer (2008b). "Multiscale stochastic simulation of emulsion polymerization". In: *Proceedings AIChE Annual Meeting*.

Hosseini, A., M. Oshaghi, and S. Engell (2013). "Mid-course control of particle size distribution in emulsion polymerization using a hybrid model". In: *2013 IEEE International Conference on Control Applications (CCA)*, pp. 728–733. DOI: 10.1109/CCA.2013.6662836.

Hosseini, Alireza, Ala Eldin Bouaswaig, and Sebastian Engell (2012). "Comparison of classical population balance models of emulsion polymerization with experimental results and a stochastic extension". In: *Chemical Engineering Science* 72(Supplement C), pp. 179 –194. ISSN: 0009-2509. DOI: https://doi.org/10.1016/j.ces.2012.01.034. URL: http://www.sciencedirect.com/science/article/pii/S0009250912000437.

Hosseini, Alireza, Ala Eldin Bouaswaig, and Sebastian Engell (2013). "Novel approaches to improve the particle size distribution prediction of a classical emulsion polymerization model". In: *Chemical Engineering Science* 88(Supplement C), pp. 108 –120. ISSN: 0009-2509. DOI: https://doi.org/10.1016/j.ces.2012.11.021. URL: http://www.sciencedirect.com/science/article/pii/S0009250912006719.

Huang, Xingyi and Pingkai Jiang (2015). "Core-Shell Structured High-k Polymer Nanocomposites for Energy Storage and Dielectric Applications". In: *Advanced Materials* 27(3), pp. 546–554. DOI: 10.1002/adma.201401310. eprint: https://onlinelibrary.wiley.com/doi/pdf/10.1002/adma.201401310. URL: https://onlinelibrary.wiley.com/doi/abs/10.1002/adma.201401310.

Huo, B. P. et al. (1988). "Effect of impurities on emulsion polymerization: Case II kinetics". In: *Journal of Applied Polymer Science* 35(8), pp. 2009–2021. DOI: 10.1002/app.1988.070350803. eprint: https://onlinelibrary.wiley.com/doi/pdf/10.1002/app.1988.070350803. URL: https://onlinelibrary.wiley.com/doi/abs/10.1002/app.1988.070350803.

Immanuel, Charles D., Ying Wang, and Nicola Bianco (2008). "Feedback controllability assessment and control of particle size distribution in emulsion polymerisation". In: *Chemical Engineering Science* 63(5). Control of Particulate Processes, pp. 1205 –1216. ISSN: 0009-2509. DOI: https://doi.org/10.1016/j.ces.2007.07.050. URL: http://www.sciencedirect.com/science/article/pii/S000925090700512X.

Immanuel, Charles David and Francis Joseph Doyle III (2002). "Open-loop control of particle size distribution in semi-batch emulsion copolymerization using a genetic algorithm". In: *Chemical Engineering Science* 57(20). Particulate Processes, pp. 4415

–4427. ISSN: 0009-2509. DOI: https://doi.org/10.1016/S0009-2509(02)00355-X. URL: http://www.sciencedirect.com/science/article/pii/S000925090200355X.

Immanuel, Charles David and Francis Joseph Doyle III (2003). "Computationally efficient solution of population balance models incorporating nucleation, growth and coagulation: application to emulsion polymerization". In: *Chemical Engineering Science* 58(16), pp. 3681 –3698. ISSN: 0009-2509. DOI: https://doi.org/10.1016/S0009-2509(03)00216-1. URL: http://www.sciencedirect.com/science/article/pii/S0009250903002161.

Jahnke, Tobias (2011). "On reduced models for the chemical master equation". In: *Multiscale Modeling & Simulation* 9(4), pp. 1646–1676. DOI: 10.1137/110821500. URL: https://doi.org/10.1137/110821500.

John, Volker and Carina Suciu (2014). "Direct discretizations of bi-variate population balance systems with finite difference schemes of different order". In: *Chemical Engineering Science* 106, pp. 39–52. DOI: https://doi.org/10.1016/j.ces.2013.11.029. URL: https://www.sciencedirect.com/science/article/pii/S0009250913007653.

Kalman, Rudolf (1959). "On the general theory of control systems". In: *IRE Transactions on Automatic Control* 4(3), pp. 110–110. DOI: https://doi.org/10.1016/S1474-6670(17)70094-8. URL: https://www.sciencedirect.com/science/article/pii/S1474667017700948.

Karolius, Sigve and Heinz A. Preisig (2018). "Approaches to Multi-Scale Modeling from Systems Engineering". In: *13th International Symposium on Process Systems Engineering (PSE 2018)*. Ed. by Mario R. Eden, Marianthi G. Ierapetritou, and Gavin P. Towler. Vol. 44. Computer Aided Chemical Engineering. Elsevier, pp. 2221 –2226. DOI: https://doi.org/10.1016/B978-0-444-64241-7.50365-7. URL: http://www.sciencedirect.com/science/article/pii/B9780444642417503657.

Kazeev, Vladimir et al. (2014). "Direct solution of the chemical master equation using quantized tensor trains". In: *PLoS computational biology* 10(3). DOI: 10.1371/journal.pcbi.1003359. URL: https://www.ncbi.nlm.nih.gov/pmc/articles/PMC3953644/.

Keil, F. J. (2012). "Multiscale Modelling in Computational Heterogeneous Catalysis". In: *Multiscale Molecular Methods in Applied Chemistry*. Ed. by Barbara Kirchner and Jadran Vrabec. Springer Berlin Heidelberg: Berlin, Heidelberg, pp. 69–107. ISBN: 978-3-642-24968-6. DOI: 10.1007/128_2011_128. URL: https://doi.org/10.1007/128_2011_128.

Kerrigan, Eric Colin (2001). "Robust constraint satisfaction: Invariant sets and predictive control". PhD thesis. University of Cambridge. URL: http://www-control.eng.cam.ac.uk/Homepage/papers/cued_control_155.pdf.

Kimaev, Grigoriy, Donovan Chaffart, and Luis A. Ricardez-Sandoval (2020). "Multilevel Monte Carlo Applied for Uncertainty Quantification in Stochastic Multiscale Systems". In: *AIChE Journal* n/a(n/a). e16262 AIChE-20-22601, e16262. DOI: 10.1002/aic.16262. eprint: https://aiche.onlinelibrary.wiley.com/doi/

pdf/10.1002/aic.16262. URL: https://aiche.onlinelibrary.wiley.com/doi/abs/10.1002/aic.16262.

Kimaev, Grigoriy and Luis A Ricardez-Sandoval (2017). "A comparison of efficient uncertainty quantification techniques for stochastic multiscale systems". In: *AIChE Journal* 63(8), pp. 3361–3373. DOI: https://doi.org/10.1002/aic.15702. URL: https://aiche.onlinelibrary.wiley.com/doi/full/10.1002/aic.15702.

Kimaev, Grigoriy and Luis A. Ricardez-Sandoval (2019). "Nonlinear model predictive control of a multiscale thin film deposition process using artificial neural networks". In: *Chemical Engineering Science* 207, pp. 1230 –1245. ISSN: 0009-2509. DOI: https://doi.org/10.1016/j.ces.2019.07.044. URL: http://www.sciencedirect.com/science/article/pii/S0009250919306086.

Kiparissides, Costas (2006). "Challenges in particulate polymerization reactor modeling and optimization: A population balance perspective". In: *Journal of Process Control* 16(3). Selected Papers from Dycops 7 (2004), Cambridge, Massachusetts, pp. 205 –224. ISSN: 0959-1524. DOI: https://doi.org/10.1016/j.jprocont.2005.06.004. URL: http://www.sciencedirect.com/science/article/pii/S0959152405000624.

Klein, A., C. H. Kuist, and V. T. Stannett (1973). "Vinyl acetate emulsion polymerization. I. Effect of ionic strength and temperature on monomer solubility in the ionically stabilized polymer particle". In: *Journal of Polymer Science: Polymer Chemistry Edition* 11(9), pp. 2111–2126. ISSN: 1542-9369. DOI: 10.1002/pol.1973.170110905. URL: http://dx.doi.org/10.1002/pol.1973.170110905.

Kumar, Pankaj and S Narayanan (2006). "Solution of Fokker-Planck equation by finite element and finite difference methods for nonlinear systems". In: *Sadhana* 31(4), pp. 445–461. DOI: https://doi.org/10.1007/BF02716786. URL: https://link.springer.com/article/10.1007/BF02716786.

Kwon, Joseph Sang-II et al. (2014a). "Enhancing the Crystal Production Rate and Reducing Polydispersity in Continuous Protein Crystallization". In: *Industrial & Engineering Chemistry Research* 53(40), pp. 15538–15548. DOI: 10.1021/ie5008163. eprint: http://dx.doi.org/10.1021/ie5008163. URL: http://dx.doi.org/10.1021/ie5008163.

Kwon, Joseph Sang-Il, Michael Nayhouse, and Panagiotis D. Christofides (2015). "Multiscale, Multidomain Modeling and Parallel Computation: Application to Crystal Shape Evolution in Crystallization". In: *Industrial & Engineering Chemistry Research* 54(47), pp. 11903–11914. DOI: https://doi.org/10.1021/acs.iecr.5b02942. eprint: https://doi.org/10.1021/acs.iecr.5b02942. URL: https://pubs.acs.org/doi/abs/10.1021/acs.iecr.5b02942.

Kwon, Joseph Sang-Il et al. (2013a). "Modeling and control of protein crystal shape and size in batch crystallization". In: *AIChE Journal* 59(7), pp. 2317–2327. ISSN: 1547-5905. DOI: 10.1002/aic.14039. URL: http://dx.doi.org/10.1002/aic.14039.

Kwon, Joseph Sang-Il et al. (2013b). "Modeling and control of shape distribution of protein crystal aggregates". In: *Chemical Engineering Science* 104, pp. 484–497. DOI: https://doi.org/10.1016/j.ces.2013.09.026. URL: https://www.sciencedirect.com/science/article/pii/S0009250913006398.

Kwon, Joseph Sang-Il et al. (2014b). "Crystal shape and size control using a plug flow crystallization configuration". In: *Chemical Engineering Science* 119, pp. 30–39. DOI: https://doi.org/10.1016/j.ces.2014.07.058. URL: https://www.sciencedirect.com/science/article/pii/S0009250914004035.

Kwon, Joseph Sang-Il et al. (2014c). "Modeling and control of crystal shape in continuous protein crystallization". In: *Chemical Engineering Science* 107, pp. 47–57. DOI: https://doi.org/10.1016/j.ces.2013.12.005. URL: https://www.sciencedirect.com/science/article/pii/S0009250913008002.

Lam, R and DG Vlachos (2001). "Multiscale model for epitaxial growth of films: Growth mode transition". In: *Physical Review B* 64(3), p. 035401. DOI: https://doi.org/10.1103/PhysRevB.64.035401. URL: https://journals.aps.org/prb/abstract/10.1103/PhysRevB.64.035401.

Li, Xiaohai et al. (2007). "Effect of additives on shape evolution during electrodeposition I. Multiscale simulation with dynamically coupled kinetic Monte Carlo and moving-boundry finite-volume codes". In: *Journal of The Electrochemical Society* 154(4), pp. D230–D240. DOI: 10.1149/1.2434686. URL: http://jes.ecsdl.org/content/154/4/D230.short.

Liotta, V., C. Georgakis, and M. S. El-Aasser (1997). "Real-time estimation and control of particle size in semi-batch emulsion polymerization". In: *Proceedings of the 1997 American Control Conference (Cat. No.97CH36041)*. Vol. 2, 1172–1176 vol.2. DOI: 10.1109/ACC.1997.609717.

Liotta, Vincenzo et al. (1997). "Manipulation of Competitive Growth for Particle Size Control in Emulsion Polymerization". In: *Industrial & Engineering Chemistry Research* 36(8), pp. 3252–3263. DOI: 10.1021/ie960643g. eprint: https://doi.org/10.1021/ie960643g. URL: https://doi.org/10.1021/ie960643g.

Lötstedt, Per and Lars Ferm (2006). "Dimensional reduction of the Fokker–Planck equation for stochastic chemical reactions". In: *Multiscale Modeling & Simulation* 5(2), pp. 593–614. DOI: https://doi.org/10.1137/050639120. URL: https://epubs.siam.org/doi/abs/10.1137/050639120.

Majumder, Aniruddha et al. (2010). "Fast High-Resolution Method for Solving Multidimensional Population Balances in Crystallization". In: *Industrial & Engineering Chemistry Research* 49(8), pp. 3862–3872. DOI: 10.1021/ie9016946. eprint: https://doi.org/10.1021/ie9016946. URL: https://doi.org/10.1021/ie9016946.

Majumder, Debarshi and Linda J. Broadbelt (2006). "A multiscale scheme for modeling catalytic flow reactors". In: *AIChE Journal* 52(12), pp. 4214–4228. ISSN: 1547-5905. DOI: 10.1002/aic.11030. URL: http://dx.doi.org/10.1002/aic.11030.

Marien, Yoshi W. et al. (2019). "Particle by Particle Kinetic Monte Carlo Tracking of Reaction and Mass Transfer Events in Miniemulsion Free Radical Polymerization". In: *Macromolecules* 52(4), pp. 1408–1423. DOI: 10.1021/acs.macromol.8b02508. URL: https://doi.org/10.1021/acs.macromol.8b02508.

Matous, Karel et al. (2017). "A review of predictive nonlinear theories for multiscale modeling of heterogeneous materials". In: *Journal of Computational Physics* 330, pp. 192 –220. ISSN: 0021-9991. DOI: https://doi.org/10.1016/j.jcp.2016.10.070. URL: http://www.sciencedirect.com/science/article/pii/S0021999116305782.

Mei, Yu et al. (2007). "Catalytic Activity of Palladium Nanoparticles Encapsulated in Spherical Polyelectrolyte Brushes and Core-Shell Microgels". In: *Chemistry of Materials* 19(5), pp. 1062–1069. DOI: 10.1021/cm062554s. URL: https://doi.org/10.1021/cm062554s.

Mesbah, Ali et al. (2009). "A control oriented study on the numerical solution of the population balance equation for crystallization processes". In: *Chemical Engineering Science* 64(20), pp. 4262 –4277. ISSN: 0009-2509. DOI: https://doi.org/10.1016/j.ces.2009.06.060. URL: http://www.sciencedirect.com/science/article/pii/S0009250909004667.

Meurer, T. (July 2017). "Some perspectives in PDE control". In: *Proc. 20th IFAC World Congress*. Accepted. Toulouse (F).

Mohammadi, Masoumeh and Alfio Borzì (2015). "Analysis of the Chang-Cooper discretization scheme for a class of Fokker-Planck equations". In: *Journal of Numerical Mathematics* 23(3), pp. 271–288. DOI: https://doi.org/10.1515/jnma-2015-0018.

Murray, Richard M. (2003). "Applications, Opportunities, and Challenges". In: *Control in an Information Rich World*. Society for Industrial and Applied Mathematics. Chap. 3, pp. 25–70. DOI: 10.1137/1.9780898718010.ch3. eprint: https://epubs.siam.org/doi/pdf/10.1137/1.9780898718010.ch3. URL: https://epubs.siam.org/doi/abs/10.1137/1.9780898718010.ch3.

Ocepek, Martin et al. (2017). "Influence of hydrophobic monomers on secondary nucleation of hydroxyl-functionalized latexes". In: *Journal of Polymer Science Part A: Polymer Chemistry* 55(13), pp. 2190–2202. DOI: 10.1002/pola.28604. eprint: https://onlinelibrary.wiley.com/doi/pdf/10.1002/pola.28604. URL: https://onlinelibrary.wiley.com/doi/abs/10.1002/pola.28604.

Odian, George (2004). "Emulsion Polymerization". In: *Principles of Polymerization*. John Wiley & Sons, Inc., pp. 350–371. ISBN: 9780471478751. DOI: 10.1002/047147875X.ch4. URL: http://dx.doi.org/10.1002/047147875X.ch4.

Omar, Hecham M. and Sohrab Rohani (2017). "Crystal Population Balance Formulation and Solution Methods: A Review". In: *Crystal Growth & Design* 17(7), pp. 4028–4041. DOI: 10.1021/acs.cgd.7b00645. eprint: https://doi.org/10.1021/acs.cgd.7b00645. URL: https://doi.org/10.1021/acs.cgd.7b00645.

Overbeek, J.Th.G. (1982). "Monodisperse colloidal systems, fascinating and useful". In: *Advances in Colloid and Interface Science* 15(3), pp. 251 –277. ISSN: 0001-8686.

DOI: https://doi.org/10.1016/0001-8686(82)80003-1. URL: http://www.sciencedirect.com/science/article/pii/0001868682800031.

Penlidis, A., J. F. MacGregor, and A. E. Hamielec (1988). "Effect of impurities on emulsion polymerization: Case I kinetics". In: *Journal of Applied Polymer Science* 35(8), pp. 2023–2038. DOI: 10.1002/app.1988.070350804. eprint: https://onlinelibrary.wiley.com/doi/pdf/10.1002/app.1988.070350804. URL: https://onlinelibrary.wiley.com/doi/abs/10.1002/app.1988.070350804.

Puschke, Jennifer and Alexander Mitsos (2016). "Robust Dynamic Optimization of a Semi-Batch Emulsion Polymerization Process with Parametric Uncertainties-A Heuristic Approach -". In: *IFAC-PapersOnLine* 49(7). 11th IFAC Symposium on Dynamics and Control of Process SystemsIncluding Biosystems DYCOPS-CAB 2016, pp. 907 –912. ISSN: 2405-8963. DOI: https://doi.org/10.1016/j.ifacol.2016.07.305. URL: http://www.sciencedirect.com/science/article/pii/S2405896316305122.

Ramkrishna, Doraiswami and Meenesh R. Singh (2014). "Population Balance Modeling: Current Status and Future Prospects". In: *Annual Review of Chemical and Biomolecular Engineering* 5(1). PMID: 24606333, pp. 123–146. DOI: 10.1146/annurev-chembioeng-060713-040241. eprint: https://doi.org/10.1146/annurev-chembioeng-060713-040241. URL: https://doi.org/10.1146/annurev-chembioeng-060713-040241.

Rasoulian, Shabnam and Luis A. Ricardez-Sandoval (2015). "A robust nonlinear model predictive controller for a multiscale thin film deposition process". In: *Chemical Engineering Science* 136(Supplement C). Control and Optimization of Smart Plant Operations, pp. 38 –49. ISSN: 0009-2509. DOI: https://doi.org/10.1016/j.ces.2015.02.002. URL: http://www.sciencedirect.com/science/article/pii/S0009250915000962.

Rasoulian, Shabnam and Luis A. Ricardez-Sandoval (2016). "Stochastic nonlinear model predictive control applied to a thin film deposition process under uncertainty". In: *Chemical Engineering Science* 140(Supplement C), pp. 90 –103. ISSN: 0009-2509. DOI: https://doi.org/10.1016/j.ces.2015.10.004. URL: http://www.sciencedirect.com/science/article/pii/S0009250915006703.

Rasoulian, Shabnam and Luis Alberto Ricardez-Sandoval (2014). "Uncertainty analysis and robust optimization of multiscale process systems with application to epitaxial thin film growth". In: *Chemical Engineering Science* 116(Supplement C), pp. 590 –600. ISSN: 0009-2509. DOI: https://doi.org/10.1016/j.ces.2014.05.027. URL: http://www.sciencedirect.com/science/article/pii/S0009250914002371.

Rawlston, Jonathan A (2010). "Multiscale modeling of free-radical polymerization kinetics". PhD thesis. Georgia Institute of Technology. URL: https://smartech.gatech.edu/handle/1853/33933.

Reinhold, Alexander and Heiko Briesen (2015). "High dimensional population balances for the growth of faceted crystals: Combining Monte Carlo integral estimates and the method of characteristics". In: *Chemical Engineering Science* 127,

pp. 220–229. DOI: https://doi.org/10.1016/j.ces.2015.01.035. URL: https://www.sciencedirect.com/science/article/pii/S000925091500055X.

Ricardez-Sandoval, Luis A. (2011). "Current challenges in the design and control of multiscale systems". In: *The Canadian Journal of Chemical Engineering* 89(6), pp. 1324–1341. ISSN: 1939-019X. DOI: 10.1002/cjce.20607. URL: http://dx.doi.org/10.1002/cjce.20607.

Rigopoulos, Stelios and Alan G. Jones (2003). "Finite-element scheme for solution of the dynamic population balance equation". In: *AIChE Journal* 49(5), pp. 1127–1139. DOI: 10.1002/aic.690490507. eprint: https://aiche.onlinelibrary.wiley.com/doi/pdf/10.1002/aic.690490507. URL: https://aiche.onlinelibrary.wiley.com/doi/abs/10.1002/aic.690490507.

Rocha-Botello, Gabriela et al. (2019). "Unexpected Secondary Nucleation in Poly(Vinyl acetate) Nanoparticle Synthesis by Ab Initio Batch Emulsion Polymerization Using Poly(Vinyl alcohol) as Surfactant". In: *Macromolecular Reaction Engineering* 13(5), p. 1900024. DOI: 10.1002/mren.201900024. eprint: https://onlinelibrary.wiley.com/doi/pdf/10.1002/mren.201900024. URL: https://onlinelibrary.wiley.com/doi/abs/10.1002/mren.201900024.

Röder, Fridolin, Richard D. Braatz, and Ulrike Krewer (2019). "Direct coupling of continuum and kinetic Monte Carlo models for multiscale simulation of electrochemical systems". In: *Computers & Chemical Engineering* 121, pp. 722 –735. ISSN: 0098-1354. DOI: https://doi.org/10.1016/j.compchemeng.2018.12.016. URL: http://www.sciencedirect.com/science/article/pii/S0098135418309013.

Röder, Fridolin, Vincent Laue, and Ulrike Krewer (2019). "Model Based Multiscale Analysis of Film Formation in Lithium-Ion Batteries". In: *Batteries & Supercaps* 2(3), pp. 248–265. DOI: 10.1002/batt.201800107. eprint: https://onlinelibrary.wiley.com/doi/pdf/10.1002/batt.201800107. URL: https://onlinelibrary.wiley.com/doi/abs/10.1002/batt.201800107.

Rusli, Effendi et al. (2006). "Robust nonlinear feedback–feedforward control of a coupled kinetic Monte Carlo–finite difference simulation". In: *Journal of Process Control* 16(4), pp. 409–417. DOI: 10.1109/ACC.2005.1470350. URL: https://ieeexplore.ieee.org/abstract/document/1470350.

Sajjadi, Shahriar and Michael Yianneskis (2003). "Semibatch Emulsion Polymerization of Methyl Methacrylate with a Neat Monomer Feed". In: *Polymer Reaction Engineering* 11(4), pp. 715–736. DOI: 10.1081/PRE-120026371. URL: https://doi.org/10.1081/PRE-120026371.

Schnoerr, David, Guido Sanguinetti, and Ramon Grima (2017). "Approximation and inference methods for stochastic biochemical kinetics—a tutorial review". In: *Journal of Physics A: Mathematical and Theoretical* 50(9), p. 093001. DOI: 10.1088/1751-8121/aa54d9. URL: https://iopscience.iop.org/article/10.1088/1751-8121/aa54d9/meta.

Schütte, Christof and Michael Wulkow (2010). "A Hybrid Galerkin–Monte-Carlo Approach to Higher-Dimensional Population Balances in Polymerization Kinetics". In: *Macromolecular Reaction Engineering* 4(9-10), pp. 562–577. DOI: https://doi.org/10.1002/mren.200900073. URL: https://onlinelibrary.wiley.com/doi/full/10.1002/mren.200900073.

Semino, Daniele and W Harmon Ray (1995). "Control of systems described by population balance equations—II. Emulsion polymerization with constrained control action". In: *Chemical Engineering Science* 50(11), pp. 1825–1839. DOI: 10.1016/0009-2509(95)00015-W. URL: https://www.sciencedirect.com/science/article/pii/000925099500015W.

Sheibat-Othman, Nida et al. (2017). "Is Modeling the {PSD} in Emulsion Polymerization a Finished Problem? An Overview". In: *Macromolecular Reaction Engineering* 11(5). 1600059, 1600059–n/a. ISSN: 1862-8338. DOI: 10.1002/mren.201600059. URL: http://dx.doi.org/10.1002/mren.201600059.

Simo, J.C. (1998). "Numerical analysis and simulation of plasticity". In: *Numerical Methods for Solids (Part 3) Numerical Methods for Fluids (Part 1)*. Vol. 6. Handbook of Numerical Analysis. Elsevier, pp. 183 –499. DOI: https://doi.org/10.1016/S1570-8659(98)80009-4. URL: http://www.sciencedirect.com/science/article/pii/S1570865998800094.

Skogestad, Sigurd and Ian Postlethwaite (2007). *Multivariable feedback control: analysis and design*. Vol. 2. Wiley New York.

Smith, Wendell V. and Roswell H. Ewart (1948). "Kinetics of Emulsion Polymerization". In: *The Journal of Chemical Physics* 16(6), pp. 592–599. DOI: 10.1063/1.1746951. eprint: https://doi.org/10.1063/1.1746951. URL: https://doi.org/10.1063/1.1746951.

Sontag, Eduardo D (1998). "Controllability is harder to decide than accessibility". In: *SIAM journal on control and optimization* 26(5), pp. 1106–1118. DOI: 10.1137/0326061. URL: https://epubs.siam.org/doi/pdf/10.1137/0326061.

Sounderya, Nagarajan and Yong Zhang (2008). "Use of Core/Shell Structured Nanoparticles for Biomedical Applications". In: *Recent Patents on Biomedical Engineering* 1(1), pp. 34–42. ISSN: 2211-3320. URL: https://www.ingentaconnect.com/content/ben/biomeng/2008/00000001/00000001/art00005.

Souza Neto, EA de, D R J Owen, and D Periae (2008). *Computational Methods for Plasticity: Theory and Applications*. Wiley: Chichester. DOI: 10.1002/9780470694626. URL: https://onlinelibrary.wiley.com/doi/abs/10.1002/9780470694626.

Srinivasan, B and D Bonvin (2007). "Controllability and stability of repetitive batch processes". In: *Journal of process control* 17(3), pp. 285–295. DOI: https://doi.org/10.1016/j.jprocont.2006.10.009. URL: https://www.sciencedirect.com/science/article/pii/S0959152406001132.

Sussmann, Héctor J and Velimir Jurdjevic (1972). "Controllability of nonlinear systems". In: DOI: https://doi.org/10.1016/0022-0396(72)90007-1. URL: https://www.sciencedirect.com/science/article/pii/0022039672900071.

Sweetman, Stephen J. et al. (2008). "Simultaneous Controllability of {PSD} and {MWD} in Emulsion Polymerisation". In: *Macromolecular Reaction Engineering* 2(5), pp. 382–397. ISSN: 1862-8338. DOI: 10.1002/mren.200800016. URL: http://dx.doi.org/10.1002/mren.200800016.

Tauer, Klaus and Hugo Hernandez (2010). "Mechanism and Modeling of Emulsion Polymerization: New Ideas and Concepts–2. Modeling Strategies". In: *Macromolecular symposia*. Vol. 288. 1. Wiley Online Library, pp. 9–15. DOI: 10.1002/masy.201050202. URL: https://onlinelibrary.wiley.com/doi/abs/10.1002/masy.201050202.

Tempo, Roberto, Giuseppe Calafiore, and Fabrizio Dabbene (2005). "Randomized Algorithms for Analysis and Control of Uncertain Systems". In: *Randomized Algorithms for Analysis and Control of Uncertain Systems*. Springer London: London. Chap. Randomized Algorithms in Systems and Control, pp. 107–115. ISBN: 978-1-84628-052-8. DOI: 10.1007/1-84628-052-4_8. URL: https://doi.org/10.1007/1-84628-052-4_8.

Tempo, Roberto, Giuseppe Calafiore, and Fabrizio Dabbene (2013). "Applications of Randomized Algorithms". In: *Randomized Algorithms for Analysis and Control of Uncertain Systems: With Applications*. Springer London: London, pp. 283–327. ISBN: 978-1-4471-4610-0. DOI: 10.1007/978-1-4471-4610-0_19. URL: https://doi.org/10.1007/978-1-4471-4610-0_19.

Tjiam, Cynthia and Vincent G. Gomes (2014). "Optimal Operating Strategies for Emulsion Polymerization with Chain Transfer Agent". In: *Industrial & Engineering Chemistry Research* 53(18), pp. 7526–7537. DOI: 10.1021/ie4032956. eprint: https://doi.org/10.1021/ie4032956. URL: https://doi.org/10.1021/ie4032956.

Tobita, Hidetaka, Yuko Takada, and Mamoru Nomura (1994). "Molecular weight distribution in emulsion polymerization". In: *Macromolecules* 27(14), pp. 3804–3811. DOI: 10.1021/ma00092a020. URL: https://doi.org/10.1021/ma00092a020.

Tronci, Stefania et al. (2011). "A stochastic approach for the prediction of PSD in crystallization processes: Analytical solution for the asymptotic behavior and parameter estimation". In: *Computers & Chemical Engineering* 35(11), pp. 2318–2325. DOI: https://doi.org/10.1016/j.compchemeng.2011.01.007. URL: http://www.sciencedirect.com/science/article/pii/S0098135411000093.

Ugelstad, J. et al. (1985). "Preparation and application of monodisperse polymer particles". In: *Journal of Polymer Science: Polymer Symposia* 72(1), pp. 225–240. DOI: 10.1002/polc.5070720125. eprint: https://onlinelibrary.wiley.com/doi/pdf/10.1002/polc.5070720125. URL: https://onlinelibrary.wiley.com/doi/abs/10.1002/polc.5070720125.

Ulissi, Z, V Prasad, and DG Vlachos (2011). "Effect of multiscale model uncertainty on identification of optimal catalyst properties". In: *Journal of catalysis* 281(2), pp. 339–344. DOI: https://doi.org/10.1016/j.jcat.2011.05.019. URL: https://www.sciencedirect.com/science/article/pii/S0021951711001680.

Urrea-Quintero, Jorge-Humberto, Silvia Ochoa, and Hugo Hernández (2019). "A reduced-order multiscale model of a free-radical semibatch emulsion polymerization process". In: *Computers & Chemical Engineering* 127, pp. 11 –24. ISSN: 0098-1354. DOI: https://doi.org/10.1016/j.compchemeng.2019.04.029. URL: http://www.sciencedirect.com/science/article/pii/S0098135419300766.

Vafa, Ehsan, Mohammad Shahrokhi, and Hossein Abedini (2013). "Solution of population balance equations in emulsion polymerization using method of moments". In: *Chemical Engineering Communications* 200(1), pp. 20–49. DOI: https://doi.org/10.1080/00986445.2012.686463. URL: https://www.tandfonline.com/doi/full/10.1080/00986445.2012.686463.

Vale, H.M. and T.F. McKenna (2005). "Modeling particle size distribution in emulsion polymerization reactors". In: *Progress in Polymer Science* 30(10), pp. 1019 – 1048. ISSN: 0079-6700. DOI: https://doi.org/10.1016/j.progpolymsci.2005.06.006. URL: http://www.sciencedirect.com/science/article/pii/S007967000500078X.

Vale, Hugo M and Timothy F McKenna (2007). "Solution of Population Balance Equations for Emulsion Polymerization: Zero- One and Zero- One- Two Systems". In: *Industrial & engineering chemistry research* 46(2), pp. 643–654. DOI: 10.1021/ie060928l. URL: https://doi.org/10.1021/ie060928l.

Varshney, Amit and Antonios Armaou (2008). "Reduced order modeling and dynamic optimization of multiscale PDE/kMC process systems". In: *Computers & Chemical Engineering* 32(9). Networked and Complex Systems S.I., pp. 2136 –2143. ISSN: 0098-1354. DOI: https://doi.org/10.1016/j.compchemeng.2008.03.004. URL: http://www.sciencedirect.com/science/article/pii/S0098135408000409.

Vicente, M, J.R Leiza, and J.M Asua (2003). "Maximizing production and polymer quality (MWD and composition) in emulsion polymerization reactors with limited capacity of heat removal". In: *Chemical Engineering Science* 58(1), pp. 215 –222. ISSN: 0009-2509. DOI: https://doi.org/10.1016/S0009-2509(02)00466-9. URL: http://www.sciencedirect.com/science/article/pii/S0009250902004669.

Vlachos, Dionisios G. (2005). "A Review of Multiscale Analysis: Examples from Systems Biology, Materials Engineering, and Other Fluid-Surface Interacting Systems". In: *Advances in Chemical Engineering*. Ed. by Guy B. Marin. Vol. 30. Advances in Chemical Engineering. Academic Press, pp. 1 –61. DOI: https://doi.org/10.1016/S0065-2377(05)30001-9. URL: http://www.sciencedirect.com/science/article/pii/S0065237705300019.

Vlachos, Dionisios G. (2012). "Multiscale modeling for emergent behavior, complexity, and combinatorial explosion". In: *AIChE Journal* 58(5), pp. 1314–1325. ISSN: 1547-5905. DOI: 10.1002/aic.13803. URL: http://dx.doi.org/10.1002/aic.13803.

Wang, Shi et al. (2020). "Isothermal emulsion polymerization of n-butyl methacrylate with KPS and redox initiators: Nucleation". In: *Journal of Applied Polymer Science* 137(2), p. 48275. DOI: 10.1002/app.48275. eprint: https://onlinelibrary.

wiley.com/doi/pdf/10.1002/app.48275. URL: https://onlinelibrary.wiley.com/doi/abs/10.1002/app.48275.

Wriggers, Peter (2008). *Nonlinear Finite Element Method*. Springer Berlin Heidelberg: Berlin, Heidelberg, pp. 1–5. ISBN: 978-3-540-71001-1. DOI: 10.1007/978-3-540-71001-1_1. URL: https://doi.org/10.1007/978-3-540-71001-1_1.

Xie, Le, Qi Liu, and Zheng-Hong Luo (2018). "A multiscale CFD-PBM coupled model for the kinetics and liquid-liquid dispersion behavior in a suspension polymerization stirred tank". In: *Chemical Engineering Research and Design* 130, pp. 1 –17. ISSN: 0263-8762. DOI: https://doi.org/10.1016/j.cherd.2017.11.045. URL: http://www.sciencedirect.com/science/article/pii/S0263876217306640.

Xie, Le and Zheng-Hong Luo (2017). "Multiscale Computational Fluid Dynamics-Population Balance Model Coupled System of Atom Transfer Radical Suspension Polymerization in Stirred Tank Reactors". In: *Industrial & Engineering Chemistry Research* 56(16), pp. 4690–4702. DOI: 10.1021/acs.iecr.7b00147. eprint: https://doi.org/10.1021/acs.iecr.7b00147. URL: https://doi.org/10.1021/acs.iecr.7b00147.

Yan, Wei-Cheng, Zheng-Hong Luo, and An-Yi Guo (2011). "Coupling of {CFD} with {PBM} for a pilot-plant tubular loop polymerization reactor". In: *Chemical Engineering Science* 66(21), pp. 5148 –5163. ISSN: 0009-2509. DOI: https://doi.org/10.1016/j.ces.2011.07.004. URL: http://www.sciencedirect.com/science/article/pii/S0009250911004647.

Yao, Ya, Jun-Wei Su, and Zheng-Hong Luo (2015). "CFD-PBM modeling polydisperse polymerization {FBR}s with simultaneous particle growth and aggregation: The effect of the method of moments". In: *Powder Technology* 272, pp. 142 –152. ISSN: 0032-5910. DOI: https://doi.org/10.1016/j.powtec.2014.11.037. URL: http://www.sciencedirect.com/science/article/pii/S0032591014009668.

Yuan, Zhihong, Bingzhen Chen, and Jinsong Zhao (2011). "An overview on controllability analysis of chemical processes". In: *AIChE Journal* 57(5), pp. 1185–1201. DOI: https://doi.org/10.1002/aic.12340. URL: https://aiche.onlinelibrary.wiley.com/doi/full/10.1002/aic.12340.

Zeaiter, J., J. A. Romagnoli, and V. G. Gomes (2006). "Online control of molar mass and particle-size distributions in emulsion polymerization". In: *AIChE Journal* 52(5), pp. 1770–1779. DOI: 10.1002/aic.10773. eprint: https://aiche.onlinelibrary.wiley.com/doi/pdf/10.1002/aic.10773. URL: https://aiche.onlinelibrary.wiley.com/doi/abs/10.1002/aic.10773.

Zetterlund, Per B. and Dagmar R. D'hooge (2019). "The Nanoreactor Concept: Kinetic Features of Compartmentalization in Dispersed Phase Polymerization". In: *Macromolecules* 52(21), pp. 7963–7976. DOI: 10.1021/acs.macromol.9b01037. URL: https://doi.org/10.1021/acs.macromol.9b01037.

Zienkiewicz, O.C., R.L. Taylor, and J.Z. Zhu (2013). *The Finite Element Method: Its Basis and Fundamentals*. Seventh Edition. Butterworth-Heinemann: Oxford, p. i. ISBN: 978-1-85617-633-0. DOI: https://doi.org/10.1016/B978-1-85617-633-

0.00019-8. URL: http://www.sciencedirect.com/science/article/pii/B9781856176330000198.